Journal Pre-proofs

NMR Crystallography of Molecular Organics

Paul Hodgkinson

Please cite this article as: P. Hodgkinson, NMR Crystallography of Molecular Organics, *Progress in Nuclear Magnetic Resonance Spectroscopy* (2020), doi: https://doi.org/10.1016/j.pnmrs.2020.03.001

This is a PDF file of an article that has undergone enhancements after acceptance, such as the addition of a cover page and metadata, and formatting for readability, but it is not yet the definitive version of record. This version will undergo additional copyediting, typesetting and review before it is published in its final form, but we are providing this version to give early visibility of the article. Please note that, during the production process, errors may be discovered which could affect the content, and all legal disclaimers that apply to the journal pertain.

NMR Crystallography of Molecular Organics

Paul Hodgkinson

Department of Chemistry, Durham University, Stockton Road, Durham DH1 3LE, UK

paul.hodgkinson@durham.ac.uk

Abstract

Developments of NMR methodology to characterise the structures of molecular organic structures are reviewed, concentrating on the previous decade of research in which density functional theory-based calculations of NMR parameters in periodic solids have become widespread. With a focus on demonstrating the new structural insights provided, it is shown how "NMR crystallography" has been used in a spectrum of applications from resolving ambiguities in diffraction-derived structures (such as hydrogen atom positioning) to deriving complete structures in the absence of diffraction data. As well as comprehensively reviewing applications, the different aspects of the experimental and computational techniques used in NMR crystallography are carefully surveyed. NMR crystallography is seen to be a rapidly maturing subject area that is increasingly appreciated by the wider crystallographic community.

Table of Contents

1 Introduction

NMR has been used to obtain crystallographic data from its earliest days, the pioneering example being Pake's measurement of the distance between the hydrogen atoms of water in gypsum ($CaSO_4.2H_2O$) via the dipolar coupling between the ^1H nuclei [1]. But despite the natural complementarity between the sensitivity of diffraction and NMR to long-range ordering and short-range environment respectively, the interactions between NMR and diffraction crystallography have traditionally been limited. The identification of crystallography with diffraction studies must have seemed complete with International Union of Crystallography's (IUCr's) 1991 re-definition of a crystal as "a material [with an] essentially a sharp diffraction pattern"[2]. Recent years have, however, seen a significant strengthening of interactions between these different ways of characterising solid materials. This is reflected in journal special issues on "NMR crystallography"[3-5], a dedicated handbook[6], and in 2014, the creation of an IUCr subject grouping (commission) in NMR crystallography[7]. There are also a number of valuable reviews of the area; Bryce's 2017 article gives a compact and wide-ranging overview[8], while Martineau et al.[9], and Ashbrook and McKay[10] have written comprehensive overviews of NMR crystallography applied to both organic and inorganic materials.

This review focusses on the applications of NMR crystallography to crystals of small molecular organics, often termed "chemical crystallography". This is a significant narrowing of the field of applications given that a major strength of NMR is its applicability to all sample types, including materials, such as polymers and glasses, that are challenging for diffraction-based methods. It is, however, the area of NMR of small molecule crystals that has seen the most rapid developments, as a result of the development of efficient Density Functional Theory (DFT) codes that allow NMR parameters to be directly correlated to crystal structures. Progress has been particularly rapid for molecular organics, aided by the fact that a relatively limited subset of nuclei (notably ^{13}C and ^1H) are sufficient for most problems. While acknowledging notable applications of NMR methods to other material types, we will try to give a comprehensive review of the state-of-the-art for molecular organic solids (up to 2018), focussed in the past decade in which DFT calculations have played an important role. Reviews of other material types with an emphasis on NMR crystallography include articles on crystalline microporous materials[11], nucleic acid components[12], peptides[13], inorganic

materials[14], pharmaceutical materials[15, 16], and supramolecular assembly[17]. Ref. [18] and citations within provide excellent illustrations of NMR crystallographic methods applied to complex biomolecules. The focus of the current review is showing how NMR has been used to provide new crystallographic insight, allowing new researchers in the field to understand what crystallographic problems can be realistically tackled via NMR methods, at the expense of excluding papers where the NMR is tangential to the crystallography.

The concept of NMR as a crystallographic tool seems unnatural for most synthetic chemists. Successful crystallisation of a product, and confirmation of its chemical identity via single-crystal X-ray diffraction (SCXRD) typically forms a tidy end-point to a synthesis. In other cases, however, the three-dimensional structure of the material is of direct interest, and characterising the different solid forms available is essential, whether these forms are amenable to single-crystal diffraction or not. This is particularly true in pharmaceutical applications, where the appearance of a previously unknown polymorph can be disastrous; well-known cases include ritonavir[19] and, more recently, rotigotine[20]. In both of these cases, the product had to be withdrawn from the market and reformulated. The importance of complete characterisation of the pharmaceutical solids, beyond single-crystal diffraction studies, is illustrated by a number of edited volumes on the topic[21-23].

The most obvious limitation of restricting crystallography to SCXRD studies is that many solid forms are not suitable for single-crystal studies. The most obvious examples are amorphous materials lacking long-range order. Although fully disordered materials are always challenging to characterise, NMR has a particularly useful role to play for disordered materials, as discussed in Section 3.9. In other cases, materials may be locally ordered, but the crystallites may simply be too small for conventional single--crystal XRD. Obvious examples are materials produced via mechano-chemistry, which typically produces fine powders that can only be characterised by powder diffraction. Significant strides have recently been made in using electron diffraction to obtain structures from very small crystals, but this is a challenging technique where the complementary information from NMR has a potentially valuable role. Powder X-ray diffraction (PXRD) is widely used to characterise finely divided crystalline solids. Much like ^{13}C solid-state NMR, PXRD can readily be used as a finger-printing tool to distinguish crystalline forms of molecular organics, but solving structures from PXRD is a considerable challenge, due to the much lower information content of a 1D diffractogram. The application of NMR to assist structure solution from PXRD and electron diffraction data is discussed in Section 3.6.

NMR would seem to have little useful role to play in characterising materials where a structure solution is already available from single-crystal XRD. It is important, however, to be aware of the intrinsic limitations of XRD. Firstly, any disorder disrupts the "inversion" of the diffraction pattern to structure. For example, even small amplitude thermal motion will distort apparent bond lengths (see Section 2.5.1), while the effects of larger amplitude motions need to be modelled, introducing an element of judgement into the fitting of the electron density pattern. Secondly, the weak scattering of X-rays by the single electron of H atoms means that XRD struggles to accurately locate H atoms. The difficulty of locating H atoms confidently is unfortunate given the importance of hydrogen bonding in structural chemistry. This is discussed in detail in Section 3.2. Thirdly, XRD struggles to differentiate isoelectronic, such as OH vs. F vs. CH_3, or near-isoelectronic species, e.g. Si vs. Al. These issues are infrequently encountered in molecular systems, but are a severe problem for materials such as aluminosilicates. The latter two limitations of X-ray diffraction can be avoided using neutron diffraction. However, much larger samples are required due to the weaker scattering of neutrons (often precluding single crystal studies), and the scale of facilities required to support neutron diffraction means it is not a panacea for the limitations of X-ray diffraction.

The bulk of the review is divided into two sections, the first dealing with the methodology of NMR crystallography, while the second reviews the applications of the method. Readers who are primarily interested in what has been achieved with NMR crystallography can skip over the methodology, hopefully to return having been convinced of the opportunities provided by combining NMR and traditional crystallography!

2 The tools of NMR crystallography

The basic principles of solid-state NMR have been set out in a number of introductory texts[24, 25] and will not be described here. Instead this section reviews the different NMR interactions and the contribution that they can make to crystallographic studies.

2.1 Information from dipolar couplings

The dipolar coupling constant between a pair of nuclei I and S is directly related to their internuclear distance, r_{IS}:

$$D_{IS} = \left(\frac{h}{4\pi^2} \right) \left(\frac{\mu_0}{4\pi} \right) \frac{\gamma_I \gamma_S}{r_{IS}^3} \tag{2}$$

Hence, measuring a dipolar coupling between a pair of nuclei provides direct information on interatomic distances. It is also worth noting that "pseudo-contact shifts" in paramagnetic systems are essentially dipolar in nature, and so can also be used to obtain distances between nuclei and paramagnetic metal centres. Such shifts have been used in NMR crystallography of, *inter alia*, lanthanide complexes[26], metal-organic frameworks[27], phthalocyanine polymorphs[28] and paramagnetic metalloproteins[29, 30]. Paramagnetic systems are not discussed further in this review.

There are, however, some important reasons why the measurement of dipolar couplings has not provided the rich source of crystallographic information that Pake may have envisaged in 1948. The primary obstacle is often isolating an individual coupling; gypsum is an atypical case where the only significant dipolar coupling involving the ^1H spins is the one of interest. In most other cases, magic-angle spinning (MAS) is necessary to obtain sufficient spectral resolution. Since MAS, by definition, averages the dipolar couplings, some form of "recoupling" using resonant radio-frequency (RF) irradiation is required to re-introduce the influence of the dipolar interactions.

For strong dipolar couplings between unlike (hetero) nuclei, this recoupling can be easily and robustly achieved by the classic cross-polarisation (CP) technique used to transfer magnetisation from an abundant spin, typically ^1H, to a dilute isotope, such as ^{13}C. For example, the distances between Sn and H in $SnHPO_3$ and $SnHPO_4$ have been measured to pm precision (1.42 vs. 2.05 Å respectively) using the $^{119}Sn/^1H$ dipolar couplings obtained from the build-up of ^{119}Sn magnetisation under CP from ^1H[31]. CP build-up curves have been similarly used to measure N–H distances in NH_2 groups (sample enriched in ^{15}N)[32]; the initial oscillations of the build-up curves were well fitted by simulations of an isolated NH_2 spin system, resulting in much more accurate and consistent N–H distances, 1.055(7) Å, than observed in the diffraction study (0.87–1.01 Å). Measuring weaker heteronuclear couplings requires more sophisticated recoupling methods, such as those based on the REDOR sequence[33]. Note that some form of isotopic labelling is generally required, either to isolate particular spin pairs and/or for sufficient signal-to-noise ratio. For example, Zhao et al. used recoupling techniques to measure $^{15}N,^1H$ dipolar couplings in ^{15}N-enriched histidine hydrochloride[34]. Experimental factors, particularly the inhomogeneity of the RF field, limited the accuracy with which the two N–H bond distances in the molecule could be measured (estimated at ±5 pm), but the *difference* in bond length could be measured both accurately and precisely, 4.0 ± 1.0 pm, comparing well with the result from neutron diffraction 4.4 ± 0.6 pm (standard error corrected). Concordant results have been obtained using "inverse detection" methods on the same model system using either REDOR-type sequences[35] or CP[36] for dipolar recoupling. Dipolar couplings are also used in a more qualitative fashion in classic heteronuclear correlation (HETCOR) experiments. These are widely used for assignment, see Section 3.1, but HETCOR experiments with longer cross-polarisation times can also reveal intermolecular interactions, as discussed in Section 3.4.1.

Strong dipolar couplings are readily measured with high precision, but it is important to note that vibrational averaging means this does not necessarily translate into high *accuracy*. The conventional model (the Independent Atom Model) used to analyse diffraction data naturally produces a set of

4

atomic positions with self-consistent interatomic distances. The effects of vibration are transferred into "atomic displacement parameters", which, perhaps unhelpfully, are treated as simple measurement uncertainties. In contrast, vibrational anharmonicity will lead to an inconsistent set of interatomic distances from dipolar couplings; since the mean dipolar coupling depends on internuclear distance as $\left\langle r_{\mathrm{IS}}^{-3} \right\rangle$, effective distances obtained from couplings averaged over an anharmonic motion will not be identical to the average distance $\left\langle r_{\mathrm{IS}} \right\rangle$. Vibrational correction to distances obtained from dipolar couplings was long appreciated as a necessary step in obtaining high-accuracy structures of molecules dissolved in liquid crystal solvents[37]. In the case of N–H distances, which are important in describing "order parameters" in peptide chains, vibrational averaging leads to effective distances that are 0.5–3% longer than the "true" (self-consistent) 0 K distance[38], with zero-point motions found to have a significant impact (up to 3 pm). Corresponding observations have been made for distances determined from dipolar couplings in molecular solids[39], although measurements of angles between dipolar tensors were found to be robust with respect to molecular vibration.

The use of dipolar couplings between like (homo) nuclei for accurate distance measurement has proved more challenging. The key problem is that the Hamiltonians for pairs, i and j, of dipolar coupled spins, $\hat{H}_{ij}^{\mathrm{D}}$, do not, in general, commute with each other, $[\hat{H}_{ij}^{\mathrm{D}}, \hat{H}_{jk}^{\mathrm{D}}] \neq 0$ when $i \neq k$. This contrasts to the dipolar Hamiltonian for heteronuclear spins (under the normal high-field conditions), which only contains spin operators involving z, and so the Hamiltonians for different spins pairs necessarily commute. Hence the effects of multiple couplings on REDOR experiments, for example, can be considered in an additive fashion. The situation is very different for Hamiltonians that are dominated by homonuclear dipolar couplings (such as those generated by "broadband" recoupling sequences under MAS). In particular, the dynamics is affected by the phenomenon of "dipolar truncation", where a strong coupling between a pair of spins, say i and j, will overpower the effect of a weaker coupling, say between i and k, making it difficult to measure the weaker coupling[40, 41]. So a cross-peak between spins i and k in a 2D correlation spectrum may be the result of a "relay" transfer involving two stronger couplings (D_{ij} and D_{jk}) rather than the direct coupling D_{ik}. The ^{1}H spins in typical organic compounds are promiscuously coupled, and so dipolar truncation is a significant problem, especially as the dominant strong couplings (such as those within a methylene, CH_2, unit) are often structurally uninteresting. The dynamics of dipolar coupled spins are most simply described in terms of the root-sum-square (RSS) coupling between a given spin j and its neighbours:

$$d_{\mathrm{rss},j} = \sqrt{\sum_{k \neq j} d_{jk}^2} \qquad (3)$$

For instance, fitting a spinning sideband manifold associated with a site j to a single dipolar coupling will return this effective coupling as a good approximation[42]. The number of spins included in the sum typically grows as a cube of the radius considered for typical materials, and so this sum converges relatively slowly, cf. Fig. 5.2 of Ref. [43]. The RSS coupling is effectively a generalisation of the "^{1}H second moment" previously widely used in wideline ^{1}H NMR, but is more suited to situations where different ^{1}H sites are resolved.

With exception of some use of ^{13}C,^{13}C dipolar couplings to probe molecular conformations, discussed in Section 3.5, structural applications of homonuclear dipolar couplings have mostly involved ^{1}H nuclei. The experimental techniques used to probe ^{1}H dipolar couplings[43-45] and their applications[46] have been recently reviewed, and we will just highlight here cases where these techniques have been most successfully applied to molecular organics. Dipolar truncation has largely thwarted the application of recoupling-type sequences to measure smaller couplings and longer distances, and recoupling has been largely used to probe dominant couplings. Such experiments have generally involved double-quantum (DQ) / single-quantum (SQ) correlation spectra, which have the advantage

(relative to simply correlating conventional single-quantum ^{1}H frequencies) that peaks are only present if double-quantum coherence can be created between the spins involved. Hence diagonal peaks are only present if they correspond to two sites with the same ^{1}H frequency (e.g. equivalent protons within a CH_2), often allowing the identification of sites that would otherwise be lost in a 1D spectrum, e.g. a key NH resonance down at 8 ppm[47]. Based on results collated up to 2007, Brown concluded that cross-peaks in a DQ/SQ correlation spectra can be observed for ^{1}H sites up to 3.5–4 Å apart[48]. Other workers have taken used a more conservative cut-off of 3 Å for expected cross-peaks in DQ/SQ correlation spectra[49]. While ^{1}H homonuclear decoupling has historically provided better resolution than simple MAS, the latter has advantages in terms of overall simplicity and robustness. For example, Sardo and co-workers[50] observed a key cross peak in a DQ/SQ correlation spectrum acquired under fast MAS (26 kHz spinning, 700 MHz NMR frequency) that was missing in the equivalent spectrum acquired with homonuclear decoupling. It is worth noting the increased availability of ultra-fast MAS probes (100+ kHz spinning rates), and the new approaches, such as inverse detection, that are opened up by the increased resolution[51].

More quantitative information can be obtained by monitoring the build-up of cross-peak intensities as a function of recoupling time. Most notably, Bradley et al.[52-54] have obtained reasonable matches of DQ build-up curves to numerical simulations of recoupling using local clusters of eight ^{1}H spins[52]. Although simulating the dynamics of dipolar-coupled networks under the effect of RF pulse sequences is in general quite challenging[55], due to multiple interacting effects such as RF inhomogeneity and pulse transient effects, the deviations between experiment and simulation are less significant for the initial build-up. Some principles were deduced from this work, most notably, that the most intense cross-peak at a given SQ frequency corresponded to the strongest coupling (and hence shortest H–H distance), and that the relative intensities of other cross-peaks were generally in proportion to the squares of corresponding coupling (excluding cross-peaks involving CH_2, which are strongly affected by dipolar truncation). Proximity information is also invaluable in probing self-assembly in supramolecular and macromolecular systems, such as polymers and host-guest systems. These are outside the scope of this article, but several examples can be found in recent reviews[44, 46, 56-58].

An alternative approach to obtaining distance information from homonuclear coupled networks is to make use of "spin diffusion", that is, the exchange of spin magnetisation via dipolar couplings. At modest MAS rates, where the effects of chemical shift differences can be ignored, the spin-diffusion build-up curves can be well fitted by simple phenomenological expressions to extract RSS couplings between sites. As discussed in Section 3.8, the set of couplings between resolved ^{1}H sites have been successfully used to obtain *de novo* crystal structures of molecular organics. The fact that spin diffusion occurs in the absence of RF, with little effect of MAS, makes such experiments very robust. The longer timescales of spin-diffusion also mean that the evolution fits to simple exponential behaviour, rather than the more complex oscillatory behaviour characteristic of RF-driven recoupling.

Finally it is important to note the role of dipolar couplings in probing dynamics; averaging of a known, strong dipolar coupling, e.g. between ^{13}C and a bonded ^{1}H, by molecular motion provides a very direct and straightforward probe of local "order parameters", e.g. to determine whether phenyl rings are dynamic on NMR timescales[59-61]. Similarly the unexpected appearance of resonances in "dipolar dephasing" experiments is often associated with dynamics, e.g. mobile butoxy groups in oxybuprocaine hydrochloride[62] and dynamic furan rings, cf. Figure 28. The experimental techniques available to measure dipolar couplings in highly dynamic materials, such as liquid crystals, have been recently reviewed[63], as has the use of dipolar couplings, and other NMR observables, to probe dynamics in biomolecules[64].

2.2 Information from J and quadrupolar couplings

Apart from the occasional use of J-coupling-based transfer for correlation experiments, J couplings have played a relatively minor role in NMR crystallography of molecular organics. Most structurally significant J-couplings, e.g. $^3J_{HH}$ couplings, with their dependence on torsion angles, are too small to

be measured in the solid state. J couplings between dilute spins are more accessible. For example, $^{2h}J_{NN}$ couplings as small as 3.8 Hz have been measured using spin-echo experiments on ^{15}N-labelled deoxyguanosine derivatives[65]. These are couplings between a pair of ^{15}N nuclei across a hydrogen bond. As well as allowing the hydrogen-bonding network to be deduced, the values of these couplings were linked to hydrogen bond strength using correlations derived from solution-state NMR. For example, the relative sizes of two couplings (6.2 ± 0.4 and 7.4 ± 0.4 Hz) were consistent with diffraction-derived N–N distances (2.83 and 2.91 Å respectively). Even smaller couplings have been measured ($^{3h}J_{NC}$ = 0.46 ± 0.24 Hz) in samples where the ^{1}H coupling network has been diluted by ^{2}H labelling[66].

Since most of the available NMR information in organic systems is naturally obtained from ^{13}C, ^{1}H and, to a lesser extent, ^{15}N NMR, NMR of quadrupolar nuclei has rarely been used. The most significant exception is ^{2}H NMR, which is widely used to study dynamics[67], but both ^{14}N and ^{17}O have been used to characterise hydrogen positioning, as discussed in Section 3.2. In principle, electric field gradients are very sensitive probes of local environment, especially where local symmetry means that electric field gradients are small, e.g. for ^{14}N in trimethylammonium[68]; the quadrupolar parameters are very sensitive to longer range effects, scaling as r^{-3} compared to isotropic chemical shifts, whose paramagnetic contributions scale as r^{-6}. In most cases, however, NMR crystallographic studies of quadrupolar nuclei are at the early stage of establishing correlations between structure and NMR measurables, such as the environment of chloride ions in pharmaceutical materials[69], rather than establishing unknown structural information from NMR data.

2.3 Information from chemical shifts

The sensitivity of NMR frequencies to local chemical environment, via the shielding effect of surrounding electrons, is central to the application of NMR to chemical systems. Hence solid-state NMR can distinguish between solid forms, whether these are different crystalline forms of the same chemical composition (polymorphs) or amorphous / disordered forms. While solid-state NMR can clearly be used to fingerprint different solid forms, the primary goal of NMR crystallography is to provide crystallographic insight. Most straightforwardly, the NMR spectrum provides direct information on Z' (the number of molecules in the crystallographic asymmetric unit, from the multiplicity of resonances of each site). Z' must be distinguished from Z, the number of molecules in the full unit cell; the ratio between the two reflects the number of symmetry elements in the space group. Cases where the apparent Z' differs between SCXRD and NMR studies may indicate a phase transition between the temperature used for SCXRD (typically 100–120 K) and the ambient temperatures typically used in NMR[70]. Note that Z' can be fractional, e.g. 0.5, if a molecule occupies a high symmetry site. Indeed, in inorganic framework materials, atoms are commonly located at high symmetry positions (so-called Wyckoff positions), and it may even be possible to deduce the relevant space group purely from NMR data by counting the multiplicity of resonances for sufficient distinct NMR-active nuclei[71]. More usually, NMR data can help significantly constrain the number of compatible space groups. This is particularly valuable in structures resulting from symmetry breaking, where the effects on the diffraction pattern are typically very subtle, but the loss of symmetry is directly observed in the NMR spectrum[72, 73]. In the case of molecular organic materials, however, the local symmetry is generally low, and it is rare to be able to provide direct crystallographic information, beyond Z'. This may, however, be an invaluable starting point in some contexts, such as solving crystal structures from PXRD data or setting up a crystal structure prediction; see Sections 3.7 and 3.8 respectively for further discussion.
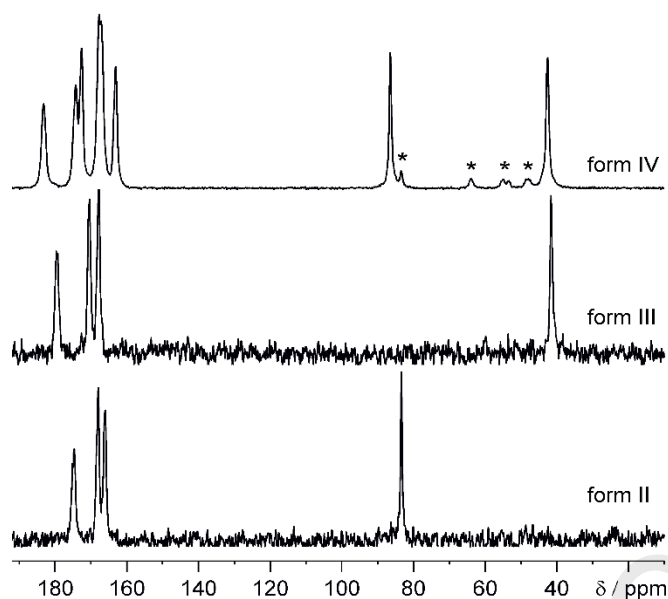
Figure 1 ^{13}C CP/MAS spectra of three forms of 2-thiobarbituric acid. The spectra easily distinguish between a keto form (resonance of CH$_2$ at about 40 ppm) and an enol form (CH resonance at about 84 ppm) of the molecule. The spectrum of Form IV clearly shows that its asymmetric unit contains both enol and keto forms. Figure adapted from Ref. 74 © 2010 Wiley-VCH Verlag GmbH&Co. KGaA, Weinheim; see reference for full details and complete figure.

In general, the connection between structural environment and chemical shift is complex, and requires computational methods to elucidate (see below). In some cases, however, chemical shifts can resolve questions of chemical identity in the solid state very directly. For instance, the ^{13}C shifts of the carbon clearly distinguish between keto vs. enol forms, as in the case of 2-thiobarituric acid[74], illustrated in Figure 1. Beyond establishing chemical identity, the most diagnostic and structurally relevant links between structure and chemical shifts are provided by hydrogen bonding[75], as discussed in detail in Section 3.2. ^{13}C shifts are also very sensitive to conformational changes, and so differences between structures associated with "conformational polymorphism" can be expected to show up clearly in the ^{13}C spectrum. For example, ^{13}C shifts of guanosine and its derivatives[76, 77] were found to reliably distinguish *syn* vs *anti* conformations of the sugar. Other examples of using shift data to establish molecular conformation are discussed in Section 3.5. In contrast, the differences will be less marked for rigid molecules, whose structures differ primarily in their packing; here ^{1}H chemical shift differences may be more pronounced, particularly where these are influenced by aromatic ring currents, as discussed in Section 3.4. In many cases there is insufficient high-quality experimental data to confidently establish empirical correlations between shifts and structure. Here the ability to compute chemical shifts on artificial structures is invaluable. For instance, the difference in shifts calculated on the full crystal structure vs. isolated molecules can be used to evaluate the strength of intermolecular interactions, see Section 3.4.

While ^{13}C solid-state NMR spectra are generally effective in discriminating solid forms, there are cases where similar conformations and packings mean that complementary data is required. For example, the ^{13}C NMR spectra of the α and γ polymorphs of glycine are very similar, but their ^{1}H NMR spectra (acquired using homonuclear decoupling) are quite distinct[78]. Similarly, the differences in ^{13}C shifts between A and B polymorphs of histidine hydrochloride are less than 1 ppm[79]. Subtle differences were visible in ^{1}H spectrum, but the forms were most cleanly differentiated by ^{1}H DQ/SQ spectra, with the differences rationalised in terms of intermolecular contacts. Particularly under fast MAS, the sensitivity of ^{1}H shifts to hydrogen bonding may be sufficient to distinguish between polymorphs, e.g. the polymorphs of acetaminophen (paracetamol), which are not clearly distinguished by vibrational spectroscopy[80].

2.4 DFT-based calculations of NMR parameters

A central theme of this review is assessing the impact of calculations of NMR parameters in solids, particularly since the development of the GIPAW (Gauge Including Projector Augmented Waves) method by Pickard and Mauri[81]. While calculation results had been used in solid state NMR with some success before this point, the rapid recent development of "NMR crystallography" is largely associated with this approach, especially through its implementation in the CASTEP code[82]. Recent work on alternative methods are discussed in Section 2.5.2. Note that there are particular challenges associated with quantum chemical calculations on paramagnetic systems, and so only diamagnetic systems will be considered here. Recent overviews of the calculations on paramagnetic systems can be found in Refs. [30, 83].

2.4.1 Overview of GIPAW calculations

Comprehensive reviews of electronic structure theory applied to molecular organics and the GIPAW method applied to both organic and inorganic systems have been written by Beran[84] and Bonhomme et al.[85] respectively. Useful overviews of quantum-chemical calculations applied to NMR spectroscopy and of DFT methods applied to solid-state can be found in Ref. [86] and Refs. [87-89] respectively, while Facelli has carefully reviewed quantum chemical calculations of chemical shift tensors, including applications[90]. Here we will simply present a digest of the key ideas behind GIPAW calculations.

The typical starting point of electronic structure theory is the non-relativistic Schrödinger equation in the Born-Oppenheimer approximation, where the electronic Hamiltonian is solved for a fixed geometry of the nuclear spins. Breakdown of Born-Oppenheimer approximation and its small, but measurable, effect on NMR parameters is considered in Section 2.5.1. Relativistic effects can mostly be ignored for molecular organics, although contributions to the shielding of light atoms from relativistic Heavy Atom effects on neighbouring Light Atoms (HALA effects) are commonly encountered[85]. For example, changes in ^{13}C shift of about 5.5 ppm were seen for carbon bonded to sulfur[91, 92]. Other examples are discussed in Section 3.4.3.

Wave-function-based methods have the advantage of offering a systematic route to improving the accuracy of solutions of the electronic Hamiltonian. Highly accurate methods, such as Coupled Cluster Theory, however, have an unfortunately poor scaling, between n^6 and n^8 (depending on choice of model), with the number of orbitals considered, n[93]. This renders application to typical molecular solids impractical. Density Functional Theory (DFT) has provided an effective compromise between ultimate accuracy and computational feasibility. The key unknown quantity in DFT calculations is the functional describing exchange correlation. The most widely used functional in GIPAW calculations is that proposed by Perdew, Burke and Ernzerhof (PBE)[94], which is expressed in terms of the local electron density, ρ, and derivatives (gradients) of ρ. This puts it in the category of the generalised gradient approximation (GGA), as opposed to Local Density Approximation (LDA) fiunctionals, which only depend on ρ.

The most natural way to account for the periodicity of crystalline systems is to exploit periodic boundary conditions. While the electron density is simply periodic, $\rho(\mathbf{r} + \mathbf{R}) = \rho(\mathbf{r})$, where $\mathbf{r}$ is a position vector, and $\mathbf{R}$ is any lattice vector describing a translational symmetry, the wavefunction is quasi-periodic

$$\Psi_{\mathbf{k}}(\mathbf{r} + \mathbf{R}) = \exp(i\mathbf{k} \cdot \mathbf{r})\Psi_{\mathbf{k}}(\mathbf{r})$$

where $\mathbf{k}$ is a wave vector. Physical properties are calculated from integrals over the wavefunction, and so need to be integrated over all the unique values of $\mathbf{k}$. The first Brillouin zone in reciprocal space is generally used as this integration range. At least in insulating materials, this integration can be easily performed over a regular grid in k-space[95], and the density of this "Monkhorst-Pack" (MP) sampling grid is one of two criteria against which the numerical accuracy of the calculations can be converged. (Note that the numerical accuracy should not be confused with the much more complex question of

the overall accuracy of the calculations.) As the unit cell size increases, the size of the Brillouin zone decreases, and it is common to find that a single k-point is sufficient for converged results. Note that the so-called Γ point, $\mathbf{k}$ = (0, 0, 0), is particularly unrepresentative and so it is common practice to shift the origin of the grid to $\mathbf{k}$ = (¼, ¼, ¼) in fractional reciprocal space. This so-called "Baldereschi point" is the "most average" point in k-space for a cubic unit cell[96], and this offset ensures that the MP grid samples non-special k-points. (The deleterious consequences of including the Γ point in the k-space averaging can be seen in Fig. 1 of Ref. [97].) The convergence of calculated NMR parameters is rarely discussed explicitly; exceptions include the convergence of ^{13}C shifts in C_{70} to within 0.2 ppm[98].

Although Gaussian-type orbitals (GTOs) can be combined with periodic boundary conditions (e.g. Ref. [99] describes an NMR crystallographic study using the GTO-based CRYSTAL09 code), a natural choice of wavefunction basis set for periodic systems is a plane wave basis:

$$\Psi_{\mathbf{k}}(\mathbf{r}) = \sum_{\mathbf{G}} c_{\mathbf{k}}(\mathbf{G}) \exp(i[\mathbf{k} + \mathbf{G}] \cdot \mathbf{r})$$

where the $\mathbf{G}$ are lattice vectors in reciprocal space, and the $c_{\mathbf{k}}$ are the expansion coefficients to be determined. Large magnitude $\mathbf{G}$ vectors in reciprocal space correspond to shorter wavelengths / higher energies, and so the size of the basis set, $\mathbf{G}$, can be expressed in terms of a cut-off energy, E_{cut}, specifying the maximum kinetic energy of the waves involved. While localised basis sets centred on atoms are not incompatible with periodic boundary conditions (and indeed, some first principles codes use these), the plane wave basis has a number of advantages, and has been used exclusively to implement the GIPAW method. Firstly, different NMR parameters have different dependencies on local vs. long-range environment; for example, the Fermi contact component of J couplings depends on the electronic wavefunction at the nucleus, while other effects, such as aromatic ring currents, involve much larger distance scales. There is the risk that different NMR parameters converge very differently with the size of localised basis sets. In contrast, the sampling of space is much more uniform with plane waves. Secondly, the cut-off energy provides a single simple convergence parameter, which is essentially independent of the convergence with respect to k-space sampling. As time taken by the calculation scales more-than-linearly with E_{cut}[100], this parameter needs to be chosen carefully. Convergence with respect to E_{cut} is determined by the most "difficult" atom, e.g. O and F[101, 102] in the 1st row elements, but otherwise is largely transferrable, i.e. it is sufficient to verify the convergence with respect to E_{cut} on one member of a set of systems with similar elemental composition. Note that the optimal E_{cut} (in terms of trading numerical convergence against time) depends on the calculation; higher E_{cut} values are typically used when calculating NMR parameters vs. geometry optimisation.

A drawback of the plane wave basis is that describing the strongly oscillating electronic wavefunctions close to the nucleus requires unfeasibly high cut-off energies. Instead, smoothly varying "pseudo-potentials" are used to describe the electronic behaviour within a certain radius of the nucleus, with the parameters of the pseudo-potentials tuned to reproduce high-quality all-electron results. Current GIPAW implementations use the "ultra-soft" pseudo-potential scheme devised by Vanderbilt[103, 104]. These smoother pseudo-potentials allow properties to be converged with lower cut-off values. The core region is, of course, critical for a correct description of the NMR parameters, and GIPAW refers to the means of determining properties within the pseudo-potential description in a gauge invariant way[81, 85].

Note that the default pseudo-potentials and their parameters are often updated between code versions, which will have an impact on calculation results. For example, a recent landmark study on the reproducibility of DFT results[105] compared calculated equations of state (calculated energy vs. cell volume) for a reference set of 71 elements between different DFT codes using the PBE functional. The agreement in results between all-electron codes (i.e. without pseudo-potentials) was generally excellent, with the variation being smaller than the uncertainties in experimental results. The variation of the pseudo-potential-based codes was slightly higher, but not significantly different from the more-exact, but more time-consuming, all-electron results. This agreement, however, only applied to recent

pseudo-potentials sets; the agreement was noticeably worse, and occasionally substantially so, when using older code versions (for example, the difference between CASTEP and all-electron predictions dropped by a nearly an order of magnitude using the OTFG9 pseudopotentials introduced in 2015 compared to the Vanderbilt-type ultra-soft potentials used in the 1998 release). Although these were all "best case" calculations, with the calculation settings carefully optimised rather than necessarily using out-the-box settings, this work does provide some confidence that the results from current codes are approaching the intrinsic limits of PBE-based DFT; see Section 4.1.2 for further discussion. It is worth noting in this context, a study in which ^{13}C and ^{1}H shifts were calculated using both CASTEP and Quantum ESPRESSO codes to aid a challenging spectral assignment[106]. Despite using different pseudo-potentials, entirely equivalent results were obtained.

2.4.2 DFT calculations of J couplings

The accurate calculation of J couplings is a considerable challenge, as the overall effects are small and involve multiple, often competing, contributions. Moreover, at least in linear-response codes, such as CASTEP, determining the couplings to a given nucleus involves breaking the local symmetry, and so it may be necessary to perform calculations on supercells of the crystal structure to obtain converged results[107]. Despite these challenges, impressive agreements have been demonstrated in a number of systems, with the most relevant for organic crystals being hydrogen-bond mediated J couplings, such as $^{2h}J_{NN}$ and $^{2h}J_{NO}$ couplings[108]; calculations quantitatively reproduced the expected inverse relationship between ^2J coupling and heavy atom distance. The methodology behind the calculation of J couplings in the GIPAW framework and its applications has been reviewed by Yates[109].

2.4.3 Dispersion-corrected DFT (dc-DFT)

The local nature of conventional GGA-based functionals, such as PBE, means that they do not account for van der Waals / dispersion interactions, which are inherently non-local. It is possible to develop non-local functionals that could account for dispersion interactions, but these are computationally expensive, and most development has involved posthoc "corrections" of DFT calculations based on conventional local functionals, accepting the limitations (argued on the basis of benchmark studies against coupled cluster calculations[110]) of this approach. This area has been comprehensively covered in recent reviews[84, 89] and overview articles[111], and so just a digest is presented here.

Early dispersion correction methods were somewhat empirical, and some intriguing work has shown that significantly improved predictions of NMR parameters can be obtained by optimising one of the key parameters of the D2 semi-empirical dispersion correction (SEDC) scheme[112, 113]. It was argued that better positioning of the atoms with the refined dispersion forces was key to the improved performance, cf. discussion around Figure 10 below. Current SEDC methods have a minimal number of fitted parameters, e.g. the widely used Tkatchenko-Scheffler (TS) scheme[114]. The TS scheme considers pairwise contributions to the dispersion interactions, while more recent approaches, such as MBD (many body dispersion)[115], have sought to include many body terms. A study involving 30 structures of molecular organics obtained at less than 50 K showed that full geometry optimisation with PBE+TS reliably reproduced lattice cell parameters[116]. Better unit cell predictions and better predictions of NMR parameters have been obtained with the TS scheme compared to earlier methods[117].

Given the evolving state-of-the-art, it is useful to consider whether dispersion corrections should be routinely included in calculations. Clearly where crystal geometries are being relaxed (see the following section) without constraints on the lattice cell parameters, dispersion correction is essential, otherwise the absence of van der Waals interactions leads to gross over-estimates of the lattice cell dimensions, and dubious results for physical properties. Similarly, lattice energies will be significantly underestimated without dispersion correction, and comparisons of calculated energies between polymorphs would have limited validity. Note that accuracies of 2–5 kJ mol^{-1} (~5% of the total lattice energy for typical molecular crystals) are currently expected for high-quality dispersion-corrected DFT calculations[84]. The significance of dispersion correction is less obvious for geometry optimisation

with fixed lattice parameters, but the minimal computational cost of most correction schemes suggests that the advantage in terms of overall correctness of the electronic structure probably outweighs the additional complexity.

2.4.4 Geometry optimisation

(a) Optimized X-ray bond lengths—compared to experimental values

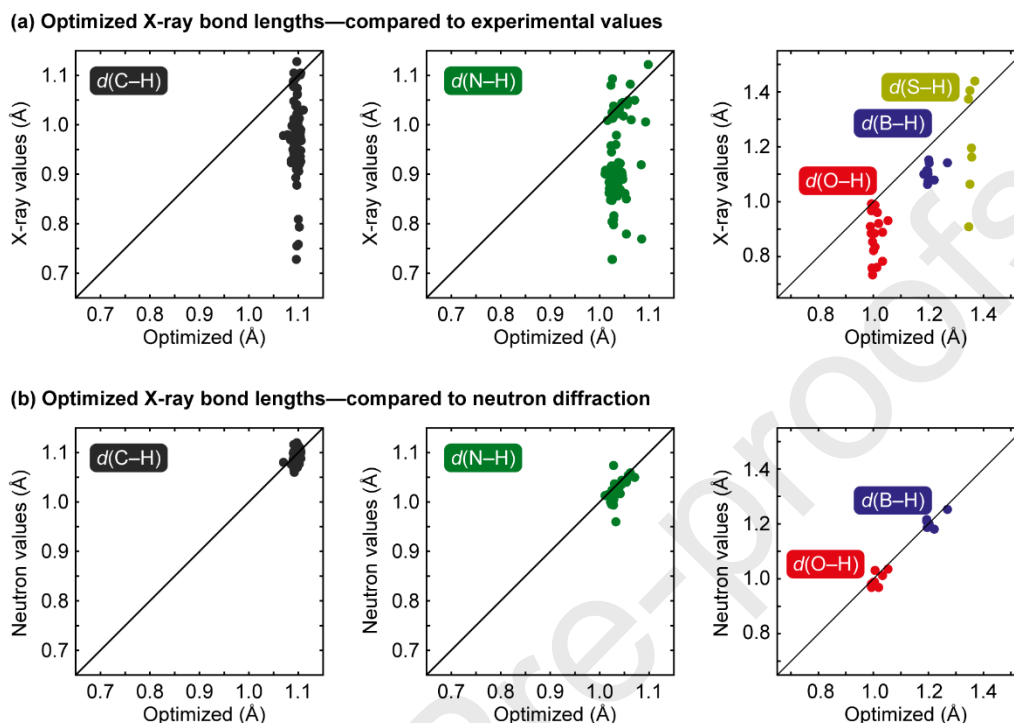**(b) Optimized X-ray bond lengths—compared to neutron diffraction**

Figure 2 Comparisons of experimental bond lengths against values obtained after optimisation of hydrogen positions using PBE-based DFT: (a) X-ray diffraction values vs. optimized lengths, (b) Neutron diffraction values vs. optimized lengths. The different bonds considered are: covalent C–H (left), N–H (middle), O–H, S–H, and B–H (right). Figure reproduced with permission from Ref. 118, copyright 2012 American Chemical Society.

It was quickly appreciated that the extreme sensitivity of NMR parameters to the local electronic structure means that calculations based on atomic positions taken directly from diffraction results are unreliable, and some form of geometry optimisation prior to calculation of NMR parameters is essential. As discussed above, H atoms are particularly poorly localised by X-ray diffraction. This is strikingly illustrated in Figure 2, which shows the effect of optimisation on the positions of 244 hydrogen atom positions derived from X-ray diffraction [118]. Excellent agreement was obtained with neutron data as a result of optimisation, which was clearly superior to standard approaches to correcting hydrogen positions (scaling bond lengths or using "standard" bond lengths). Similar observations have been made in the context of OH bond lengths[119]; in the geometry optimisation of solid isocytosine[120], the range of initial C–H distances (0.94–1.09 Å) was significantly reduced (to 1.08–1.09 Å) on optimisation, while N–H bonds lengthened by 0.06–0.15 Å. The effect of optimisation on ^{15}N shifts in particular was considerable (up to 24 ppm). In other cases, significant movements of atoms during optimisation may indicate problems with the initial structural model, for example, missing hydrogen atoms[54]. Other examples, such as disordered solvent molecules, are highlighted in Section 3.9.

Geometry optimisation involves calculating the forces on the atoms in the current geometry, iteratively adjusting the atomic positions until convergence on a lower energy structure. Its iterative nature means that geometry optimisation is generally the most time-consuming part of a calculation. Simultaneously optimising the unit cell parameters introduces significant additional degrees of freedom and slows down convergence. In some cases, authors have used step-wise geometry

12

optimisation[121, 122], first optimising with a fixed unit cell, then relaxing again without constraints. The focus of these studies was identifying faulty starting structures, and so initial fixing of the unit cell might be a suitable precaution. More generally, however, initial restriction of the degrees of freedom might make it more difficult to find the overall global energetic minimum. In some cases, for example, when comparing predicted NMR spectra for alternative structures obtained by diffraction[123], fixing the non-hydrogen ("heavy") atoms at their diffraction-predicted positions and only relaxing the hydrogen positions is appropriate, since structural relaxation is likely to eliminate the difference between the starting structures. Such "structure validation" is considered in detail in Section 3.6.

In an explicit study of geometry optimisation in the context of NMR crystallography, three model crystal structures derived from powder diffraction data (naphthalene, acetaminophen and adenosine) were optimised prior to calculation of NMR parameters. Judged on the basis of improved agreement with neutron structures, GGAs functionals (PBE and PW91) gave significantly better results than a simple LDA functional, and PBE was used for the remainder of the study[124]. The optimisation improved agreement with experimental ^{13}C tensor data. Although optimisation of hydrogen atoms had the most effect, changes in heavy atom positions (from a full optimisation) further improved agreement with the tensor data. Perhaps counter-intuitively, the movement of hydrogen atoms on optimisation was often greater for structures obtained from SCXRD data compared to PXRD, presumably because the hydrogens in PXRD structures are often positioned at "standard lengths" derived from neutron studies. Optimisation of different starting structures did not always fully converge, for example, methyl groups sometimes optimised to different orientations. In a later study involving a total of 39 ^{15}N shift tensors measured on five compounds[125], GIPAW geometry optimisation reduced the RMSD between experiment and theory from 54 to 7 ppm; the large shift range covered (380 ppm) implied that the ^{15}N tensor values were very sensitive to local geometry. The average movements of atoms on optimisation were approximately an order of magnitude larger than uncertainties on diffraction positions. Note that the tensor components were measured at natural abundance for two of the samples, requiring up to six days of spectrometer time.

In an early study of the effect of geometry optimisation on the accuracy of predicted ^{13}C shift tensors, data from 14 organic single crystal studies were compared with DFT predictions calculated from neutron structures[126]. The good positioning of hydrogen atoms in neutron structures was reflected in the good agreement between calculated and experimental shifts found without refinement, but the RMSDs dropped slightly on optimisation. The largest atomic movements involved lengthening of methyl C–H and hydroxyl O–H, which is suggestive of dynamics. The RMSDs successively reduced when using all six tensor components, the three principal values, and the isotropic shift (e.g. 3.05 ppm vs 1.85 ppm vs 0.89 ppm for aromatic carbons). This will partly reflect cancellation of errors (the isotropic shift being calculated from the average of the three principal components), but will also reflect the differing effects of dynamics on isotropic vs. anisotropic components (see Section 2.5.1). Note that the "icosahedral representation"[127] was used to express the symmetric component of the shielding tensor in terms of six independent components.

The iterative nature of geometry optimisation means that the degree of convergence potentially affects predicted NMR parameters. This has been investigated using a disordered co-crystal system formed between caffeine and citric acid[128], as shown in Figure 3. The convergence parameters for the geometry optimisation needed to be significantly tightened from their default values for the lattice energies of symmetry-related structures to match within about 1 kJ mol^{-1}. Optimisation with a variable cell showed one configuration pair to be the most stable, but the disordered arrangement (corresponding to fixing the cell at measured geometry) will be preferred at ambient temperature on entropic grounds. On the other hand, this had a limited impact on the calculated ^{13}C chemical shifts of symmetry-related sites (the mean difference dropping from just over 0.2 ppm to just over 0.1 ppm). There was no visible impact on the overall RMSD between experimental and calculated shifts, but reducing the uncertainty in calculated shifts due to geometry optimisation convergence may be

13

significant when investigating very small differences in shifts; as noted in Section 2.5.2, calculations can reproduce very subtle effects when comparing sites in similar electronic environments.
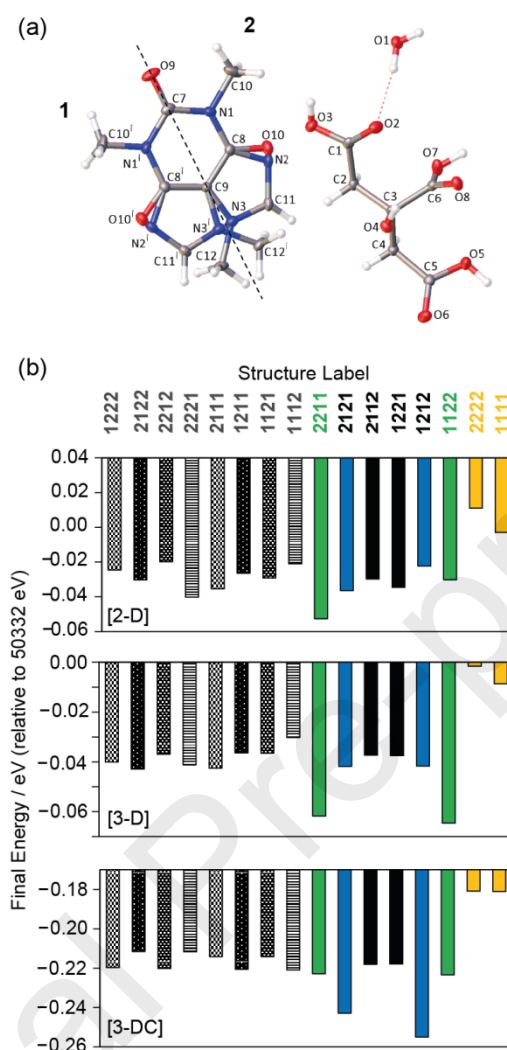

Figure 3 (a) Asymmetric unit of a caffeine citric acid cocrystal in which the caffeine is disordered about a pseudo-rotation axis (dashed line), with the two positions labelled **1** and **2**. The disorder configuration in the full unit cell (*Z* = 4) is denoted **1112** etc. (b) Energies of the 16 configurations after different dc-DFT geometry optimisations. The energies of symmetry-related pairs (indicated by colour and hatching) only agree if tight optimisation parameters are used, [3-D] (fixed cell) and [3-DC] (variable cell) optimisations. Figure adapted from data published in Ref. 128, licensed under CC BY 3.0.

2.4.5 Using DFT-calculated chemical shifts

DFT calculations in molecular systems have been most widely used to predict isotropic ^{13}C and ^{1}H chemical shifts. First principles calculations always provide shieldings (more specifically full shielding tensors), and so an initial question is the referencing needed to relate shielding values, σ, to experimental chemical shifts, δ, i.e.

$$\delta_{iso} = \frac{\sigma_{ref} - \sigma_{iso}}{1 - \sigma_{ref}}$$

where σ_{ref} is the shielding of a reference compound. Since we are not dealing with heavy elements, the shielding values are in ppm, and it is safe to simplify this to $\delta_{iso} = \sigma_{ref} - \sigma_{iso}$. Different approaches to referencing in solid-state NMR[100] and solution-state NMR[129] have been discussed previously, and are summarised briefly here. Rather than use some form of absolute referencing with respect to

a calculated reference shielding of, say, the carbonyl signal of α-glycine (using the same calculation settings), it is generally preferable to establish the shielding scale directly against experimental results to maximise cancellation of errors. For example, if calculating a set of shielding values for aliphatic sp^3 carbons, referencing against an sp^2 carbonyl shift is likely to introduce additional uncertainty associated with the systematic limitations of DFT (see Section 2.5.2). A common practice when making qualitative comparisons is to establish the reference from the average of calculated shieldings and experimental shifts, i.e. $\sigma_{ref} = \langle \sigma_{iso} \rangle + \langle \delta_{iso} \rangle$. Spectra do, of course, need to be at least partially assigned in order perform regression; a useful strategy when working with a set of related compounds is to establish the referencing using a subset of well-resolved spectra[130].

In practice, the slope of plots of calculated isotropic shieldings vs. experimental shifts often deviates from –1 (as discussed further in Section 2.5.2). Hence it may be necessary, particularly when trying to quantitate the agreement between calculation and experiment, to rescale the calculated shieldings via linear regression, i.e. fitting the points, i, to $\delta_{expt,i} = \sigma_{ref} - m\sigma_{calc,i}$. Having fitted the reference shielding, σ_{ref}, and slope, m, the shieldings can be converted to predicted shifts, $\delta_{calc,i}$. The limited shift range for ^{1}H means that m is generally not different from –1 outside its standard error, and so it is more reasonable to use $\sigma_{ref} = \langle \sigma_{iso} \rangle + \langle \delta_{iso} \rangle$. The overall agreement between calculated and experimental shifts is then typically expressed as a root-mean-square deviation (RMSD):

$$\text{RMSD} = \sqrt{\frac{1}{N} \sum_{i}^{N} (\delta_{expt,i} - \delta_{calc,i})^2}$$

where N is the number of data points. It could be argued on statistical grounds that the denominator above should be N–2 or N–1 (depending on whether m is a fitted parameter or not), but the RMSD should probably be regarded as a pragmatic measure of the deviation between experiment and calculation, rather than a strict standard deviation of residuals between experiment and calculation. Note that the distribution of residuals between calculated and experimental shift values has been described as "somewhat Gaussian"[131] (based on the fractions of values within one and two standard deviations), but a greater number of outliers than expected from a normal distribution was also noted using the same data set[132]. Some literature uses the "standard deviation", which is ambiguous (the usual sample standard deviation would use a denominator of N–1), while other literature uses the term RMSD, but with a denominator of N–2; these differences will be minor for a statistically significant number of data points (say >5). Some literature uses the mean absolute error, $\text{MAE} = \sum_{i} \left| \delta_{expt,i} - \delta_{calc,i} \right| / N$, which is a reasonable alternative. On the other hand, "correlation coefficients" are less useful since their values depend strongly on the range of chemical shifts as well as the discrepancies (a widely dispersed shift range will automatically give a better correlation coefficient).

The RMSD quantifies the agreement of a calculation result with experiment, but does not, of itself, provide a probability that the experimental and calculated results are in agreement. In one approach to attaching greater statistical significance to RMSD values, GIPAW calculations of a reference set of 15 organic structures were used to determine typical ranges for isotropic shift RMSDs[133], 0.33 ± 0.16 ppm for ^{1}H, and 1.9 ± 0.4 ppm for ^{13}C. These ranges are stated elsewhere to be expressed as ± one standard error[134], which means these should not be treated as absolute limits, particularly as a different set of reference compounds and different calculations (e.g. improved pseudo-potentials, as discussed in Section 2.5.2) will give different ranges. Similar ranges are quoted elsewhere e.g. 2.2 ± 0.5 ppm for ^{13}C[135]. Note that it is common practice to exclude data from atoms bound to heavy atoms since these are indirectly, but measurably, influenced by relativistic effects, see e.g. Ref. [136]. Reduced χ^2 statistics have been used to give more quantitative measures of agreement between experiment and calculation, although the systematic nature of the deviations between experiment and DFT results means that such analyses need to be used carefully.
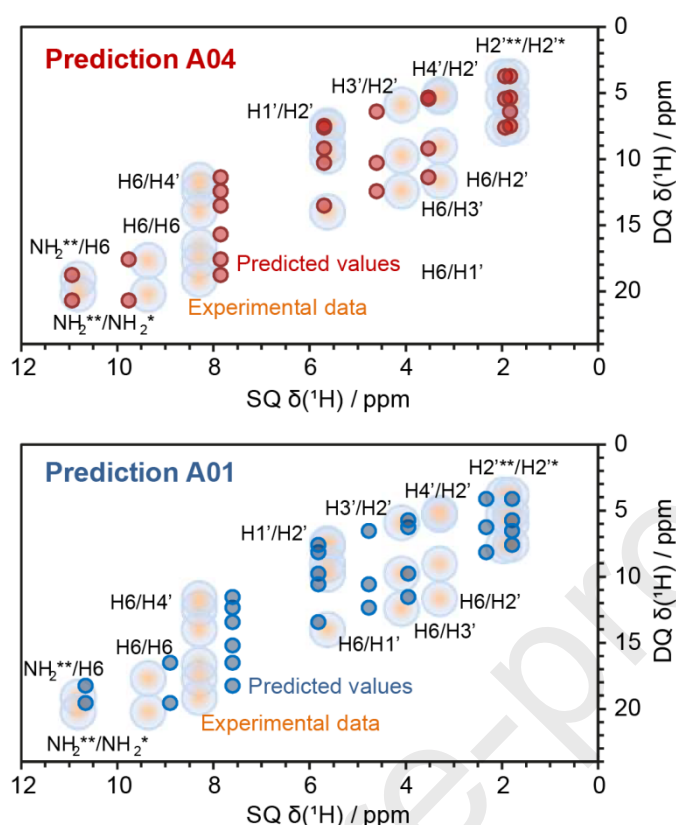
Figure 4. Schematic visualization of the agreement between experimental ^{1}H SQ/DQ correlation experiments and shifts calculated from two model structures obtained from a crystal structure prediction. The overall agreement is seen to be better for model A04. Figure reprinted with permission of the authors from Ref. 170.

Goodness-of-fit statistics for comparisons involving more than one calculated parameter are more difficult, as there is the question of the "weighting" given to the different parameters. In one of the few literature examples, a χ^2 statistic combined ^{17}O isotropic shift and quadrupole coupling parameters, with the scaling provided by the *experimental* uncertainties[137]. This is not a general approach since the experimental uncertainties on, say, ^{13}C isotropic shifts are much less than the accuracy of the calculations. On the other hand, minimising the distance between experimental and predicted cross-peaks on a 2D plot (which is equivalent to this measure, but with scaling factors effectively determined by the aspect ratio of the plot), is a widely used pragmatic, and visually intuitive, solution. Simply plotting predicted cross-peak positions over the experimental spectrum, as illustrated in Figure 4, is particularly relevant when spectral features are incompletely resolved. One metric that has been proposed is the covariance of the deviations between the pairs of calculated vs. experimental parameters[138]:

$$\rho_{XY} = \frac{1}{N}\sum_i^N \left(d_i^X - \left\langle d_i^X \right\rangle \right)\left(d_i^Y - \left\langle d_i^Y \right\rangle \right)$$

where d_i^J is the i'th deviation between calculated and experimental results for parameter J, and $\langle \ \rangle$ is a mean deviation (which will be zero if the experimental and calculated values have been regressed against each other). Note this differs slightly from the parameter originally proposed[139]. These parameters should be zero for a large enough number of uncorrelated deviations. The convergence behaviour is, however, poor (e.g. pairs of values can make equal and opposite contributions) and it was necessary to also consider the individual RMSDs for parameters *X* and *Y* when using this metric to distinguish between different assignments[138].

2.4.6 Tools for working with DFT-calculated NMR parameters

A powerful feature of quantum chemical calculations of NMR parameters is that they provide full interaction tensors. While it is possible to measure the principal components experimentally of most chemical shift and quadrupolar coupling tensors, it is not possible to determine the absolute orientation of tensors (i.e. with respect to crystal axes) from experiments involving powder samples. Being able to efficiently calculate and visualise full interaction tensors is therefore very helpful. A number of software tools are available for visualising NMR tensors, see citations in Refs. [140, 141]. Here we highlight some tools which are particularly relevant for NMR crystallography.

Typically, the results of quantum chemical calculations are written out in lengthy text files without strictly defined formats, meaning that tools to parse them are at the mercy of format changes. The magres file format[140] is an easily parsed and well-defined format for storing the results of magnetic resonance calculations, which is suited to archiving and as input to different computational tools. The format has been adopted by the two major codes that implement the GIPAW method, CASTEP[82] and Quantum ESPRESSO[142]. MagresView[140] provides a web browser-based interface[1] for visualising the contents of a magres file and for exporting into different formats. TensorView[141] is a Mathematica-based tool that provides a more programmatic approach to visualising and manipulating NMR tensors. Notably tensors can be displayed in an "ovaloid" form[143], which is a more correct means of representing tensors with a non-zero trace, such as chemical shift / shielding tensors, than the traditional "ellipsoid" form.

Programmatic tools for manipulating calculation results are desirable when dealing with large quantities of data and/or automating workflows. In particular, many scientific tools currently provide interfaces for the Python programming language, such as PyCIFRW[144] for reading / writing Crystallographic Information Files (CIFs), MagresPython[140] for working with magres files, and the application programming interface (API) for working with the Cambridge Structural Database[145]. Current versions of CASTEP allow atomic sites to be associated with user-defined labels, which simplifies the task of keeping calculation results associated with specific crystallographic sites; since each crystallographic site in a CIF file is guaranteed to have a distinct label, automated workflows can be developed that produce predicted spectra with resonances associated with corresponding crystallographic sites. It is also worth noting more comprehensive Python-based frameworks for setting up, running, and analysing calculations, such as the Atomic Simulation Environment[146].

2.5 The reliability of computed NMR parameters

The robustness of DFT-calculated results clearly needs to be understood before relying on them. The two largest sources of discrepancy between computed NMR parameters and experimental results are expected to be the effects of temperature / thermal motion, and the systematic limitations of the calculations themselves.

2.5.1 The effects of temperature on comparisons between calculation and experiment

In many ways it is surprising that NMR crystallography based on calculated chemical shifts has been successful, since it typically involves comparing NMR parameters derived from experiments at ambient temperature, with DFT calculations performed without considering temperature (i.e. 0 K calculations) based on atomic co-ordinates obtained from diffraction, typically at 100–120 K. Various studies, however, have demonstrated that temperature has a relatively limited effect, at least on

—————
[1] URL: h

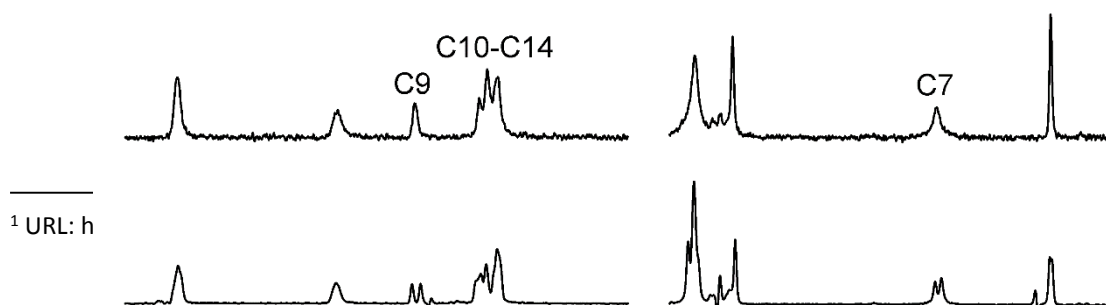Figure 5. ^{13}C CP/MAS spectra of the dioxane solvate of phenobarbital at (top) ambient temperature and (bottom) −80 °C. The labelled resonances indicate a change in *Z′* from 1 to 2 at lower temperature. Figure adapted with permission from Ref. 70, copyright 2014 American Chemical Society.

isotropic chemical shifts, with obvious exceptions, such as illustrated in Figure 5, where there is a phase change between NMR and XRD measurement temperatures.

This topic is subtle since there are a number of interacting effects as well as different levels of approximation in the methods used to assess the effects of temperature; a useful overview of incorporating finite temperature effects in calculations can be found in Ref. [147]. The conceptually simplest approach is to use molecular dynamics (MD) simulations to model the behaviour of the atoms at finite temperature, calculating NMR parameters at regular "snapshots" of the simulation and averaging the tensors[148, 149]. Although, in DFT-based MD, the forces are being calculated from first principles, and anharmonic effects are automatically included, the vibrational motion is being treated classically, which is only appropriate for relatively low frequency vibrations (energies much less than $k_B T$, 207 cm^{-1} at 298 K), such as lattice modes. Localised vibrational modes, such as C–H stretching, will be in the ground state at 298 K, although zero-point "motion" will still be present. Another drawback of MD methods based on snapshots is relatively poor convergence; the expense of using *ab initio* forces means that simulated times run to a few fs, limiting the quality of sampling of the dynamics, particularly for slower processes. Perhaps as a consequence, some researchers have found no systematic improvement when using such techniques[150]. Robinson and Haynes[151] developed complementary approaches for improving dynamical averaging; using Langevin dynamics to sample the configurational space while avoiding correlations caused by sampling too rapidly, plus creating a custom force-field for classical atomistic MD based on fitting the behaviour under DFT MD. Using a standard atomistic force field (GAFF) to generate configurations gave poor results for the predicted vibrational corrections to the chemical shifts of L-alanine, while the DFT-derived custom force field gave equivalent results to DFT-MD. Although the vibrational corrections reduced the deviations between calculated and experimental chemical shifts, the limited number of data points makes it difficult to judge the generality of these computationally expensive approaches. In a study using five solid forms used for chemical shift calibration, including adamantane[152], vibrational corrections to chemical shifts allowed the set of 14 ^{13}C chemical shifts to be fitted to experimental values with an excellent RMSD (2.0 ppm) while using a single reference shift. MD simulations were run on a supercell to reproduce the dynamics of adamantane. This would be too large for *ab initio* DFT, and so snapshots for NMR calculations were derived from a separate simulation on a single unit cell, but which used the average lattice parameters observed in the supercell simulation. In follow-up work, "tailor-made" force fields derived using an automated method from dc-DFT calculations[153] were used to determine vibrational corrections for structures of cocaine generated by crystal structure prediction (see Section 3.8), and to assess whether this provided better discrimination between correct and incorrect structures[154]. While the DFT-derived force fields resulted in objectively more realistic behaviour in MD simulations than the default force field (COMPASS), the vibrational corrections did not significantly improve discrimination.

An alternative to MD-based methods is to calculate vibrational frequencies and vibrational modes (i.e. evaluate the phonon spectrum) and determine the probability distributions for the amplitude of the different modes at a given temperature (treating each mode independently and within the simple harmonic approximation). Average properties can then be calculated by Monte Carlo (MC) sampling using these distributions[149]. The probability distributions can be calculated for the quantised simple harmonic oscillator, and hence including the effects of zero-point motion, but again the precision of results is determined by the degree of MC sampling. Further references on vibrational corrections of calculated parameters can be found in Refs. [155] and [156].

These two methods have been compared for calculating motionally averaged shielding tensors in small peptides[149]. They gave similar results in terms of the effect on the isotropic shielding; indeed, there was no significant difference between the thermal correction within the harmonic approximation when evaluated at $T = 0$ (i.e. zero-point motion only) and $T = 293$ K. This presumably reflects the small size of the effects and the relatively large "error bars" associated with Monte Carlo sampling using just 64 points. Significantly, the effects of thermal motion on isotropic shifts were

largely systematic, and largely led to changes in the fitted referencing value, σ_{ref}, rather than changing the relative values of shieldings. In contrast, a clear effect of temperature was observed on ^{13}C shielding anisotropies, with vibrational averaging reducing anisotropies by about 15%, significantly improving agreement with experimental values for L-alanine. This study also examined the effect of thermal expansion on the calculated shieldings. The initial 60 K neutron structure of L-alanine was relaxed with unit cell parameters fixed at experimental lattice parameters measured at 120, 220 and 300 K, and the shielding tensors calculated. The changes in isotropic shielding (of the order of ±0.2 ppm for ^{13}C) were significantly smaller than those directly due to thermal motion. In contrast, anisotropic thermal expansion has a major effect on diffraction results, making it difficult to compare PXRD patterns obtained at very different temperatures[157].

In a study of the effects of thermal motion on ^{13}C shift tensors of the phenyl resonances of solid ibuprofen[158], experimental measurements of the principal components at ambient temperature were compared to values calculated from DFT calculation and a motional model involving ring libration and bending of the C–H bonds. After fitting the vibrational effects, the RMSD between corrected and DFT-predicted values was reduced to about 3 ppm (compared to nearly 20 ppm for the δ_{11} component initially). In follow-up work, the temperature dependence of the aromatic chemical shift tensor principal components was measured down to 129 K[159], and the values fitted to a simpler model of ring libration and in-place C–H bending with a linear dependence of motional amplitude on temperature. The fitted root-mean-square amplitudes of the motions at 295 K (16° for ring libration and 14° for C–H bending) are in line with other studies discussed here. In other work, GIPAW calculations on snapshots of DFT-MD simulations of a tripeptide reduced the RMSD between calculated and experimental ^{13}C shifts from 4.2 to 3.3 ppm[160]. It was necessary, however, to use classical MD simulations to determine the common sidechain conformations, and perform vibrational averaging on each of the ten resulting conformations. The difficulty of sampling the conformations of alkyl chains, possibly compounded by referencing issues, may explain the modest size of the improvement, and the atypically large final RMSD values.

Table 1. [17]O quadrupolar couplings (in MHz) calculated on static structures and with the inclusion of dynamics, average re-orientation angle β of the EFG tensor, and experimental couplings.

Compound	O site	CSD	CSD+MD	β / °	Exp[b]
Glycine HCl	O1	8.53	8.38	6	8.40 ±0.05
	O2	−7.69	−7.51	6	7.60 ± 0.05
Valine HCl	O1	8.59	8.41	7	8.40 ± 0.05
	O2	−7.60	−7.45	6	7.35 ± 0.05
Phenylalanine HCl	O1	8.62	8.65	7	8.54 ± 0.05
	O2	−7.79	−7.56	7	7.46 ± 0.05
Tyrosine HCl	O1	8.40	8.38	10	8.22 ± 0.05
	O2	−7.37	−7.31	10	7.35 ± 0.05
	O3	8.82	−8.72	7	8.56 ± 0.05
Glutamic acid HCl[a]	O1	−7.41	−7.33	7	7.45 ± 0.05
	O2	8.40	8.40	7	8.16 ± 0.05
	O3	8.62	8.44	7	8.31 ± 0.05
	O4	−7.86	−7.64	7	7.49 ± 0.05
Alanine	O1	8.32	8.19	6	7.86 ± 0.1
	O2	6.81	6.83	8	6.53 ± 0.1
Cytosine	O1	7.72	7.68	6	7.20 ± 0.05
Thymine	O2	6.96	6.88	15	6.65 ± 0.05
	O4	9.08	8.39	6	8.40 ± 0.05

[a] Calculated for LGLUTA structure from the Cambridge Structural Database (CSD) with optimised position of O4-H hydrogen atom.
[b] See Ref. [148] for sources of experimental data.

These results are consistent with a DFT-MD study of the effects of thermal motion at 300 K on NMR

tensors using a set of nine reference compounds[148]. Fluctuations of the chemical shift and electric

field gradient tensor orientations (measured as the average deviation of the principal axis) were of the

order of 5–15°. This reorientation automatically leads to a net reduction in the tensor anisotropies,

and significant improvements in agreement of calculated ^{17}O quadrupolar parameters with

experiment, as shown in Table 1; note how initially poor agreement in the case of glutamic acid

highlighted a poorly placed hydrogen. As observed for other interactions, the degree of averaging of

the tensors was not consistent between sites, i.e. a single scaling factor to correct anisotropies for

thermal motion would be a crude approximation. Another significant aspect of this study concerned

the effect of thermal motion on the structure observed by diffraction. As discussed in Section 2.1, the

result of conventional diffraction is a set of atomic positions, **r**, plus associated anisotropic

displacement parameters (ADPs), giving the impression that the only effect of increasing temperature

is to enlarge the ADP ellipsoid. This would only be true, however, if each atomic site were vibrating

harmonically about its 0 K position, which is not generally true for molecular materials; anharmonic

motion means that interatomic distances measured on the average structure reported by diffraction,

$\left| \langle \mathbf{r}_A \rangle - \langle \mathbf{r}_B \rangle \right|$, are not the same as the average $\mathbf{r}_{AB}$ bond length, $\langle \left| \mathbf{r}_A - \mathbf{r}_B \right| \rangle$ (where $\left| \mathbf{r} \right|$ represents the length of vector $\mathbf{r}$ and $\langle \ \rangle$ the time average over thermal motion). Although thermal ellipsoids (ADPs) are typically envisaged as independent "uncertainties" in atomic positions, the thermal motions at adjacent sites are highly correlated due to bonding. Unless some form of vibrational correction has
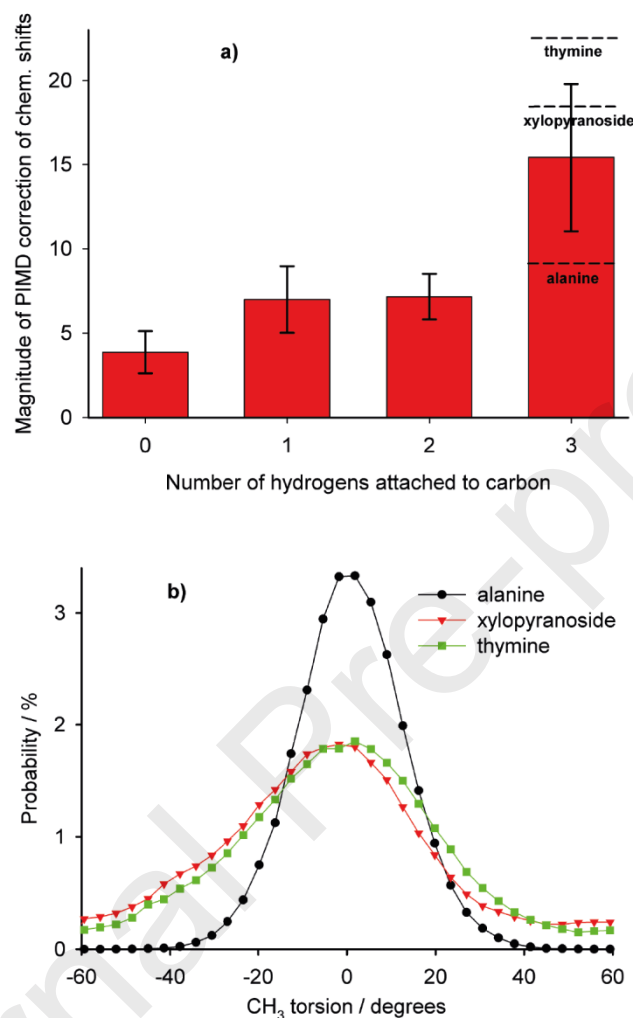

Figure 6. Effects of nuclear delocalisation on NMR parameters obtained from path integral MD calculations. (a) Dependence of the PIMD corrections of the isotropic ^{13}C chemical shift on the number of attached hydrogen atoms. Dashed lines indicate individual PIMD-induced shifts for methyl groups. "Error bars" indicate one standard deviation. (b) Probability distribution of CH_3 torsions relative to equilibrium geometry for the methyl-containing systems. Figure reproduced with permission from Ref. 166 © 2014 Wiley-VCH Verlag GmbH & Co. KGaA, Weinheim.

been applied, interatomic distances in diffraction-derived structures tend to *decrease* monotonically with increasing temperature, and so apparent bond lengths measured from room temperature structures have significant systematic errors[161]. In the above DFT-MD study, thermal motion was shown to have measurable effects on chemical shifts calculated from a neutron structure obtained at 301 K. DFT optimisation of the 301 K structure allowed bond distances to relax to values close to those in an XRD structure obtained at 23 K. Analogous observations have been made when geometry optimising H positions for 24 neutron structures[162]; in particular DFT optimisation significantly lengthened apparent C–H distances in methyl groups (where significant libration-type motions are expected) towards more typical C–H bond lengths. These results suggest that geometry optimisation of all the atomic positions (not just H) is advisable when structures have been obtained at higher temperatures.

36

The convergence properties of sampling-based methods discussed above significantly limit their precision. Arguably the most precise predictions of thermal effects on isotropic shifts have come from a "functional" analysis of trajectories from Path Integral Molecular Dynamics (PIMD) simulations[155]. Path integral (PI) methods allow full quantum mechanical behaviour to be incorporated into MD simulations. Although still using the Born-Oppenheimer approach of separating nuclear and electronic coordinates, the PI method combines multiple copies (replicas) of an MD simulation into a model that increasingly approximates to a fully quantum treatment as the number of replicas increases. By allowing the nuclear positions to behave quantum mechanically, effects such as nuclear delocalisation and tunnelling can be described. These effects are particularly significant for light nuclei, such as H, and in turn have measurable effects on chemical shifts. PI methods are computationally very expensive; a PIMD simulation using 16 replicas, for example, is the equivalent of running 16 DFT-MD simulations in parallel. Although there is great interest in developing more efficient ways to incorporate nuclear quantum effects, e.g. Refs. [163-165], PIMD has the merit of being implemented in the CASTEP code, allowing the effects on NMR parameters to be directly studied. In this study, rather than sample the PIMD simulation directly, the dependence of the nuclear shielding on a set of geometrical parameters of glycine was calculated and the dependencies fitted to quadratic functions. Distribution functions for the various distances and bond angles were determined from the PIMD simulation and "convoluted" with the parameterised shielding dependencies. The predicted changes in chemical shift with temperature were in good agreement with experiment, particularly given the size of the changes (~0.2 ppm for ^{13}C, ~0.5 ppm for ^{15}N). Striking agreement was also found for the ^{2}H C_Q of the strongly hydrogen-bonded H in 2-nitromalonamide, which, unusually, is observed to increase with temperature. The PIMD calculations successfully predicted the sign and magnitude of the thermal effect.

More than one study[149, 166] has noted a tendency for the ^{13}C chemical shifts of alkyl carbons (CH$_2$ of glycine) to increase due to thermal motion relative to those of sites with high chemical shift, such as the C=O of glycine. This will lead to slight, but observable, changes to the gradient of a referencing plot of calculated shielding vs. experimental shift. This is consistent with changes in shift values associated with motion calculated from PIMD simulation[166], as illustrated in Figure 6. These calculated effects vary with the number of attached hydrogen atoms, and were particularly large, and variable, for methyl carbons (up to 23 ppm!). The correction factors were very small for ^{1}H, except for methyl groups where large quantum effects were again observed (maximum change 2.8 ppm). Methyl groups aside, including the PIMD corrections did not improve the overall agreement with ^{13}C experimental shifts due to the error bars associated with sampling.

A similar observation was made in a study of more efficient approaches to incorporating vibrational averaging [167]; a fairly modest improvement in the RMSD (from 3.5 to 2.5 ppm) between experiment and calculation was observed for ^{13}C shifts of a crystalline dipeptide at 293 K. The improvement was much more marked for ^{1}H, with the RMSD dropping from 0.49 to 0.21 ppm when vibrational effects are included. Note that anharmonic effects had a negligible effect, whereas shift corrections due to zero-point motion (i.e. nuclear delocalisation) were relatively large (up to ~−1.0 ppm for ^{1}H), contributing a major fraction of the vibrational correction at temperatures between 0 K and ambient. Interestingly similar estimates (of 30–60%) have been made for the fractional contribution of zero-point motion on expansion coefficients[147]. Although the corrections due to motion were relatively modest for ^{13}C shift anisotropies (up to −6 ppm at 200 K), the effects on ^{15}N and ^{17}O were surprisingly large and variable (between ~0 and −80 ppm), implying that quantitative comparison between experimental and calculated CSAs would be difficult without accounting for finite temperature effects.

Depending on the potential energy curve for the hydrogen bond, ^{1}H shifts for hydrogen-bonded hydrogens are often significantly temperature dependent. For example, in a study of β-maltose, the OH shifts varied monotonically with temperature[168], and linear extrapolation of these shift values down to 0 K provided improved agreement with the GIPAW calculations. Hence OH and NH protons

are sometimes excluded from shift vs. shielding regression plots in order to obtain satisfactory RMSDs[169, 170]. Ref. [118] also discusses the effects of temperature on OH and NH bond lengths.

Although there is continued interest in developing efficient ways to account for vibrational effects on NMR and other physical properties[156], the overall conclusion is that NMR parameters, and isotropic chemical shifts in particular, are remarkably robust with respect to thermal motions. Moreover, linear regression of experimental shifts and calculated shieldings will remove most of the effects, both through the referencing value, and the fitted gradient. Although deviations of the fitted gradient from −1 are generally assumed to reflect systematic errors in DFT, the contribution of finite temperature and nuclear delocalisation effects is probably significant. How to address this issue will depend whether the goal is accurate referencing or "fitting out" the limitations of 0 K DFT calculations. Analogous recommendations on using scaling to correct for both rovibrational and DFT errors have been made for calculations of solution-state NMR parameters[129].

2.5.2 Limitations of current DFT functionals

As discussed in Section 2.4, Density Functional Theory has proved a highly successful compromise between accuracy and computational practicality. Inevitably, however, there are circumstances in which this compromise is a limiting factor.

One important problem area for DFT is the description of hydrogen bonding. The conclusion of a recent survey of the ability of DFT to reproduce reference interaction energies (from coupled cluster calculations) for sets of molecular pairs interacting via hydrogen bonds was that DFT had some way to go[171]. Notably PBE was amongst the poorer performers, as has been previously observed[172]. Including dispersion correction (D2 and D3 methods) further worsened agreement, highlighting that improved ability to predict long-range interactions may come at the expense of describing short-range interactions. In a study of 30 molecular organic structures, GGA-based functionals consistently predicted N−H and O−H distances in hydrogen bonds to be at least 2 pm longer than observed experimentally[116]. The description of short, strong hydrogen bonds is expected to be particularly challenging, since such bonds often exhibit temperature-dependent proton migration, implying that the balance between the hydrogen lying on the donor vs acceptor side is very subtle. The consequences of poor description of hydrogen bonding are illustrated in Figure 7, where a PBE-based optimisation leads to incorrect predictions[173]. Other examples of this behaviour include Ref. [130]. Hence significant movements of hydrogens in H-bonds should be viewed with suspicion. Other researchers have encountered significant discrepancies for ^{15}N and ^{1}H chemicals shifts (deviations of ~10 ppm for N) for sites involved in hydrogen bonding[174], or poor correlations between calculated and experimental shifts for OH and NH hydrogens[169]. It is important to note, however, that valuable information can be obtained about hydrogen bonding from DFT calculations, despite these caveats. In other cases, for example, DFT geometry optimisation correctly re-positions hydrogen-bonded hydrogens that have been misplaced, as in the structure of flurbiprofen (CSD refcode FLUBIP)[175]. These limitations are not restricted to hydrogen bonding. For example, the carbon shift in a C≡N was found to be overestimated as a result of geometry optimisation, due to PBE-DFT over-estimating the C≡N bond length by ~0.03 Å[176].
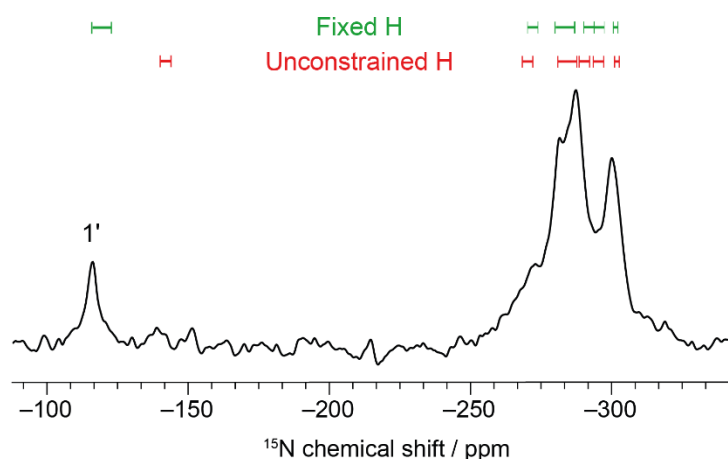
Figure 7 ^{15}N CP/M...).64 MHz. Overlaid are the calculated ^{15}N ... top, green) where the hydrogen-bonded H has been restrained during optimisation. Without the constraint, the H moves across the O−H…N hydrogen bond, leading to a clearly incorrect predicted shift for the associated nitrogen (1'). Figure adapted from Ref. 173, licensed under CC BY 3.0.

The systematic limitations of DFT have been recently explored using bench-marking studies,

comparing different functionals and alternative fragment-based approaches to calculating solid-state

shifts[131]. These methods are carefully explained by Beran[84], and will not be discussed in detail here, beyond remarking that they are significantly more sophisticated than previous "cluster-based" approaches to calculating shifts in the solid state. Because the fragment-based methods typically use localised Gaussian-type orbitals, it is practical to use "hybrid" functionals; hybrid functionals in combination with plane-wave bases are prohibitively computationally expensive. Benchmark data sets of ^{1}H, ^{13}C, ^{15}N and [17]O isotropic chemical shifts were established from unambiguously assigned literature data (plus some additional ^{15}N experimental results) and the quality of agreement assessed using RMS deviations from linear regression of experimental shift vs. calculated shielding. Puzzlingly, fragment-based methods consistently give lower RMS errors for [1]H (~0.34 ppm), even when comparing fragment+PBE calculations to GIPAW+PBE (0.43 ppm); very similar results were obtained were obtained using PBE with either fragment or GIPAW methods for other nuclei. For nuclei other than ^{1}H, significantly improved agreements were found using the hybrid functionals B3LYP[177] and PBE0[178], e.g. RMS errors of ~1.5 ppm for ^{13}C compared to 2.2 ppm for GIPAW+PBE. This was consistent with a previous bench-marking study of ^{13}C shifts[179]. These benchmarking results show that the dominant source of uncertainty is the DFT functional (note that the same GIPAW+PBE-optimised structures were used as input for all calculations, ruling out geometry optimisation as a factor). In contrast, the performance of the fragment-based methods was consistently poorer for [17]O shifts compared to GIPAW (e.g. RMSD of 9.8 ppm for fragment+PBE0 compared to 7.2 ppm for GIPAW+PBE). This was ascribed to a greater importance of many-body effects for oxygen shieldings. It was argued that these data sets provided robust experiment vs. calculation regression data for referencing purposes. It is worth noting, however, some features of experimental studies on a set of histidine-based salts in the same paper using this referencing. In particular, the RMS errors for ^{15}N were much larger than observed in the test set (6.9 vs 4.2 ppm), and the relative order of the ^{15}N shifts for one of the molecules was consistently mispredicted. This was traced to the particular N environment (hydrogen-bonded sp^2 N) having larger discrepancies from the regression fit. This highlights the difficulty of establishing shift calibrations based on a set of compounds; the systematic rather than random nature of the discrepancies means that the appropriateness of the calibration set will vary depending on the balance of different chemical functionalities present. In some cases, different regressions have been used for different chemical functionalities, e.g. for sp^2 vs. sp^3
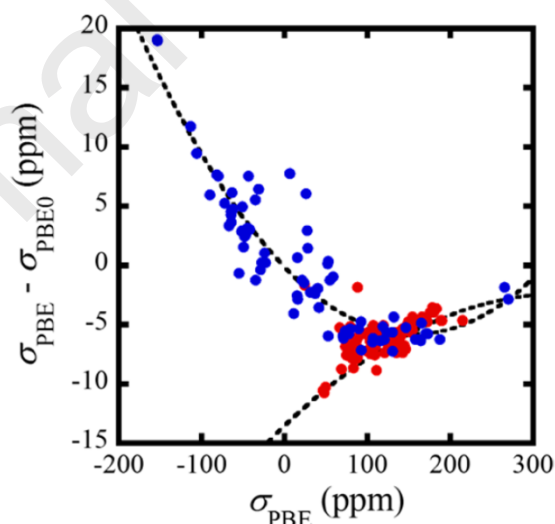
Figure 8 Difference between PBE- and PBE0-calculated ^{13}C principal shielding values for sp^3-hybridized (red points, lower curve) and sp^2- and sp-hybridized (blue points, upper curve) sites in a set of 72 crystal structures. The trend lines are guides for the eye. Figure reprinted with permission from Ref. 182, copyright 2015 American Chemical Society.

hybridised carbons[180], and aromatic vs. carbohydrate (sp^3) carbons[126]. Benchmarking work on NMR shifts relevant to inorganic systems has similarly highlighted the limitations of GGA-based functionals[181].

Dybowski and co-workers have developed sophisticated cluster-based methods (distinct from the "fragment" methods above). The clusters are sufficiently large that the environment around the central molecule has the same symmetry as the crystal, excluding translation (typically involving 11 molecules). Initial work showed that these provided robust predictions of ^{13}C tensor principal values[162]. Follow-up work used these methods to assess performance of different functionals[182]. Hybrid and so-called "meta GGA" functionals (which go beyond GGAs in incorporating higher derivatives of electron density) performed better for ^{13}C than did PBE, although the RMSDs were generally quite large (5.0 ppm for PBE), suggesting that there is a significant contribution from experimental uncertainties and motional effects on the principal values. Statistical analysis showed that sp^2 vs sp^3 predictions fell into distinct sub-populations, as illustrated in Figure 8, which shows distinct trends in the differences between PBE and PBE0 values for the different carbon types. In contrast, no sub-populations were observed in the results from PBE0, a hybrid functional. For ^{15}N, the best performance was for meta GGAs, while hybrid functionals performed the worst. In particular, the meta GGA improved results from highly correlated systems, e.g. in N=N double bonds. The agreement between calculated and experimental ^{15}N tensor principal values has recently been re-considered[183]. While the literature values of RMSDs (typically exceeding 10 ppm) appear high, this should be weighed against the large shift range (~1000 ppm) for nitrogen. Significantly lower RMSDs (about 5 ppm) were found when considering up a subset of environments, specifically nitrogen in amide sites, with modest improvements found over GIPAW when using PBE0 and cluster/fragment-based methods.

In the previous benchmarking study[182], hybrid functionals give a shift/shielding fitting gradient for ^{19}F that was significantly closer to the expected −1. A follow-up study[184] showed that increasing the fraction of Hartree-Fock exchange to 50% (compared to 25% in PBE0) further improved the regression slope, although the RMSDs (not calculated) did not seem to significantly improve. This is consistent with the idea the systematic limitations of DFT are often due to "self-interaction / delocalisation" errors[84] associated with the exchange energy correlation functional, which are reduced by decreasing the contribution of the PBE functional. The impact of these systematic errors varies from element to element, with O and F appearing to be particularly "exposed", in contrast to C and H where PBE generally performs very well.
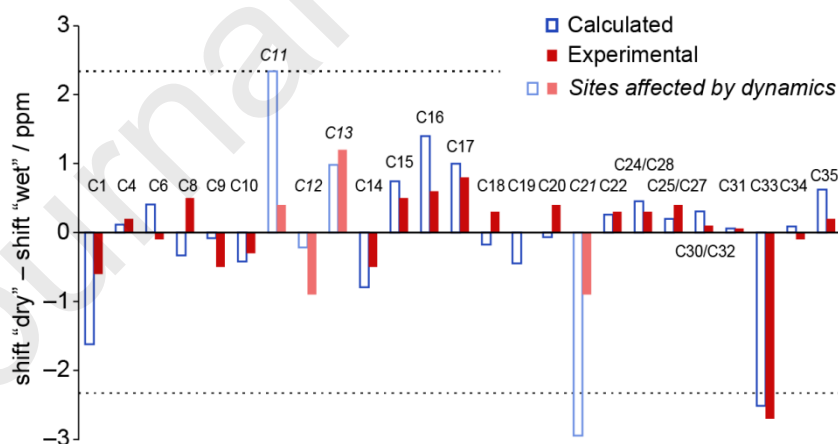
Figure 9 Calculated (blue, unfilled bars) vs. experimentally observed (red, filled bars) differences in ^{13}C chemical shift between dehydrated and hydrated sildenafil citrate (shifts of overlapped peaks have been averaged). Sites affected by dynamics are marked by paler colours and italic labels. Dotted lines indicated expected one-standard deviation residuals expected if individual "errors" were uncorrelated. Figure adapted from Ref. 189, licensed under CC BY 3.0.

On a positive note, as well as demonstrating the potential for improved functionals, the systematic nature of discrepancies between calculation and experiments means that quite subtle variations in calculated parameters can be considered, provided these involve chemically similar sites. An early example is the use of GIPAW calculations to assign the ^{13}C spectrum of α-testosterone[185], a system

with $Z' = 2$. ^{13}C INADEQUATE spectra allowed the resonances to be assigned to one of the two molecules, but GIPAW calculations were essential to determine which set of resonances corresponded to which molecule in the asymmetric unit. The overall RMSD for calculated vs. experimental ^{13}C shifts was 2.3 ppm (full linear regression). If this represented a standard deviation on individual shift values, then we would expect a difference in two uncorrelated shifts to be predicted with a standard deviation of 3.2 ppm, whereas the RMS difference between computed and experimental shift differences (considering only the assigned pairs) is only 0.9 ppm. Other researchers have observed similarly good correlation between calculated and experimental ^{13}C and/or ^{15}N $Z' > 1$ splittings [186, 187], although the assignment of individual lines in these cases was assumed to agree with the calculations, which limits the quantitative significance of the agreement. Another striking example is of RMSDs of only about 1 ppm for ^{13}C tensor principal components in two forms of α-glucose[188], which presumably reflects the very limited range of chemical environments. An example of a practical application of this principle involves the change of ^{13}C shifts upon hydration of the sildenafil citrate[189]. Shift differences were calculated starting from a geometry-optimised structure in which the water sites were fully occupied and the same structure in which the water molecules had been removed. As illustrated in Figure 9, the calculated differences in ^{13}C shift were small, but correlated extremely well with experimentally observed changes, to the point where they could be used to resolve uncertainties in assignment.
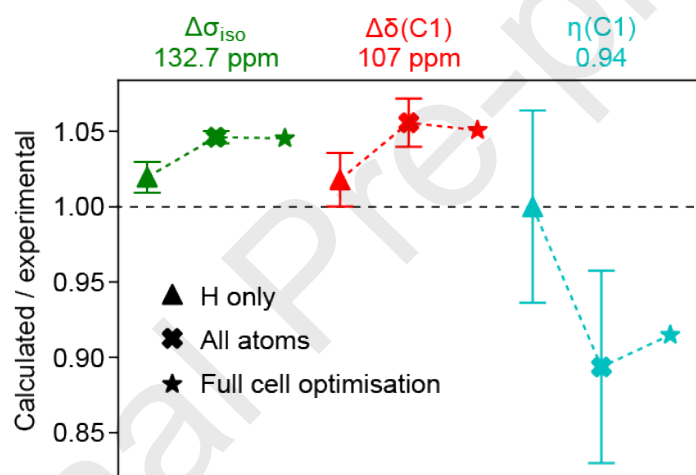

Figure 10: Accuracy of calculated ^{13}C NMR parameters as a function of DFT geometry optimisation for 34 alternative crystal structures of α-glycine: difference in isotropic shielding between C1 and C2, shift anisotropy for C1, and CSA asymmetry for C1 (experimental values shown). The "error bars" indicate the standard deviation of the 34 values (insignificant for full cell optimisations). Note that the results without optimisation are not shown since the errors are too large for the scale used. Figure plotted from data presented in Ref. 190. Dashed lines are guides for the eye only.

An interesting reversal of the usual approach to comparing calculated and experimental data is provided by a study involving 34 distinct crystal structure determinations contained in the Cambridge Structural Database for α-glycine[190]. Different geometry optimisations using PBE with TS dispersion correction were used to evaluate the convergence of calculated NMR results with the degree of optimisation. As shown in Figure 10, the standard deviation of the set of calculated NMR parameters decreases as the geometries converge, but this does not improve the *accuracy* of the overall agreement with experiment. Indeed, the best results are arguably obtained with optimisation of the hydrogen atoms alone. The systematic deviations between calculation and experiment cannot be simply ascribed to the effects of temperature since the experimental results involve a wide variety of temperatures (10–427 K), and the same trends are observed on three approximately independent parameters. This wide temperature range means that the standard error on the experimental mean

cell volume, 305.6 ± 1.7 Å^3 (quoted to one standard error), is high, but this value is nevertheless in clear disagreement with the mean cell volume of the fully optimised structures, 311.81 ± 0.04 Å^3.

3 Applications of NMR crystallography

This larger part of the review considers different topics in NMR crystallography, giving a critical assessment of the state-of-art of the art in the different areas. The first topic considered is that of assignment of the NMR spectrum. Although assignment does not itself provide new crystallographic information, some degree of assignment is an essential first step, and the advent of reliable DFT calculations for periodic systems has had a considerable impact in this area. Moving to more direct crystallographic insights, Section 3.2 discusses how NMR has been used to clarify hydrogen positioning and protonation states. Section 3.3 discusses other cases where problems with crystal structures have been identified via NMR crystallographic studies, often as a result of DFT geometry optimisation. Section 3.4 shows how both dipolar and chemical shift information have been used to establish intermolecular interactions, e.g. hydrogen bonding between crystal components. Section 3.5 discusses how NMR can be used to establish molecular conformation without requiring solution of the full crystal structure. Section 3.6 discusses how NMR can be used to confirm the validity of structures derived from powder and electron diffraction techniques, while Section 3.7 presents the various ways in which NMR crystallography has been used directly to assist structure solution from powder diffraction data. Section 3.8 discusses different approaches to solving structures directly from NMR data without relying on diffraction data. Finally Section 3.9 considers how these methods have been applied to systems containing disorder.

3.1 Spectral assignment

Only limited information can be drawn from NMR spectra without first assigning the signals to specific molecular sites. In contrast to solution-state NMR, where resolved ^{1}H spectra and J-couplings make assignment a relatively straightforward process for small organic molecules, the tools available in solid-state NMR are much more limited. Historically assignment has often been made with reference to assigned solution-state NMR shifts, but the very dependency of chemical shifts on conformation and packing that make NMR a powerful tool for characterising solid forms means that solution-state shifts are an unreliable guide to assignment for solid-state spectra. In this context, calculated solid-state shifts with a typical RMSD of ~2 ppm for ^{13}C make assignment much more straightforward. The use of calculated shifts for assignment is now routine, and here we will simply highlight informative cases. It is important to note, however, that spectral overlap, together with the significant uncertainties in calculated results, means that assignment is still far from being an automated process, and classic tools, such as "dipolar dephasing" (or "interrupted decoupling") to identify non-protonated carbon sites, are still vital. Assignments made purely based on calculated results should be viewed with caution.

The robustness of assignments can be significantly improved if multiple parameters are considered. In an early example of using GIPAW calculations, the ^{17}O spectrum of the zeolite material ferrierite was assigned with the aid of both ^{17}O isotropic chemical shift and C_Q values[137]; neither parameter on its own would have been sufficient for unambiguous assignment. Despite the limited range of ^{1}H shifts, two-dimensional ^{13}C/^{1}H correlation spectra have been widely used to aid assignment for organic systems. Typically, HETCOR experiments with short cross-polarisation periods provide the ^{1}H shifts of hydrogens attached to protonated carbons. Taken together with calculated ^{1}H shifts, this is often sufficient to distinguish sites with similar ^{13}C shifts. Additional cross-peaks appearing at longer cross-polarisation periods often allow further assignments to be made. Lee-Goldburg (also termed off-resonance) cross-polarisation is generally employed when using long contact times to reduce the effects of spin-diffusion during the contact time, but the PRESTO recoupling sequence has also been used for the same purpose[191]. Long-contact time HETCOR spectra can also sometimes be usefully simplified by exchanging of labile hydrogens for ^{2}H[180, 189]. While dipolar-based HETCOR experiments have been the most widely used, other researchers have used refocused ^{1}H,^{13}C INEPT

(i.e. J-coupling-based) experiments, e.g. Refs. [76, 192-194], or a combination of both dipolar and J-based experiments[49]. A potential drawback of INEPT-based methods is that signals from CH_2 groups can be strongly attenuated by dipolar dephasing during the relatively long recoupling times; this may result in missing peaks in correlation spectra[195, 196]. Inverse-detected HETCOR experiments used for assignment[59, 60, 197, 198] have the advantage of providing accurate ^{1}H shifts without the complications of the scaling of the ^{1}H shift axis associated with homonuclear decoupling in conventional HETCOR. [1]H-^{14}N HMQC experiments have also been used for assignment, using different recoupling times to identify one-bond and longer-range N,H correlations[76, 77], while 3D experiments have been used to filter ^{1}H DQ/SQ spectra by proximity with [14]N[199]. Correlation experiments with other nuclei, e.g. [19]F[200] and [11]B[201], have often been necessary for assignment in individual cases.
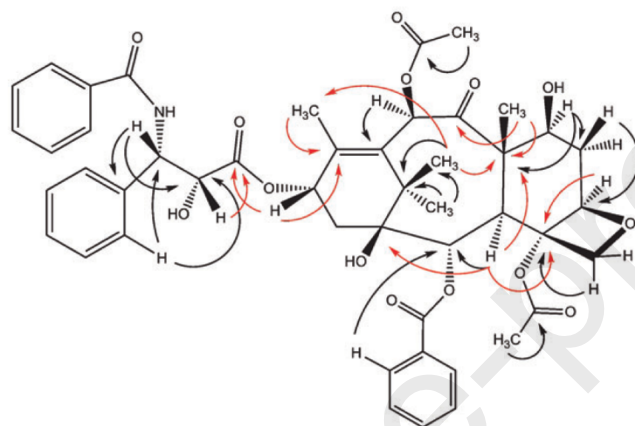

Figure 11 Schematic illustration of correlations observed in ^{13}C,[1]H HETCOR experiments that provided signal assignments in paclitaxel (*Z'* = 2). Correlations shown in red allowed signals to be assigned to individual crystallographic sites, while assignment only to molecular sites was possible using correlations indicated by black arrows. The resolution was insufficient to make assignments for the phenyl carbons. Figure reproduced with permission from Ref. 203 © the Owner Societies 2007.

Resonance assignment is particularly challenging in *Z'* > 1 systems. As illustrated in Figure 11, HETCOR experiments may provide sufficient resolution to assign the carbons of interest[123, 202-204], but lengthy INADEQUATE spectra were required in other cases to fully assign resonances to individual crystallographic sites[185, 205]. A striking example is the assignment of a system with *Z'* = 6, where all ^{1}H and ^{13}C shifts were assigned using 2D ^{1}H,[13]C INEPT spectra and GIPAW calculations[195], aided by favourable ^{1}H resolution. Assignment is more difficult if DFT-calculated shifts are not available (for example, where structures are being predicted from NMR data). In such cases, ^{13}C refocused INADEQUATE spectra may be required[192, 206], although these are unfeasible if the T_1 relaxation times are too long[192]. The presence of heteroatoms may prevent full tracing out of the carbon skeleton, but full assignment may still be possible with the aid of complementary experiments[61].

Signal assignment is generally challenging for saccharides, due to limited shift ranges. 2D spectra have been acquired on β-maltose monohydrate doped with $MnCl_2$ to shorten T_1 relaxation times[168]. [1]H DQ, ^{13}C SQ refocused INEPT experiments were particularly useful for regions where the ^{1}H DQ/SQ spectrum was too crowded. These 2D spectra show linked pairs of peaks corresponding to neighbouring CH groups, and single peaks for correlations involving CH adjacent to OH; the latter enable ^{1}H shifts of hydroxyl groups to be established. In a related study, the ^{1}H DQ, ^{13}C SQ experiment was again found to have excellent resolving power[196], although sensitivity was an issue (80 h of spectrometer time was needed compared to 1 h for corresponding homonuclear ^{1}H DQ/SQ experiment). Further discussion of multi-dimensional experiments to aid assignment can be found in both Refs. [45] and [207], with the former discussing N-rich materials. Note that in some cases, the dispersion of the ^{1}H spectrum under fast MAS[208, 209] may be sufficient for ^{1}H assignments to be
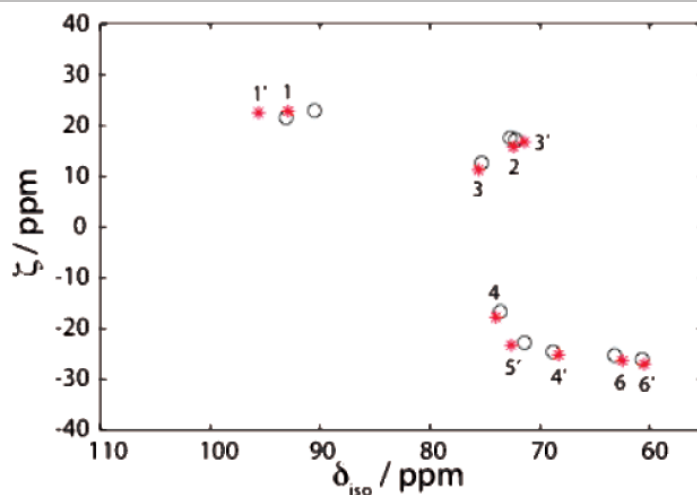
made purely from ^1H DQ/SQ spectra. In less favourable cases, however, long T_1's (commonly encountered in co-crystal systems) may preclude the use of 2D techniques for assignment[210].

Figure 12 Plot of the shift anisotropy, ζ, against the isotropic shift (circles) measured using ^{13}C CSA amplification and (asterisks) calculated for α,α-D-trehalose, labelled by carbon site. Note that the calculated anisotropies were scaled by 0.76 to match experiment. Figure reprinted with permission from Ref. 218, copyright 2007 American Chemical Society.

Assignments have been made in a semi-automated fashion on model systems solely using ^{13}C and ^1H shifts obtained from ^{13}C CP/MAS and ^{13}C,^1H HETCOR experiments[138]. Using this approach, conflicting literature assignments of the shifts of solid naproxen were investigated, confirming an assignment based on calculated shifts and HETCOR spectra[49], and challenging an assignment made without the aid of calculated shifts[211]. GIPAW calculations on 6-aminopenicillanic acid showed that an assignment made using cross-polarisation build-up rates contained errors[212], and confirmed an earlier assignment aided by solution-state NMR shifts[213]. Other examples of using DFT-calculated shifts to correct previous assignments include Refs. [99, 189, 214-217]. These examples highlight the frequency of problems with literature spectral assignments.

Tensor information has often proved valuable In cases where isotropic shifts have been insufficient to make assignments. For example, CSA amplification methods have been used to measure chemical shift anisotropies (CSAs) in three disaccharides[218], where, as noted previously, assignment is difficult due to the narrow chemical shift range. As illustrated in Figure 12, comparing DFT-calculated and experimental anisotropies dramatically improved the confidence of assignment, although the calculated anisotropies needed to be significantly scaled to match experiment. Similarly, ^{13}C tensor components measured on the highly polymorphic system ROY have been used to aid assignment in a case where sites had very similar isotropic shifts[219].

Improving the quality of DFT predictions, e.g. using hybrid functionals in combination with fragment-based methods discussed in Section 2.5.2 should lead to better discrimination between structures. A reduced χ^2 statistic has been used to quantify the ability to discriminate between correct and incorrect assignments of dilute-spin shifts of a set of polymorphs[132]. In all cases considered, the discrimination between correct and next-best "assignment" was increased using fragment-based PBE0 relative to GIPAW+PBE, although this difference was small in some cases, e.g. if swapping the assignment of molecules in a Z' = 2 structure. Including ^{15}N isotropic shifts did not significantly improve discriminating power in most cases, often because range of ^{15}N shifts was small, and the RMS errors of ^{15}N isotropic shifts are significantly larger, e.g. 5.5 ppm for GIPAW+PBE.

3.2 Confirmation of H positioning and protonation state

A common application of NMR crystallography is establishing / confirming the positions of hydrogen atoms. While hydrogen atoms can readily be observed in difference maps derived from high-quality

XRD data[220], this locates the centroid of the electron density, which is not the same as the nuclear position, leading to systematic errors in apparent bond lengths. Calculating NMR parameters from un-optimised X-ray diffraction results consistently yields poor results as a consequence. Analyses that go beyond the independent atom model can reduce these systematic errors. For example, Hirshfeld Atom Refinement uses DFT-calculated electron densities to model the diffraction data, allowing hydrogen atoms to be placed much more accurately and reducing the discrepancy between reference neutron data by about an order of magnitude[221]. It is unlikely, however, that such "quantum crystallography" will be applied in routine crystallographic studies. In other cases, e.g. where the diffraction data is of limited quality, or in powder diffraction studies, it is often not possible to locate hydrogen atoms with any confidence. For example, it is often difficult to distinguish between different tautomeric states of the same molecule, particularly from PXRD data, whereas different tautomers are readily differentiated by NMR, e.g. Ref. [135] and references within. See Section 3.7 for other examples where NMR data is necessary to distinguish between alternative positionings of hydrogen atoms.

In the context of pharmaceutical materials, it is important to know whether a solid form contains the active pharmaceutical ingredient (API) as a neutral molecule (as in a co-crystal form) or in an ionised state (salt form); this difference typically reduces to knowing the position of a single H atom within hydrogen bond. The difference in pK_a between acid and base components (defined as $\Delta pK_a = pK_a[\text{protonated base}] - pK_a[\text{acid}]$) is only a useful predictor of proton transfer where the difference is large (> 3), since pK_a's for molecules in solution have limited relevance for predicting the relative lattice energy of salt vs. co-crystal solid forms; see Ref. [222] and references within for further discussion. Examples, such as pyridine and formic acid[223], where the same components can form both co-crystals and salts, illustrate this clearly. Note that there are important systems where the hydrogen positions are intrinsically ambiguous, for instance, temperature-dependent hydrogen migration in carboxylic acid dimers. These are interesting and well-studied systems in their own right; we focus here on cases where hydrogen does have a well-defined position, but where this is not precisely known from diffraction studies.

For convenience, the following examples of using NMR to probe hydrogen position are divided by the key NMR nucleus used.

3.2.1 Via ^{13}C NMR

Most cases of using ^{13}C NMR to determine H positions have involved the different chemical shift of carboxylic vs. carboxylate carbon. Even so, the increase in ^{13}C isotropic chemical shift on deprotonation of CO_2H is relatively small, up to 7 ppm stated[224], and has often been used to confirm a protonation state established by other means, e.g. using ^{15}N shifts[225]. In a set of salts / co-crystals of venlafaxine, the carboxylate resonance in one of the five salt forms was found be at lower, rather than higher, chemical shift than the neutral form[224]. Quantitative correlations between ^{13}C shifts and hydrogen bonding have often been elusive. For example, in a multi-nuclear study of hydrogen bonding in benzoic acid and group I hydrogen dibenzoates[226], there was a good correlation between the ^{1}H isotropic shift and O...O donor/acceptor atom distance, but the correlation with the δ$_{22}$ shift of the carbon of the carboxylic acid was less than clear than expected from previous literature in which the σ$_{22}$ shielding principal value of the carboxylic/carboxylate carbon of amino acids was quite sensitive to protonation state[227]. In contrast, ^{13}C shifts have been successfully used in a more qualitative manner to distinguish between two structures for terbutaline sulfate form B in the CSD, which differ only in the orientation of a single hydroxyl group[123]. There were significant differences in calculated ^{13}C shieldings for the carbons adjacent to the OH. These show that the hydrogen was correctly positioned in ZIVKAQ (hydrogen placed at standard positions and distances), and incorrectly in ZIVKAQ01 (hydrogen positions refined). See Figure 20 in Section 3.6 for a similar example.

As previously noted in Section 2.3, the principal values of shielding tensors are often more informative than isotropic shieldings. For example, the crystal structure of lauric (*n*-dodecanoic) acid, like other

alkyl carboxylic acids, contains carboxylic acid dimers. The agreement of experimental ^{13}C shift principal values with calculations was good after geometry optimisation for all carbons except for the carboxylic acid (C1), with disagreements consistently exceeding 10 ppm[228]. Moving the hydrogens across a model butyric acid dimer showed that much better agreement with NMR data could be obtained at two different O–H distances (1.16 and 1.46 Å), in significant disagreement with the neutron-derived data. It was concluded that the H pair was likely be tunnelling between the two almost-energetically-equivalent dimer arrangements, and so the NMR measurement is reporting an averaged tensor. In follow-up work on polymorphs of palmitic acid, only one of which has known structure, two model structures were created based on known arrangements, one based on carboxylic acid dimers and the other catemeric[229]. An f-test was used to assess agreement between calculated shifts from clusters and experimental ^{13}C principal components, which showed poor agreement with the catemer model, and consistently better agreement with *trans* rather than *cis* arrangements of alkyl torsion angles adjacent to the dimer. As noted previously, the ^{13}C principal values readily distinguished between localised vs. disordered hydrogen positions. "ADPs" were modelled by Monte Carlo methods; the hydrogen positions were adjusted randomly, and compared to experiment, retaining only structures in which the calculated shifts were within one standard deviation (8 ppm for the carboxyl C) of the experimental values. The volumes of the resulting ellipsoids were ~4 times smaller than those from XRD and ~1.8 times smaller than those from neutron studies. Analogous work on estimating "ADPs" from ^{1}H shifts[230] is discussed in Section 3.2.3. ^{13}C and ^{15}N shift tensors calculated on isolated molecules have also been shown to be quite sensitive, via the σ_{22} principal value, to the position of hydrogen within an intramolecular O...H...N bond in a pair of Schiff bases[231]. The NMR data was determined to be compatible with an N–H distance of 1.1–1.26 Å.
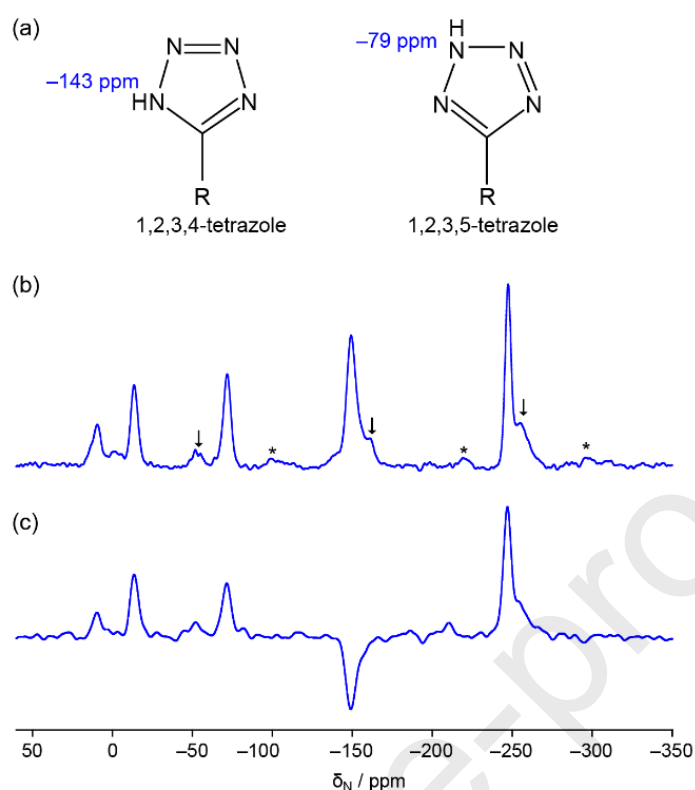
3.2.2 Via ^{15}N (and ^{14}N) NMR

Figure 13 (a) Possible tautomeric forms of the tetrazole ring. Figures show the shift of the protonated nitrogens in forms A and B of irbesartan, which contain the 1,2,3,4 and 1,2,3,5 tautomers respectively. (b) ^{15}N CP/MAS spectrum of a semi-crystalline form of valsartan acquired at 50.65 MHz. (c) The ^{15}N inversion-recovery CP/MAS spectrum of the same material clearly identifies the protonated nitrogen, whose shift indicates that valsartan contains the 1,2,3,4 tautomer. Arrows indicate "conformational defects" in this partially ordered material. Figure adapted from data published in Ref. 236, copyright 2016 American Chemical Society.

Despite its poor sensitivity, ^{15}N NMR has been used very successfully to establish and confirm hydrogen positions in the solid-state. Applications to tautomerism in both solution and solid states have been recently reviewed[232].

A very direct approach to positioning hydrogen atoms relative to nitrogen is to measure N,H dipolar couplings, as previously discussed in Section 2.1. For example, the hydrogen atom in a $N^+…H…N^+$ bonding arrangement was shown to be symmetrically positioned[233] using N,H dipolar couplings measured simply using the spinning sideband pattern of the ^{15}N MAS spectrum (the coupling being sufficiently large for recoupling not to be needed). In contrast, different DFT calculations gave inconsistent predictions of the H position (associated with the limitations of DFT in strongly H-bonded systems), and the uncertainties in the H position from diffraction data were too large to distinguish between these predictions. CP build-up curves have also been used to determine N,H distances, and hence protonation state[234]. This was more reliable than using "dipolar dephasing" to test the N protonation site. In a similar vein, N,H dipolar couplings have been measured by inverse-CP methods in four two-component solids[222] to determine the degree of H transfer in a PyN…H–O– bonding arrangement. Such inverse measurements are advantageous if an N site may be coupling with multiple hydrogens; a simple sideband pattern at low spin rates would give an effective (root-mean-square) coupling, while the inverse method under fast MAS will pick out the dominant coupling of interest. The resulting measurements were in good agreement with neutron data. In most systems, XRD also cleanly distinguished between salt and co-crystal, but the XRD data was ambiguous in one intermediate case, confirming the value of NMR in cases where ΔpK_a is between 1 and 3. Again classic "dipolar dephasing" experiments do not reliably distinguish between protonated and non-protonated

49

nitrogen, and "inversion recovery CP"[235] was used to identify protonated the nitrogen in imidazole rings[236], as illustrated in Figure 13.

Dipolar-coupling-based experiments may be misleading in cases where dynamics are present. In these cases, J-based experiments, such as solid-state version of the Attached Proton Test (APT)[237], can reliably distinguish protonated and non-protonated N sites[238]. ^{14}H/^{1}H HMQC experiments were also used in this case to establish N protonation state, with the advantage that experiments with longer mixing times (600 μs) often (although not always) also showed correlation peaks corresponding to H...N in a N–H...N bonding arrangement, hence providing valuable insight into intermolecular hydrogen bonding. Different protonation states of imidazole rings have also been clearly observed in ^{1}H,^{14}N HMQC spectra[79], which were acquired in less than an hour using 90 kHz MAS at 14.1 T. N,H proximity has also been investigated by ^{1}H NMR, e.g. ^{1}H spectra acquired at 90 kHz MAS with and without ^{14}N decoupling clearly H atoms bonded to nitrogen[80].

The ^{15}N chemical shift is generally extremely sensitive to the number of attached hydrogens and has been widely used to confirm or infer protonation state, e.g. to distinguish salt from co-crystal forms[239], to distinguish between protonation of N vs. O sites[174], and showing the DFT optimisation was incorrectly moving the hydrogen across an O–H...N bond, cf. Figure 7. ^{15}N shifts clearly distinguished between alternative hydrogen bonding arrangements in a co-crystal between theophylline and pyridoxine hydrochloride, where one H could be forming an intramolecular H-bond with an O acceptor or intermolecular bond with an N acceptor[240]. A change of ^{15}N chemical shift of >13 ppm showed that relevant N is an acceptor in pure theophylline, but not in the co-crystal, while ^{14}N/^{1}H experiments confirmed the protonated N sites. In a study of co-crystals/salts of a poorly soluble pharmaceutical with three dicarboxylic acids[241], the ^{15}N shift showed clear correlation with H position, with shifts to lower frequency >80 ppm on proton transfer to heterocyclic N, compared to 20–40 ppm on formation of a stronger H bond. In a study of four salts / co-crystals of ketoconazole, XRD was able to locate the hydrogen in three cases[225]. In one case, however, the positioning was ambiguous, and the ^{13}C shifts were also insufficiently distinctive, but the ^{15}N shifts and C–O bond lengths were consistent with a co-crystal (i.e. presence of carboxylic acid rather than carboxylate). A change in ^{15}N shift from ~16 ppm to 25–29 ppm was used to show protonation of a tertiary amine, i.e. salt formation, in four solid solids of lidocaine with dicarboxylic acids[242]. Similarly, the absence of a significant change in the ^{15}N shift was used to show that protonation state of an NH$_2$$^+$ was unchanged on the formation of a cocrystal of ezetimibe[243].

In other studies of solid forms of theophylline, a distinctive ^{15}N shift on protonation of the imidazole ring nitrogen was used to distinguish salts and co-crystals[244, 245], which was confirmed in a follow-up study on wider range of compounds[246]. There was a good correlation between N–H bond length and calculated change in shift on protonation. The magnitude of changes, however, varied significantly between N type: around −50 ppm for protonation of imidazole of theophylline vs. −69 ppm for protonation of pyridine of isonicotinamide, whereas shifts >−100 ppm were observed for the pyridine of an API. These differences partly reflect differences in H-bonding strength, e.g. changes of up to −33 ppm were observed on formation of a co-crystal, i.e. without H transfer. In contrast, changes to amine shifts were much smaller e.g. −14 ppm, hence DFT calculations were very helpful in confirming the significance of the change. X-ray photoelectron spectroscopy (XPS) was also used in this study to examine protonation. Although the resolution of XPS spectra is relatively poor, the chemical shifts in N 1s binding energy are much less sensitive to changes in intermolecular interaction, and so do cleanly distinguish between protonation states. Changes to lower ^{15}N chemical shift of >10 ppm have similarly been observed protonating NH$_2$ [247], while consistent changes >10 ppm to *higher* frequency were observed on protonating tertiary amines[224] (consistent with the lidocaine example above). In the latter case, the protonation was confirmed using ^{14}N/^{1}H HMQC. In another example of using ^{14}N shifts, ^{14}N NMR (at 14.1 T and 70 kHz MAS) was used to separate NH and NH$_3$$^+$ resonances of alanine polypeptides, based on their very different isotropic quadrupolar shifts[248].

The utility of calculations to predict the magnitude of shift changes is illustrated in a study of co-crystals formed between an imidazole and morpholinium iodide[249]. Based on the good agreement with GIPAW-calculated shifts and the ^{13}C and ^{15}N spectra of the starting materials, it was assumed that proton transfer had not occurred between species. Surprisingly, however, the calculated ^{15}N shift of solid morpholine was in the same range as the morpholinium ion, and so additional NMR evidence was sought to confirm the protonation state. The ^{15}N CSA asymmetry parameters, however, were sufficiently distinct for static CSA patterns to confirm the presence of morpholinium.

3.2.3 Via ^{1}H and ^{2}H NMR

At a simple qualitative level, strong hydrogen bonding is expected to decrease magnetic shielding and hence increase the ^{1}H chemical shift of the associated hydrogen. Clear empirical correlations have been be derived from ^{1}H chemical shifts for, for instance, O–H...O hydrogen bonds involving carboxylic acid donors or carboxylate acceptors[250], amide protons in peptides[251], in N...H–O vs. N$^+$–H...O$^-$ interactions[252], O...H...O and N...H...O interactions[253], N–H...O=C hydrogen bonds in polyalanines[254], or more generally[255, 256].

In one of the earliest applications of DFT-calculated solid-state shifts, the H shielding was calculated, using a dimer model, as a function of position in the N–H...O hydrogen-bond in methylnitroacetanilide (MNA)[257]. The experimental ^{1}H shift was then used to determine the N–H distance as 1.03 ± 0.02 Å. Applying the same methodology on L-histidine hydrochloride gave N–H distances in excellent agreement with neutron diffraction results. This approach of relating shifts directly to distances has not, however, been widely adopted. This may reflect uncertainty in the referencing used to relate experimental shifts and calculated shieldings; as in the case of measuring N–H distances via dipolar couplings discussed in Section 2.1, relative changes in bond length can be determined with significantly greater confidence than absolute bond lengths. For example, the structure of a naproxen–picolinamide cocrystal contained two independent carboxylic acid dimers in the asymmetric unit, with almost identical donor-acceptor distances, but with donor–H distances differing by 12 pm[258]. The uncertainty on H positioning, however, means that the confidence intervals on the donor–H distances almost overlap within one standard error. In contrast, a straightforward ^{1}H MAS spectrum showed a difference in ^{1}H shifts of less than 1 ppm, meaning that the actual donor-H distances must differ by only a few pm (based on the empirical corrections above). Plots of the lattice energy as a function of the position within the carboxylic acid showed well-defined minima and confirmed the positioning of the hydrogen. In a similar way, using ^{1}H shifts to confirm the similarity of hydrogen bonding environments is helpful in cases where one structure is unknown[54].

An alternative approach to estimating the accuracy with which hydrogen atoms can be located via ^{1}H shifts used molecular dynamics (MD) simulations to generate perturbed structures from which shifts were calculated[230]. The results were used to determine how much positional variation corresponds to a given RMSD between experimental and calculated shifts. The results varied with the system, with, for instance, a 0.49 ppm RSMSD corresponding to a mean positional variation of 0.17 Å for cocaine. Although smaller than typical ADPs of hydrogen in XRD studies, these uncertainties are an order a magnitude larger than the 2 pm uncertainty estimated for MNA above. This reflects the fact that the 0.49 ppm RMSD is dominated by the global systematic limitations of DFT, and so over-estimates the uncertainty of positioning an atom within a given type of local environment.

A good example of the use of ^{1}H shifts to establish the correct positioning of hydrogen atoms is provided by a study of three different XRD structures of α-D-galactose present in the CSD[259]. Geometry optimisation of the H atom positions resulted in two of these structures converging, but the remaining pair of structures still differed in hydrogen atom positioning and in hydrogen bonding arrangements. The mean average error on ^{13}C NMR parameters calculated from optimised structures and compared to experiment, was only slightly lower (0.9 vs 1.4 ppm) for the structure with the lower calculated lattice energy (difference of 2 eV per unit cell, corresponding to ~200 kJ mol^{-1}). (To put this figure in context, computational studies[260] have shown that most polymorphs differ in lattice energy by less than 2 kJ mol^{-1}.) In contrast, the predicted ^{1}H NMR spectra for the alternative structures

were significantly different (despite the modest magnetic fields and MAS rates used), as shown in Figure 14, confirming the structure with the lower lattice energy.
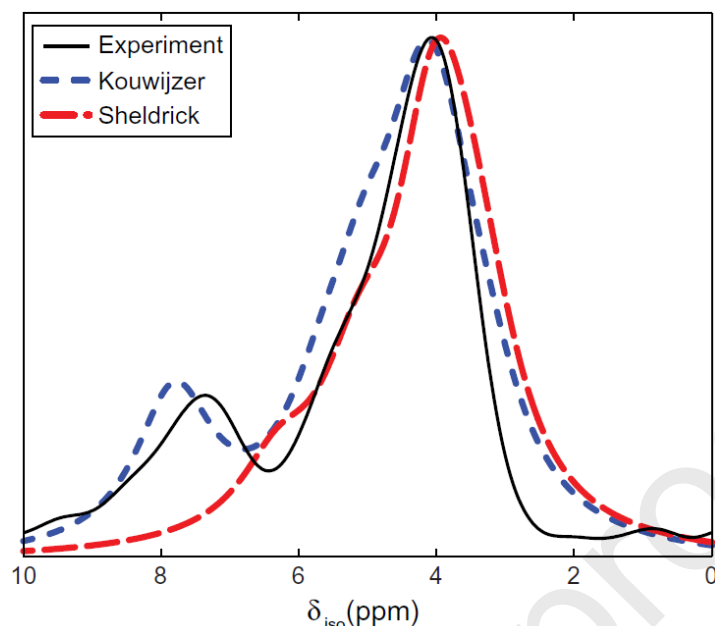

Figure 14 Comparison of an experimental (solid black line) ^{1}H NMR spectra for α-D-galactose with simulated spectra for the H-position optimised XRD structures determined by Kouwijzer *et al.* (short blue dashes) and Sheldrick (long red dashes) structures (CSD refcodes ADGALA03 and ADGALA10 respectively). Experimental spectra were acquired at 300.07 MHz and 12 kHz MAS. Figure taken from Ref. 259, copyright Elsevier (2010).

^{1}H chemical shift anisotropies have also been shown to be very sensitive to hydrogen positioning. 2D experiments correlating ^{1}H CSA and isotropic shifts have been compared to calculated values obtained from X-ray and neutron structures of L-ascorbic acid with and without optimisation of the hydrogen positions[261]. Excellent agreement was obtained in both cases after optimisation, with the neutron structure giving reasonable (but not perfect) agreement without optimisation. Similarly ^{1}H CSA parameters clearly distinguish the polymorphs of acetaminophen[80].

^{2}H quadrupolar couplings are also sensitive to the hydrogen bonding, with the ^{2}H C_Q decreasing strongly with increasing hydrogen bonding strength, cf. Ref. [262] and references therein. For example, the positioning of the hydrogen-bonded H in trimethylammonium chloride was examined using a variety of NMR parameters, including hydrogen shifts and ^{2}H C_Q[263]. The measurements were consistent with a moderately strong H bond, although the overall accuracy of positioning was comparable to previous dipolar-based measurements.

3.2.4 Via ^{17}O NMR

^{17}O NMR has not been widely used in NMR crystallography due to its poor sensitivity at natural abundance and the expense and/or difficulty of isotopic labelling. More information about ^{17}O NMR in the solid state can be found in recent review articles and book chapters[264-266]. Here we focus on the limited number of cases where ^{17}O NMR has been used to understand hydrogen positions.

As for nitrogen, very strong changes in chemical shift are observed on changing oxygen protonation state, e.g. the isotropic shift of phenol oxygens was observed to increase by ~60 ppm on ionisation, while the quadrupolar parameters were only slightly affected[267]. This was larger than the effect (although similar in proportion to the shift range) on the associated ^{13}C shift (about −10 ppm). Variable success has been reported in correlating calculated and experimental ^{17}O parameters. For example, the ^{17}O parameters of enriched salicylic acid and aspirin were measured and used to follow double-H exchange in the carboxylic dimers present in their structures as a function of temperature[268]. A good match with GIPAW calculated parameters was reported (at least compared to simple cluster-based calculations), with an RMSD between experimental and calculated shifts of 20 ppm. In contrast,

a study of hydrogen bonding in benzoic acid and group I hydrogen dibenzoates reported relatively poor correlation between GIPAW calculations of ^{17}O parameters and experimental values, limiting conclusions that could be drawn[226].

In possibly the most detailed application of ^{17}O NMR to pharmaceutical systems, diflusinal was ^{17}O-labelled at the carboxylic acid positions and studied in its Form I, co-crystal and two amorphous dispersions[269]. The ^{17}O shielding was observed to be very sensitive to changes in H-bonding environment, with the donor OH shielding increasing by 150 ppm Å^{-1} with H…O (acceptor) distance, compared to shift changes on hydrogen bonding of ~2 ppm for ^{13}C in a C=O acceptor. The spectra were relatively easy to acquire due to short relaxation times, and chemically distinct O sites were resolved without need for 2D techniques. Favourable ^{1}H relaxation times allowed ^{1}H/^{17}O HETCOR to be performed, which resolved an intermolecular correlation associated with an O–H…O hydrogen bond (otherwise difficult to characterise via ^{13}C NMR). 2D spectra were even acquired from solid dispersions, allowing changes in H-bonding to be observed that would be too subtle for ^{13}C/^{1}H HETCOR experiments, and impossible for classic diffraction methods. It was therefore argued that isotropic enrichment might be justified for late-stage compounds.

3.2.5 Via ^{31}P NMR

The protonation state of phosphate groups, which are widely encountered in biological systems, is readily established via NMR, in particular, using the ^{31}P chemical shift anisotropy[270]. Dipolar-based experiments have also been used to establish the presence of P–OH groups. For example ^{31}P and ^{13}C inverse HETCOR experiments distinguish between C–OH and P–OH acid protons[271]. Combined with ^{1}H DQ/SQ spectra, these experiments showed the hydrogen bonding to be distinct from the known structure of a related form of the molecule.

3.3 Correcting other problems with diffraction-derived structures

The use of NMR to address limitations of diffraction studies is discussed implicitly in a number of sections, e.g. positioning of hydrogen atoms in the previous section or characterising disorder in Section 3.9. Here we briefly consider other cases where NMR crystallography has identified otherwise unsuspected problems in structures derived from single-crystal data.
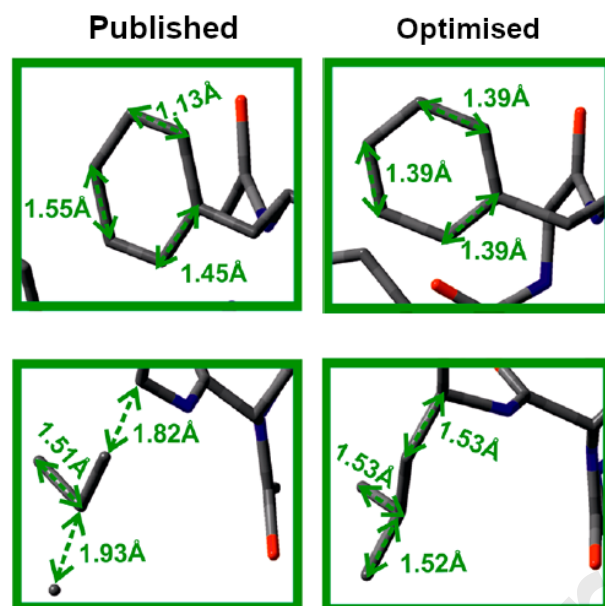
Figure 15 Sections of the crystal structure of a penta-peptide enkephalin: (left) as originally published (CSD refcode LENKPH11) and (right) after DFT geometry optimisation. Figure adapted from Ref. 59, copyright 2014 American Chemical Society.

Such problems have most commonly been identified in poor correlations between experimental and calculated ^{13}C shifts. For example, calculated and experimental shifts of two forms of thiamine hydrochloride showed significant deviations (up to 10 ppm) for one form[272], associated with an unusually short C–O bond (1.18 Å compared to 1.40 Å in the other form), which was presumed to be associated with dynamics. Full structural optimisation reduced the RMSD between experiment and calculation from 5.3 to 3.3 ppm (results for PBE functional). Similarly, very poor agreement was observed between experimental ^{13}C shifts and those calculated from CSD crystal structures for tiotropium bromide, both as anhydrous (GUYGOX03) and hydrate (GUYGUD01) forms[273]. Again, full geometry optimisation provided more reasonable bond lengths and improved agreement with experimental shifts. In a study of two pentapeptides[59], three structures were found in the CSD, all involving complex structures with multiple molecules, including water, in the asymmetric unit and poor *R*-factors (between 9 and 14%). DFT geometry optimisation was essential to obtaining agreement with experimental shifts, and substantially altered some structures, which in one case featured very unreasonable bond lengths, as seen in Figure 15. Similar observations involving adjustment of water molecule positions on optimisation have been observed in other hydrate materials[198].

3.4 Confirming and rationalising intermolecular interactions

This section discusses the various ways in which solid-state NMR has been used to probe intermolecular interactions[274]. NMR parameters are a very powerful tool for probing intermolecular interactions, since they are directly connected to changes in electronic structure, e.g. due to hydrogen bonding. In contrast, intermolecular interactions can only be inferred indirectly from diffraction studies, based on statistical evidence. In most cases, however, NMR has been used to rationalise or quantify the strength of interactions, rather than as route to solving / verifying crystal structures, which is the focus of the current article. Hence this is not an exhaustive summary of the literature.

3.4.1 Intermolecular interactions established from dipolar/J-based experiments

As discussed above, dipolar couplings have frequently been used to directly probe H positioning within hydrogen bonds. In other cases, dipolar coupling has been used more qualitatively to examine intermolecular association via hydrogen bonds. For example, cross-peaks observed at longer mixing times in ^{14}N/^{1}H experiments have shown the presence of O–H…N hydrogen bonding in a co-crystal of

nicotinamide and palmitic acid[275]. The limited resolution of ^{14}N and ^{1}H spectra made it difficult to resolve individual correlations, but changes in hydrogen-bonding arrangement could be observed. Interestingly, because the ^{14}N shift is sensitive to both the chemical shift and the isotropic component of the second order quadrupolar interaction, some large changes in shift (of ~60 ppm) between were seen in HMQC spectra of a pure API (acetaminophen) and its amorphous dispersions in polyvinylpyrrolidone, while negligible changes in isotropic shift were observed in corresponding ^{15}N experiments.

The ability of solid-state NMR data to test co-crystal formation via observing intermolecular contacts has been assessed on a set of ten systems[276]. Provided distinctive ^{1}H chemical shifts due to moderate-to-strong hydrogen bonding could be seen, ^{13}C/^{1}H HETCOR was always able to prove association, and both chemical shifts and APT experiments were used to confirm protonation state, e.g. distinguishing between neutral vs. zwitterionic states of β-piroxicam. In the case of carbamazepine.nicotinamide, however, the hydrogen bonds are relatively weak and the ^{1}H shift was insufficiently distinctive to allow association to be proved. [13]C,[1]H HETCOR was used in later work for showing co-crystal formation, with ^{1}H DQ/SQ spectra and ^{1}H shifts providing some insight into hydrogen bonding patterns and strengths[277]. [13]C,[1]H HETCOR experiments at longer contact times are commonly used to show interactions between the carbons and the hydrogens of a carboxylic acid dimers e.g. Ref. [258]. Similarly, long contact-time FSLG HETCOR experiments revealed a number of intermolecular contacts[278] in a multicomponent solid form of tolfenamic acid obtained from mechano-chemistry (i.e. no SCXRD structure could be obtained), see Figure 16. Intermolecular interactions involving O–H…O hydrogen bonding has also been observed via ^{13}C/^{1}H HETCOR spectra[279], corresponding to C,H distances around 1.9–2.2 Å. HETCOR experiments have established presence of hydrogen bonds between carbonyl and OH and NH groups in four salts of lidocaine with dicarboxylic acids[242], with ^{1}H DQ/SQ spectra establishing intermolecular proximity.
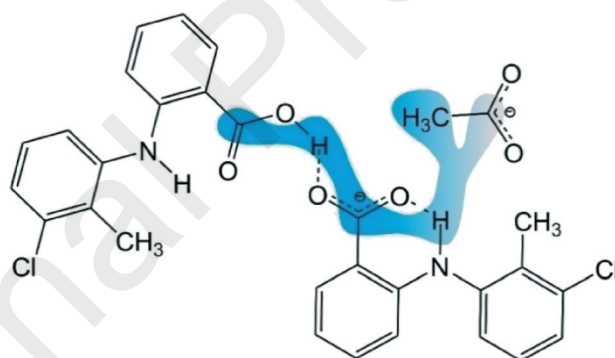

Figure 16 H,C proximity information deduced between components of a mixed salt co-crystal form of tolfenamic acid from ^{1}H,[13]C HETCOR experiments. Figure reproduced from Ref. 278, with permission from The Royal Society of Chemistry.

As previously noted in Section 2.1, ^{1}H DQ/SQ correlation experiments have frequently been used to observe intermolecular contacts. For example, 100 kHz MAS has been used to obtain well-resolved ^{1}H DQ/SQ spectra from host-guest complexes which could not be characterised by SCXRD[193]. The observed correlations were consistent with a specific orientation of the methyl and para-phenyl hydrogens of the toluene guest relative to the host, in agreement with DFT calculations on isolated host-guest complexes. In another example, there are four possible supramolecular "synthons" that would link indomethacin and nicotinamide in a co-crystal[280]. [1]H DQ/SQ experiments clearly ruled out the presence of a carboxylic acid dimer, but showed strong correlation of the carboxylic H with either aromatic CH or amine. In principle, the ^{13}C,[1]H refocused INEPT experiment was sufficient to show this correlation involved aromatic CH, and hence identify the synthon present, but a ^{14}N,[1]H HMQC experiment provided additional unambiguous evidence for the presence of an O–H…N hydrogen bond. [1]H DQ/SQ correlation experiments have been used to distinguish between parallel vs

anti-parallel β-sheets in alanine polypeptides, including larger polypeptides where single crystal structures were unavailable[248]. [14]N NMR (at 14.1 T and 70 kHz MAS) was used to separate NH and NH$_3^+$ resonances based on their very different isotropic quadrupolar shifts. [1]H DQ/SQ spectra have similarly been used to discriminate between polymorphs of alanine tripeptides[254], with the presence/absence of diagonal peak linked to a key intermolecular contact. The build-up of ^{1}H DQ coherences was used to study intermolecular interactions in γ-indomethacin[53]; the build-up of coherences between the carboxylic acid OH and either the neighbouring OH in the acid dimer or the aromatic protons were found to be in line with predictions and with numerical simulation. In addition, ^{1}H DQ / [13]C refocused INEPT experiments were used to obtain DQ build-up curves from sites that could not be resolved by their ^{1}H shifts. This permitted the resolution of a strong build-up associated with a close (2.2 Å) proximity between a specific pair of aromatic hydrogens. In contrast to the spin-diffusion evolution curves discussed below, however, it seems difficult to discriminate between similar structural models using DQ build-up data. Apart from the DQ auto-correlation peak observed for the acid OH, which clearly indicates the presence of a carboxylic acid dimer[47, 52, 200, 281], the interpretation of build-up data is strongly dependent on the existence of a structural model. A similar pattern emerges from work on polymorphs of sibenadet hydrochloride[54], where the presence of cross-peaks in DQ/SQ ^{1}H correlation spectra highlighted proximities between pairs of NH's (H–H distance of 2.62 Å) and between OH and NH (H–H distance of 2.87 Å). This was consistent with the hydrogen bonding arrangement of the known form (Form I), and identical behaviour of DQ build-up curves implied that the hydrogen bonding arrangement in the unknown form (Form II) was very similar. Note it was important to consider the "effective" RSS dipolar coupling (see Eq. 2) for sites at similar distances to multiple hydrogens. In other cases DQ/SQ correlation spectra have provided clear finger-prints for different hydrogen bonding motifs, for example, allowing different assemblies of deoxyguanosine derivatives be identified[196], as illustrated in Figure 17. As discussed in Section 3.6, such information about bonding networks is invaluable when trying to solve structures when only powder diffraction data is available.
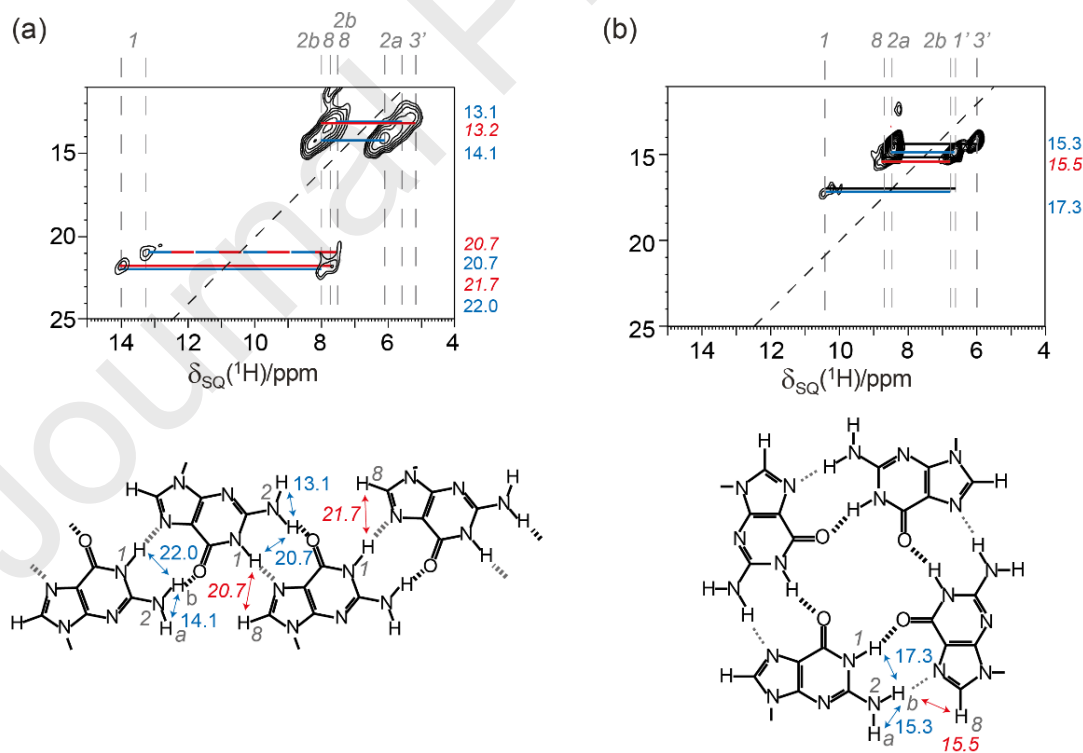
Figure 17 Sections of ^{1}H (600 MHz) DQ/SQ NMR spectra, acquired at 12.5 kHz MAS and using homonuclear ^{1}H decoupling in both dimensions, for deoxyguanosine derivatives adopting (a) ribbon-like, and (b) "quartet" structures. Blue and red horizontal bars highlight DQ coherences arising from intra- and inter-molecular contacts respectively. The H,H proximities are labelled in the structures with their ^{1}H DQ chemical shift (blue roman and red italic typeface for intra- and inter- molecular contacts respectively). Figure adapted from results published in Ref. 196, copyright 2011 American Chemical Society.

Although not strictly fitting into the category of small molecular organics, Ref. [282] is an interesting example of combining shift, dipolar and J information from 2D NMR experiments to establish the packaging arrangement of DNA base analogues that self-assemble into a complex "rosette" nanostructure, as illustrated in Figure 18. Differences in ^{13}C linewidths clearly distinguished the ordered core from disordered pendant groups. This local packing information was nicely complementary with PXRD, which could be used to establish the overall packaging of the assemblies, despite the width of the diffraction peaks due to the disorder.
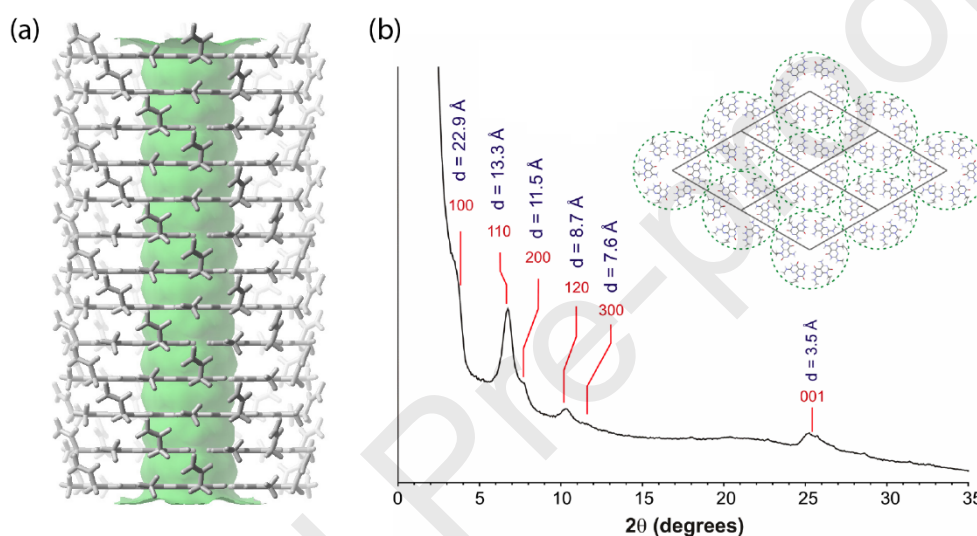

Figure 18 (a) Molecular model of "rosette stack" formed by self-assembly of a synthetic DNA base analogue. (b) Powder XRD pattern of the solid formed, indexed according to the illustrated hexagonal packing model. Adapted with permission from Ref. 282, copyright 2016 American Chemical Society.

3.4.2 Rationalising the effects of intermolecular interactions on chemical shifts

In contrast to approaches using couplings, probing intermolecular interactions via chemical shifts requires comparison to the shifts in isolated molecules. The difference in chemical shift of a given site in the crystalline lattice compared to the isolated molecule is a combination of short-range effects (changes in the local bonding environment) and long-range effects, mostly due to nearby ring currents. The effects of surrounding molecules on the overall chemical shift are obtained by calculating the chemical shift tensor at general points in space, rather than just at nucleus positions (hence "nucleus independent"). The resulting maps of Nucleus Independent Chemical Shifts (NICS) show the change in chemical shift at a particular position due to surrounding lattice[283, 284]. Since NICS calculations

Figure 19 Map of the isotropic component of the nucleus-independent chemical shift for nicotonamide in a cocrystal with indomethacin, showing the effect of ring currents on the NMR chemical shifts of nuclei as a function of spatial position. Figure reproduced from Ref. 117 with permission from The Royal Society of Chemistry.
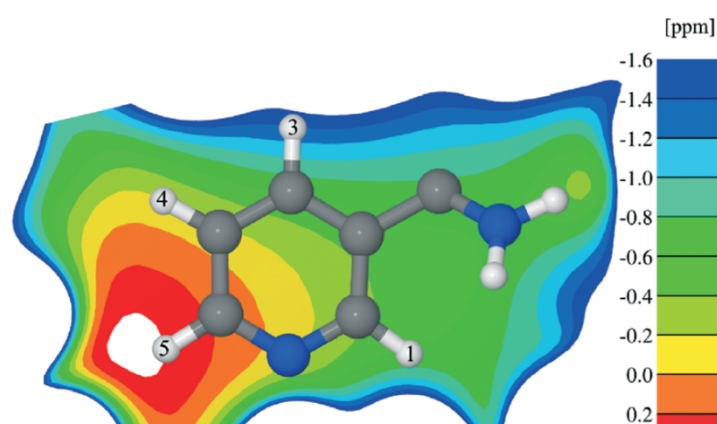
involve removing individual molecules in order to map out the effect of the surrounding lattice, it is often necessary to consider larger super-cells to avoid "self interaction" between a missing molecule and its image in an adjacent unit cell. NICS maps, such as Figure 19, are very useful for visualising the effects of CH…π interactions since these are strongly anisotropic. Quantitative insight into the strength of *short-range* intermolecular interactions require such long-range effects to be corrected for. A recent study on visualising the different contributions to shielding due to intermolecular effects[285] concluded that the dominant contributions to the changes in chemical shift were local for row 2 elements, such as C, while long-range effects were more significant for light atoms, notably H. This is consistent with the general observation that ^1H shifts are sensitive to the overall packing arrangement, for example, a shift to low frequency of 1.2 ppm of aromatic protons has been used to infer the stacking of aromatic rings[286].

As illustrated in Figure 19, NICS maps have been used to analyse intermolecular interactions in an indomethacin.nicotinamide cocrystal[117]. Computing the difference in shifts for sites in the crystal lattice and the isolated molecules, and subtracting off the NICS component, the changes in shift due to intermolecular interactions were estimated to be between −0.2 to 1.7 ppm. Simple differences between lattice and isolated molecule shifts have been used to examine intermolecular effects in a co-crystal system[287]. Many differences larger than 1 ppm corresponded to CH…π interactions (associated with ring currents), but a large (3.6 ppm on ^1H) difference between lattice and isolated molecule shifts was linked to N–H…O hydrogen bonding, and there was also evidence for a weak C–H…O hydrogen bond (from a difference of 2.0 ppm). The effects of CH… π interactions were similarly observed via an outlying ^1H aromatic shift in γ-indomethacin[53]. The largest changes (lattice minus isolated molecule) in ^1H shift were, unsurprisingly, observed for hydrogen in carboxylic acid dimers, but differences of −1 and −1.9 ppm were seen for H pointing towards aromatic rings. Similar observations have been observed in other systems[195, 284], with an aromatic shift as low as 3.8 ppm in naproxen providing a very striking example of the potential size of such shift changes[49]. A noteworthy feature of another study using NICS maps to rationalise intermolecular interactions[176] was the use of "converse" approaches to calculating chemical shifts. In contrast to "linear-response" methods used by codes such as CASTEP, which determine the response of the system to a bulk magnetic field, converse methods consider the magnetisation induced by point dipoles placed at atomic centres. Although it is necessary to calculate the response at each nuclear site of interest and in three orthogonal directions to obtain the full shift tensor, the relative simplicity of the calculations means these approaches can be competitive in terms of calculation time. The NICS were relatively large (3.8–7.3 ppm), and so removal of these effects was essential to determining the short-range intermolecular effects (which ranged from −0.5 to 1.8 ppm). For example, the overall calculated intermolecular contribution to the ^1H shift in a particular NH was +1.6 ppm, a significant change in shift due to the formation of a hydrogen bond, but the experimental shift was only 5.4 ppm, which, without the insight from NICS calculations, would have suggested minimal H-bonding.

Changes in shift due to intermolecular interactions have been used to examine desolvation processes. For example, simple differences in shifts calculated on the crystal lattice and isolated molecules were used to examine intermolecular effects in orotic acid and its salts with lithium and magnesium[288]. As previously remarked for ^{13}C shifts, the changes in ^{15}N shifts were numerically larger than those on ^1H, but relative to uncertainties on the calculated shifts (i.e. RMSD value), the changes in ^1H shift were ultimately more distinctive. The magnesium salt showed complex dehydration behaviour with some of the eight waters per formula unit proving easier to remove. Significant changes in some aromatic ^{13}C shifts were predicted after removing six water molecules and relaxing the geometry, which were consistent with experimental observations, although it was not possible to be more definitive. Note that simulated PXRD patterns of the dehydrated structures did not match experiment, but matching PXRD patterns is often difficult due to the extreme sensitivity of the patterns to the lattice parameters[289]. In a study of dehydration of solid forms of ciprofloxacin[204], water molecules were removed from the structure and NICS calculations performed to study effect of hydration and intermolecular interaction on ^{13}C and ^1H shifts. Changes of up to 5 ppm were seen on hydration on

58

[13]C, although the changes of up to 1 ppm change in ^{1}H shifts are again proportionately larger. The largest intermolecular effects on ^{1}H shifts on hydration were found to be from NH$^+$ ... O$^-$ (+4.6 ppm) and CH...π interactions (up to −4.0 ppm). In a study of dehydration of the dihydrate form of the tetra-peptide Tyr-D-Ala-Phe-Gly, subtle changes in NMR spectra were observed on dehydration[198], e.g. [1]H DQ/SQ experiments distinguished the forms, but showed that the overall intermolecular interactions were substantially unchanged. [1]H spectra calculated for material with water removed gave excellent agreement with the observed spectrum, suggesting that the desolvate was essentially isomorphic with the initial hydrate.

Lattice vs. isolated molecule calculations are particularly helpful when probing the effects of hydrogen bonding. For example, weak C–H...O hydrogen bonding in α and β maltose was investigated using changes in calculated ^{1}H isotropic shifts[290]. Differences of up to 1.9 ppm were observed and correlated with local geometry, both H...O distance and C–H...O angle (i.e. the directionality of the hydrogen-bonding interaction). In contrast, the effects of intermolecular interactions on ^{13}C isotropic shifts were smaller (as a function of the shift range) and complicated by additional interactions. Similar approaches were used to study weak C–H...O weak hydrogen bonding in uracil and 4-cyano-4'-ethynylbiphenyl[291]. Long-range effects (from NICS calculations) were confirmed to make small (~10%), but significant, contributions to shift changes. The short-range effects of chemical shift were not found to depend significantly on C hybridisation, with consistent changes of about 2 ppm in these systems where weak hydrogen bonding is expected to play a significant role (H...O distances < 2.5 Å and bond angles close to linearity). The ^{1}H shift in NH has been used to distinguish between different motifs of hydrogen bonding in self-assembled guanosine derivatives which do not form diffraction-quality crystals[196]. The NMR linewidths were generally sharp, despite the peaks in the PXRD patterns rapidly deceasing in intensity with scattering angle, which suggests some dynamic disorder of the alkyl chains.

Again, stepping into host-guest chemistry rather than classic small molecule crystallography, the ^{1}H chemical shifts of pyridine and toluene have been compared between solution and when included as part of solid-state host-guest inclusion complex with calixarene. The "complexation-induced shift" was modelled computationally comparing the shifts in the free molecule vs. positioned in cavity according to the SCXRD structure of the complex[292]. Using the equivalent of a NICS map obtained by placing a probe He atom in different positions within the calixarene host, the "depth" of binding in cavity could accurately predicted from the complexation-induced shift. A similar approach has been used to reveal the location of guest molecules in host-guest system using ring current shifts[293].

3.4.3 Halogen bonding

The halogen bond, which is a non-covalent interaction involving a central halogen atom, has an important role in supramolecular chemistry and crystal engineering. Specialist techniques are often required to obtain NMR data from halogen nuclei, and the experimental and computational challenges of obtaining / calculating NMR parameters where heavy elements are involved means that NMR crystallography of halogen bonding is mostly at the stage of establishing potentially useful correlations between NMR data and local structure. This section highlights a few examples that illustrate the potential of NMR in this area. Further information can be found in recent reviews and overview articles[8, 294-296].

Dipolar couplings, specifically between ^{15}N and [127]I, have been used to estimate N,I bond distances in a molecular system expected to self-assemble by N...I halogen bonds[297]. The estimated distance of 2.7–2.9 Å was significantly shorter than sum of van der Waals radii, consistent with formation of a halogen bond.

Most studies of chemical shifts and halogen bonding have involved the shift of ^{13}C attached to the halogen. For example, consistent changes in [13]C (and ^{19}F) isotropic shifts were observed on forming co-crystals containing strong N...I halogen bonds, up to −11 ppm for [13]C[298]. Trends in ^{13}C shift with halogen bonding strength have been qualitatively reproduced[68, 299], and correlated to changes in

C–I bond length via DFT with the Zero Order Regular Approximation (ZORA) method of including relativistic effects, although quantitative agreement for ^{13}C bonded to I was still relatively poor. Relativistic effects have been discussed as part of a recent extensive review of shift calculations for ^{13}C[300].

3.5 Establishing molecular conformation

As discussed further in Section 3.7, understanding the conformation adopted by molecules in the solid state is a significant help in solving crystal structures from powder diffraction data. Again, both dipolar and chemical shift-based approaches have been used to address this question.

The strengths and weaknesses of using dipolar couplings to obtain quantitative information on molecular geometry are illustrated by work on the polymorphic drug molecule cimetidine. This is a challenging system for structure solution since the molecule has seven degrees of torsional freedom, allowing a wide variety of conformations to be adopted. In an early study, two ^{13}C labels were introduced at approximately opposite ends of the molecule, and four forms (anhydrates A, B and C plus a monohydrate form, M1) crystallised[301]. The primary geometrical information was obtained using rotational resonance, which is a simple means to selectively recouple dipolar interactions between pairs of sites. The effects of ^{13}C,^{13}C dipolar coupling were unambiguously observed in forms A and M1, and robust distance measurements of <4 Å were clearly consistent with the known "bent horseshoe" configuration. In contrast, the molecule adopts an extended configuration in form D, with a distance of 9.1 Å between the labels, resulting in a coupling that is too small to be measured (the upper limit being stated to be 6 Å for closely related double-quantum methods). The rotational resonance curves of forms B and C were both fitted to a C,C distance of 5.5 ± 0.3 A, and the molecule was predicted to adopt a "corkscrew" conformation. In a recently determined structure of cimetidine form C[302], however, the molecule was found to adopt an extended conformation in which the ^{13}C,^{13}C coupling would be unmeasurably small; the decay of the signal in the rotational resonance experiments must have been due to relaxation rather than coupling. In follow-up studies, a ^{15}N label was introduced at a single site, and four distinct C,N distances measured (with uncertainties between 0.1 and 0.2 Å) in form A using a constant-time version of REDOR[303]. CH/CH$_2$-selective cross-polarisation was used to simplify the ^{13}C spectrum and increase the number of measurable dipolar couplings. These distances were used to obtain the conformation of the molecule in the solid state via a molecular dynamics simulation in which the four C,N distances were constrained to the values obtained via the dipolar couplings. Structure solution from PXRD data was greatly facilitated by the reduction of the number of conformational degrees of freedom from 7 to effectively zero; Section 3.6 below discusses in more detail the role of NMR data in solving structures from powder diffraction data. In the most recent study[304], ^{13}C and ^{15}N labels were inserted at two sites at opposite ends of the molecule in which the label was attached to a single H atom, and a set of dipolar-based restraints were used to constrain the conformational space. The remaining compatible conformations fell into two groups, with the lowest energy group corresponding to the known conformation in form A. Upper limits of 4.3 Å, 5 Å and 6 Å were stated for C–N, N–H and C–H distances to be measured from dipolar couplings respectively.

In other applications of ^{13}C,^{15}N REDOR-type experiments, the conformation adopted by *N*-octyl-D-gluconamide in three distinct solid forms was investigated using a sample with a single ^{15}N label, but natural abundance in ^{13}C[305]. As above, this allowed multiple (up to six) C,N distances to be measured. Here the dependence of chemical shifts on the local conformation of alkyl chains (the "γ-gauche" effect) was used to reduce the range of conformations compatible with the dipolar coupling data. As well as showing that the dipolar data was consistent with the molecular conformation in the form with known crystal structure, a distinct molecular conformation was predicted for the two forms with unknown crystal structure. Note that the dipolar coupling was also helpful in establishing the assignment of carbon signals close to the N site. In a different system, the bonding in methoxycarbonylurea restricted each torsion angle to either 0 or 180°. Even so, the limited distance range probed via ^{13}C,^{15}N dipolar couplings meant that more than one isotopically labelled sample was

required to establish the molecular conformation[306]. ^{13}C,^{15}N REDOR experiments on mixtures of labelled and unlabelled compounds were used to measure an intermolecular distance of < 4 Å, which was found to be compatible with a limited number of packing arrangements via molecular modelling studies. Recently C,N distances up to 3.3 Å have been measured via dipolar couplings between ^{13}C and ^{14}N at natural abundance[307], giving access to a small number of angles between internuclear vectors in a pair of complex molecules. Such experiments have the advantage of not requiring labelling, with the drawback that dilution in unlabelled samples cannot be used to distinguish between inter- vs intra-molecular couplings[308].

^{13}C chemical shift tensor data has also been used to reduce the possible conformational space. For example, the torsion angles in the molecule paclitaxel were varied and conformations only retained if calculated ^{13}C principal component values were compatible (at an 80% confidence level) with experimental NMR data[203]. This, however, still left 13 out of the original 600 structures. Note that these calculations, by necessity, involved isolated molecules, rather than the (unknown) full crystal structure. ^{13}C tensor information in combination with isolated molecule calculations has also been used to determine the backbone conformation of a tripeptide amide[309]. Similarly, the agreement between experimental isotropic ^{13}C shifts for a set of eight compounds and those calculated for isolated molecules in different conformations observed in related materials were used to identify the most likely molecular conformation in the solid state[310].

3.6 Validation of crystal structures derived from diffraction

The solution of crystal structures from powder X-ray diffraction data is a well-established technique[311]. However, in contrast to single-crystal XRD, where (in the absence of significant complications, e.g. due to disorder) the structure solutions are essentially unambiguous, the compression of the diffraction peaks into a single data axis of intensity vs. scattering angle means that structure solution from powder data necessarily requires modelling. Even the initial peak indexing required to obtain the unit cell dimensions can be far from straightforward and subject to ambiguity. The most common route to structure solution then involves placing molecules within the determined unit cell and calculating a trial diffractogram and associated R factor (which quantifies agreement between experimental and trial data). Rietveld refinement, involving iterative adjustment of the atomic positions and diffraction parameters to minimise R, is then used to optimise structures with reasonable initial R factors. The difficulty of finding initial structure "hits" for subsequent refinement scales quickly with the number of structural degrees of freedom, e.g. the number of independent molecules in the unit cell (Z'), torsion angles etc. Model structures will generally be built with as few parameters as possible, e.g. omitting hydrogen, fixing aromatic rings at standard planar geometries etc. These parameters can be re-introduced at later stages of the refinement process. However, it is important to remember that, in contrast to NMR where the peak positions are sensitive to structure, the peak positions in the diffractogram are fixed by the space group and unit cell parameters; the atomic positions within the unit cell only change the peak intensities, and the effects of hydrogen atoms in particular on the peak intensities is often too small to determine their positions.

NMR has a strongly complementary role in this context. Section 3.7 discusses cases where NMR information has been used to guide the process of solving structures from powder diffraction data. The current section considers cases where NMR data has just been used to validate the structures obtained from potentially ambiguous diffraction. Examples will be seen where the NMR and/or DFT has helped to correct initial solutions.

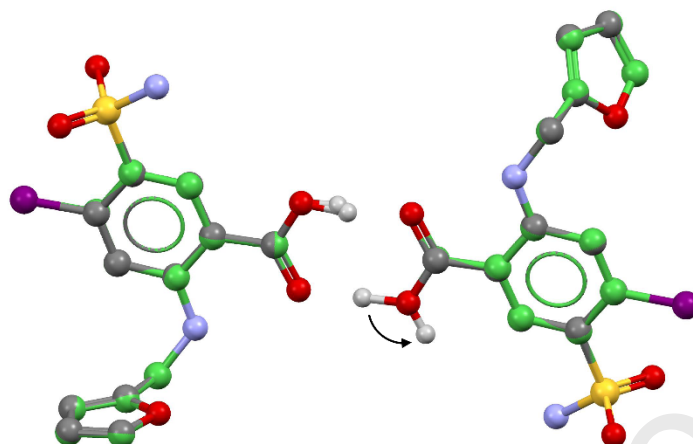*3.6.1 Validation of structures from single-crystal XRD data*

Figure 20 Overlay of the asymmetric units of two CSD structures, FURSEM01 (C atoms in grey) and FURSEM17 (C atoms in green), of furosemide form 1. H atoms are generally omitted except for the critical carboxylic acid groups, which form a classic dimer in FURSEM01, but not FURSEM17; the arrow head points toward the H position in FURSEM17. Figure reproduced from Ref. 134, licensed under CC BY 3.0.

Although NMR has been most widely used to validate structures derived from powder diffraction data, examples have already been presented, e.g., in Figure 14, Section 3.3 and the terbutaline sulfate example of Section 3.2.1, of problems with structures derived from single-crystal diffraction being identified via NMR. In most cases, the issues are associated with poorly positioned hydrogen atoms. This illustrated in Figure 20 for two alternative structures of form 1 of furosemide present in the CSD. While FURSEM01 has a conventional carboxylic acid dimer, one hydrogen in FURSEM17 is rotated out of the dimer. RMSDs for ^{13}C and ^{1}H isotropic shifts predicted from FURSEM17 gave values outside typical ranges (2.78 ppm and 0.77 ppm for ^{13}C and ^{1}H respectively) and significantly higher than FURSEM01[134]. In particular, the calculated shift of the mispositioned H was clearly incompatible with experimentally observed shift obtained from ^{13}C,^{1}H HETCOR. The significant difference in calculated lattice energies (25 kJ mol^{-1} molecule^{-1}) was also too large for FURSEM17 to plausibly be a different polymorphic form. DFT refinements and validation via NMR shifts have also been used to validate structures from single-crystal data where the crystal diffracted weakly[312].

A very recent study has also focussed on the ability of NMR crystallography to distinguish between alternative structures; such "distinction" between alternative models is a relatively straightforward problem since we only need to rank structures by agreement with NMR data, as opposed to "verifying" an individual structure, which would require calculation of probabilities that a given structure agrees with the NMR data. This survey of repeat structure determinations in the CSD found that over 20% of 3132 pairs of alternative structures for the same system exhibited structural differences (mostly of hydrogen atoms) greater than 0.25 Å (i.e. significantly larger than would be expected from experimental uncertainties)[313]. DFT geometry optimisation resolved these differences in most cases, but in other cases the alternative structures solutions minimised to distinct structures. Ignoring differences in methyl group orientations, the largest fraction of unresolved structural differences were associated with hydroxyl groups (as in the majority of the individual examples discussed above). In most cases a combination of either ^{13}C or ^{1}H isotropic chemical shifts would be expected to distinguish these alternative structure solutions, but in a small number of cases the structures differed only in long-range ordering, which would be difficult to characterise via NMR methods. This systematic study helps to position NMR crystallography in a sequence of methods of increasing complexity / expense (single-crystal diffraction, DFT optimisation, solid-state NMR, neutron diffraction) for distinguishing between alternative solutions arising from X-ray diffraction studies.

3.6.2 Validation of structures from powder XRD data

Verification of crystal structures is relatively straightforward where the proposed structure from PXRD is essentially isostructural with a known structure; NMR can show that the structures have the same hydrogen bonding arrangements and intermolecular interactions, e.g. using ^{1}H fast MAS, ^{1}H DQ/SQ and ^{13}C,[1]H HETCOR experiments, without the need for detailed assignment. For example, the similarity of the NMR data for succinate and fumarate salts of lidocaine supported the solution of the succinate salt structure from powder data, starting from the structure solution of the fumarate salt[242]. Similarly, NMR is often used selectively to confirm hydrogen bonding arrangements. For example, ^{1}H DQ/SQ spectra of di- and tri- *p*-benzamides confirmed that carboxylic acid groups were present as dimers[47] (via the characteristic high-frequency diagonal peak, as noted in Section 3.4.1). These materials are relatively insoluble, forming crystals that are unsuitable for single-crystal XRD, hence the structures were solved from PXRD data aided by lattice parameters obtained from electron diffraction. In the case of a new polymorph of metergoline solved from PXRD data, ^{13}C NMR identified that *Z′* was 2, while ^{13}C,[1]H HETCOR cross-peaks between resonances associated with different molecules confirmed intermolecular interactions predicted from the proposed structure[314]. Other examples of using dipolar information to confirm predicted intermolecular contacts in structures solved by PXRD include Ref. [224]. In other cases, dipolar information has been more ambiguous. For example, in a study of a second polymorph of a drug system, ^{13}C and ^{1}H NMR indicated that the overall structure was very similar to that of the known form, but with some slight differences, such as a different conformation for a propionic side chain inferred from an absent cross-peak in a ^{1}H DQ/SQ spectrum[281]. The form 2 structure was solved from PXRD data, with DFT used to optimise geometries between stages of Reitveld refinement. Adjustment of dimer conformation to match NMR data, however, did not lead to an overall improvement of the *R* factor or predicted ^{13}C shift principal components. On the other hand, the proposed structure had the qualitative characteristics (stronger hydrogen-bonding, increased ring stacking) that had been predicted from chemical shift-based arguments.

Full validation of proposed crystal structures requires the assignment of ^{13}C and ^{1}H shifts, and quantitative assessment of the agreement between experimental shifts and those calculated from the proposed structure. For example, in a cocrystal of theophylline produced by grinding, where the structure needed to be determined from powder data, ^{13}C and ^{1}H isotropic chemical shifts (together with proximity information from ^{1}H DQ/SQ experiments) were used to confirm the proposed structure[315], while the structure of a theophylline-nicotinamide cocrystal derived from PXRD was validated against ^{13}C and ^{15}N shifts[316]. In the case of a new polymorph of the drug praziquantel obtained by grinding, the structure could be solved from synchrotron PXRD data, although this was challenging due to peak broadening[317], which was presumably associated with small crystal size, rather than lack of crystallinity *per se*, as the ^{13}C spectra resonances were sharp. The RMSD of ^{13}C isotropic shifts was 2.4 ppm (compared to a stated expected range of 2.2 ± 0.5 ppm for a correct solution), helping to validate the proposed structure. The structure of *O*-phospho-DL-tyrosine was solved from PXRD, but the accuracy was limited by the lack of high-angle peaks[271]. The structure was refined by DFT optimisation to give reasonable agreement with the assigned ^{1}H and ^{13}C shifts, and was compatible with predictions of intermolecular interactions from dipolar correlation experiments. The structure of an anhydrous form of cimetidine hydrochloride, obtained by dehydration of a monohydrate phase, needed to be solved from PXRD data[318]; desolvation processes often produce finely powdered materials due to strain associated with the change in lattice parameters. Here only minor movements (up to 0.18 Å for H) were observed on geometry optimisation, and qualitatively good agreement was found between calculated chemical shifts and experiment, which clearly differed from shifts calculated from the starting hydrate form. The very different ^{13}C shifts for the two phases were assumed to reflect the distinct conformation of the cimetidinium cation in the two forms. Combined with ^{1}H DQ/SQ spectra, these experiments showed the hydrogen bonding to be distinct from that in the known structure of a related form of the molecule.

NMR was used to validate the structure solution of polymorphs of ixazomib citrate from synchrotron powder data[169]. This is a challenging system as $Z' = 2$, and there is uncertainty about stereochemistry, and how the boron is co-ordinated in solid state. The co-ordination geometry was investigated with a 2D [11]B experiment, which clearly discriminated the two forms, and the shift ranges agreed with predicted local B environment (shared between two 5-membered rings). The build-up of [11]B DQ coherences was used to estimate the shortest B…B distance to be 6.3–6.5 Å, in agreement with proposed structure.

An important aspect of structure validation is confirming hydrogen bonding arrangements. An early example, before the widespread use of periodic DFT, involved the crystal structure of anhydrous theophylline determined from powder XRD data[319]. Two viable solutions were found with different H-bonding arrangements (N–H…N vs. N–H…O), but significantly better agreement was found for experimental ^{15}N chemical shifts calculated for molecular trimers having an N–H…N structure; this was consistent with other indicators, such as lower lattice energy and better R factor for the N–H…N arrangement. It is often difficult to obtain diffraction quality structures from sugars, while their acetate derivatives often crystallise more readily. The crystal structures of acetates of three methyl glycosides were determined and the conformation of the molecules used as the basis for structure solutions[320]; the acetate was replaced by H in a random orientation and a unit cell constructed in the relevant space group before geometry optimisation using dispersion-corrected DFT. In two cases, the resulting structures were in good agreement with the known crystal structures, and showed good matches with predicted ^{13}C shifts. In the remaining case, a large discrepancy in ^{13}C shift identified an OH which was incorrectly oriented; optimisation with a re-positioned H provided a satisfactory solution.

Note that in some cases the DFT optimisation required for good estimates of NMR parameters has itself improved the structure solution (see Section 3.3 for further examples). For example, in the solution of the structure of a cocrystal from PXRD data, all-atom DFT refinement of the initial Rietveld-refined structure decreased the R factor from 11% to 5%[50], presumably by pushing the structure out of a local minimum. GIPAW-calculated ^{13}C, ^{1}H and ^{15}N shifts were then used to validate the resulting structure. In another example of using geometry optimisation to aid structure solution, the structure of the drug ethoxzolamide was solved from PXRD[321]. This produced 20 structures with similar R factors (13–14%), which fell into groups with two different molecular packings and two orientations of the sulphonamide. DFT was used to relax representative examples of four solutions from the four groups, which lowered the R factors on subsequent Rietveld refinement (9% for the best solution). DFT refinement changed many H positions (by up to 0.65 Å), again possibly allowing new minima to be explored. The resulting structures were validated using experimental isotropic shifts; ^{13}C isotropic shifts were not found to be very distinctive, but ^{15}N shifts clearly favoured one packing (although failing to distinguish between alternative orientations of the sulphonamide group). Geometry optimisation had a similarly important role in a study of two structures available for β-piroxicam[322]. As illustrated in Figure 21, geometry optimisation of the two structures brought them into agreement with only minor adjustment of atomic positions. The resulting calculated ^{13}C shifts were in good agreement with experiment (<2 ppm RMSD), and ^{1}H DQ/SQ and ^{14}N/^{1}H HMQC spectra were used to confirm spatial correlations in the structure. Here NMR crystallography helped to validate an essentially correct structure that might otherwise be viewed suspiciously due to its poor R factor.
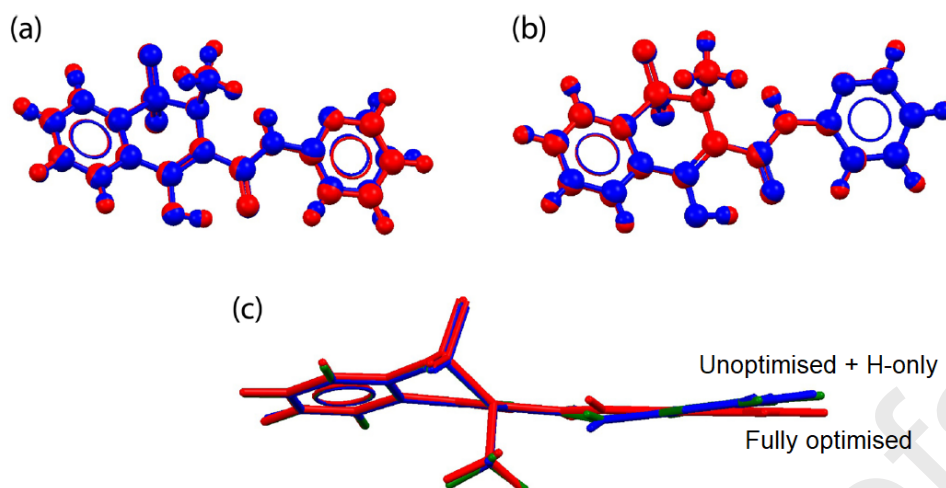
Figure 21 Ball and stick representations before (blue) and after (red) geometry optimization of crystal structures of β-piroxicam derived from (a) PXRD and (b) SCXRD. The *R* factor of the PXRD structure (CSD refcode BIYSEH03) is much higher (19%) than that of the SCXRD structure (refcode BIYSEH13), but geometry optimisation leads to only a minor adjustment of the pyridine ring orientation, highlighted in (c) which shows an overlay of the PXRD structure before geometry optimization (blue), and with geometry optimization of proton positions only (green), and all atoms (red). Figure reprinted with permission from Ref. 322, copyright 2018 American Chemical Society.

3.6.3 Validation of structures from electron diffraction data

The extremely strong scattering of electrons by the electron density of molecular systems makes it possible to obtain diffraction data from extremely small crystals. The strong interaction between electrons and matter means, however, that the conventional "kinematical" model of the diffraction experiment begins to break down. Hence even quantifying the agreement between experimental and trial data with a conventional *R* factor can be problematic. Developments in experimental techniques and data analysis are, however, allowing structures to be solved directly from electron diffraction (ED) data, e.g. Ref. [323]. DFT calculations have a potentially significant role, both to help predict diffraction patterns, but also in refining the approximate co-ordinates obtained from ED studies[324], in much the same way as geometry optimisation is used in NMR crystallography. For example, the pigment fluorescein has two polymorphs which contain different tautomers: a red form, with a quinoid tautomer, and a yellow form with unknown structure thought to contain a zwitterionic tautomer[130]. The PXRD pattern of the yellow form produced by rapid crystallisation shows broad peaks, precluding structure solution directly from the PXRD data. Instead, crystal structure prediction (see Section 3.8) was used to generate possible structures, and the calculated diffraction pattern from the structure with the third highest lattice energy showed the best fit to experiment. This was used to obtain a structure by Reitveld refinement, which also gave the best fit to ED data. Figure 22 shows the result of validating the proposed structure using ^{13}C isotropic shifts; reasonable RMSDs are obtained if the experimental shifts are compared with the correct structure, and unreasonable values (of about 4 ppm) obtained if structures are swapped around.
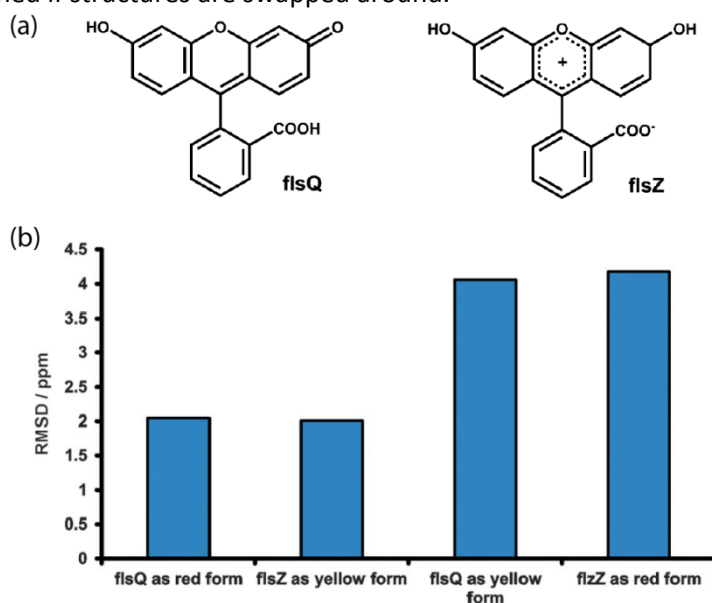
Figure 22 (a) Two possible tautomeric forms of fluorescein. (b) RMSD between experimental ^{13}C chemical shifts for the red and yellow solid forms of fluorescein compared to shifts calculated from the proposed structures of the two forms. Figure adapted from Ref. 130 (Creative Commons Attribution licence).

3.7 Assisting the structure solution process from powder X-ray diffraction data

NMR data has been used in a variety of ways to directly assist structure solution from PXRD data. The first key stage of structure solution is determining a unit cell that indexes the positions of the diffraction peaks. The number of molecules in the unit cell, Z, can then be inferred using typical densities of molecular organics. Information from NMR about Z' can be very helpful at this stage in reducing the number of space groups that need to be considered. For instance, in the structure solution of unusual mixed organic inorganic materials obtained by grinding barbituric acid with alkali metal salts, standard analysis tools gave a space group of $P2_1/c$ and a unit cell with $Z = 8$ and $Z' = 2$[325]. ^{13}C and ^{79}Br NMR, however, showed only one unique molecule of barbituric acid and one Br$^-$ per asymmetric unit, while ^{23}Na NMR showed two distinct Na sites. This information was used to establish that the structure was best described in the higher-symmetry $C2/c$ space group. Where component molecules have high symmetry, NMR can reveal fractional values of Z', e.g. the value of $Z' = 0.5$ inferred from ^{13}C NMR similarly significantly constrained the number of space groups to be considered[326]. The value of Z' is not always evident from ^{13}C spectra; DFT calculations are helpful in these cases to confirm that symmetry independent sites have locally very similar environments[157, 327].

NMR can also be invaluable in determining the molecular basis for building the crystal structure. In a particularly striking example, ^{13}C NMR clearly showed that the material commercially sold as "hexaketocyclohexane octahydrate" is actually dodecahydroxycyclohexane[328], which was obviously essential to solving the structure from PXRD data. As discussed in Section 3.2, NMR can generally easily identify protonation sites. For example, ^{13}C shifts were used to determine which one of the two aromatic nitrogens in an aminopyrimidinium moiety was protonated, providing key input in a structure solution from PXRD data[329]. Similarly, questions of tautomeric state need to be established prior to solving structures. For example, cyameluric acid has potentially 17 tautomers. The ^{1}H NMR spectrum combined with a cross-polarisation polarisation inversion experiment showed that the tautomeric protons must all be N–H, while calculated ^{15}N shifts for the isolated molecule then narrowed the options to two tautomers[330]. These were difficult to distinguish even when using ^{13}C tensor principal components, as the most sensitive parameter (the asymmetry of the CSA) is influenced by intermolecular effects, such as hydrogen bonding. Nevertheless, a preferred tautomer was identified, and its DFT-optimised structure used to solve the structure. Note, however, that the hydrogen positions could not be located, and so the refinement produced two structural models with different hydrogen bonding networks. These could be distinguished from their very different lattice energies, with ^{13}C and ^{15}N isotropic shifts being supportive of this choice rather than definitive. In an unusual case of the re-investigation of a structure derived with the aid of NMR, Li et al. reinvestigated[331] a structure obtained from PXRD where NMR had been used to confirm $Z' = 1$[332]. Specifically, it was questioned whether the correct amine vs. imine tautomer had been identified. Refitting the original PXRD data with different model structures gave indistinguishable fits, but the RMSD agreement of ^{13}C shifts improves markedly (from 4.0 ppm to 1.9 ppm), and individual discrepancies reduce from over 10 ppm to less than 4 ppm when the correct tautomer was used. Note

66

that DFT relaxation of the published structure gave a RMS displacement of the non-H atoms of over 0.3 Å, which indicates a problematic structure[121].

As discussed in Section 3.5, NMR has been used to assist structure solution by reducing the size of the conformational space that needs to be considered. A common application has been restraining the orientations of OH groups, which can rarely be determined with any confidence from PXRD data. In solving the structure of (+)-catechin 4.5 hydrate from PXRD data, cross-polarisation build-up rates were used to determine the orientations of five OH groups[180]. Comparison of experimental and calculated ^{13}C tensor principal components for ten model structures of isolated molecules narrowed this to two models which refined equally well against PXRD data. Note that structures were geometry optimised with frozen OH torsion angles to maintain the conformation. In the structure solution of ambuic acid from PXRD data, DFT optimisation of the molecular geometry improved the agreement with ^{13}C shift principal values without affecting the R factor, i.e. the NMR is more sensitive than is PXRD to small changes in local geometry[333]. Regions of the structure where agreement was poor helped to identify torsion angles requiring optimisation, leading to improved R factors. The ^{13}C principal values were observed to be very sensitive to OH orientation, allowing the orientations of the hydroxyls to be identified based on agreement between experimental and calculated data.

The conformation of the three hydroxyls of quercitin is similarly difficult to determine from PXRD data[215]. In an initial study, molecular mechanics was used to explore conformational landscape, and the three lowest minima used as input for PXRD structure solution of anhydrous quercetin. The structure with the lowest energy after DFT optimisation was validated by the RMSD of ^{13}C isotropic shifts. Follow-on work obtained the same solution by a more comprehensive search of conformational space using 8 orientations of the three OH's (torsion angles of either 0° or 180°)[334]. In contrast to systems noted elsewhere, no clear correlations were found between hydroxyl orientation of an OH and the isotropic ^{13}C shift of adjacent atoms. The same method was applied to a dioxane solvate of quercetin[335], with ^{13}C and ^{1}H shifts used to validate the structure determined from PXRD using multiple Rietveld refinement stages alternating with DFT optimisation. The solution of the structure of lisonopril dihydrate was complicated by the ambiguous orientation of two carboxylic acid units[336]. Exploration of conformational space resulted in three models which fitted with similar R factors. DFT optimisation significantly reduced the energies of two of the structures, one of which had a better overall fit with ^{13}C and ^{1}H data and so was used as input to Rietveld refinement. After optimisation of the water positions, this refinement produced a structure with both good R factor and good agreement with NMR data. Subsequently both SCXRD and PXRD structures of the material were published. The solution from PXRD + NMR was almost identical to the SCXRD structure, and was in significant disagreement (matching only the overall conformation) with the PXRD-only solution.

As discussed in Section 3.4, NMR has been widely used to establish intermolecular connections, which can potentially assist structure solution. For example, 3',5'-bis-O-decanoyl-2'-deoxyguanosine has interesting supramolecular behaviour, but is not available as single crystals. Previous NMR work had established the presence of N–H…N hydrogen bonds, which helped constrain starting models for solving the structure [337]. DFT was used to optimise the initially obtained structure, resulting in some significant conformational changes in the decanoyl chains and an improved R factor on subsequent Rietveld refinement.

In other cases, agreement with NMR parameters has simply been used to discriminate between alternative solutions compatible with the PXRD data. The determination of crystal structures produced by photodimerization is complicated by the disintegration of the crystals as a result of the change in cell volume. PXRD showed that the product is crystalline, but eight possible structures were found with the same overall packing, differing only in orientation of t-butyl ester groups[338]. The agreement with NMR data was quantified using a reduced chi-squared statistic, which consistently ruled out two structures, leaving six with very similar packing motifs. Out of the different NMR data sets evaluated, the ^{1}H shifts, the ^{13}C shifts, and ^{13}C principal values all had similar discriminating power in this case.

A number of studies have combined multiple aspects of NMR crystallography to determine structures from PXRD data. For example, C.I. Pigment Yellow is a commercial pigment with unknown crystal structure and three possible tautomeric forms, labelled CH, NH, OH[135]. IR spectra were inconclusive, solution-state NMR ruled out the CH tautomer, and DFT calculations on isolated molecules indicated that NH tautomer had the lowest energy by about 60 kJ mol⁻¹. Strong scattering from eight Cl atoms per molecule made it impossible to determine the tautomeric state from PXRD. Structure solutions for OH and NH tautomers were geometry optimised. The H changed tautomeric state on optimisation (using PBE), but the given the known limitations of DFT in such cases, noted in Section 2.5.2, energies and NMR parameters were also calculated for H explicitly positioned in 3 alternative sites across the hydrogen bond. ^{13}C spectra failed to distinguish between NH and OH tautomers, while ^{15}N spectra suggested NH. The tautomeric state was proved more definitively using ^{1}H-^{14}N HMQC and ^{13}C,^{1}H HETCOR spectra.
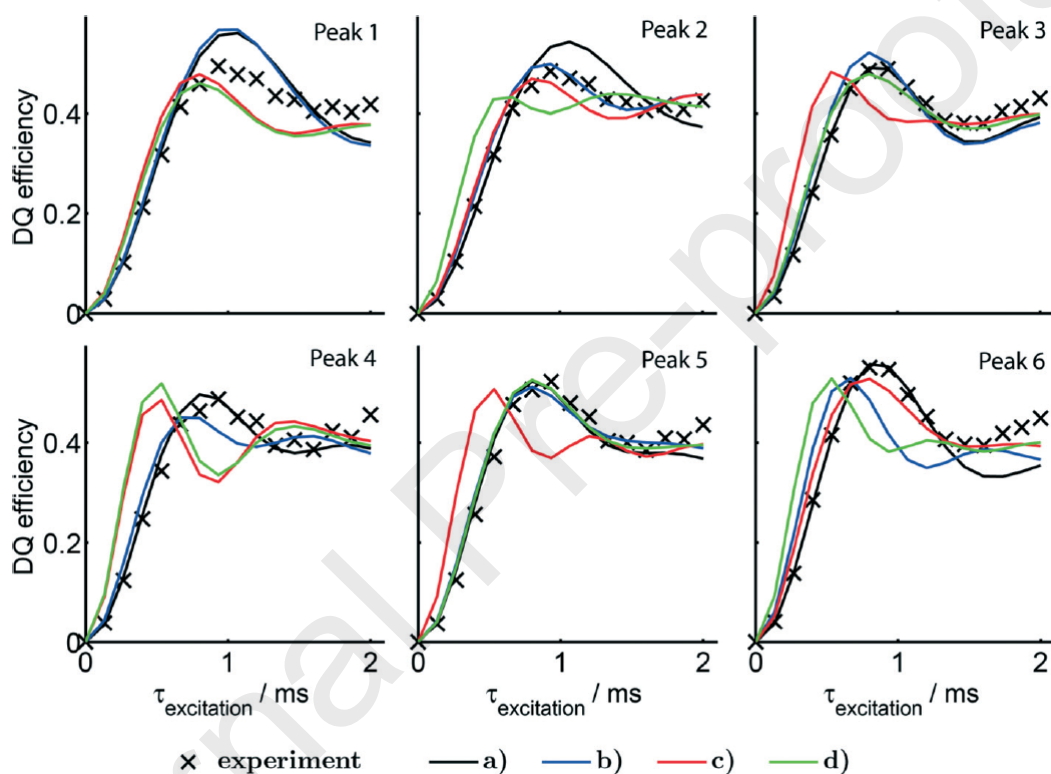

Figure 23 Experimental ^{19}F double-quantum coherence build-up curves plus corresponding simulated curves for four structural models compatible with PXRD data. Model **a** (black line) provided the best overall fit to the NMR data. Figure reproduced from Ref. 339 with permission from The Royal Society of Chemistry.

When solving the structure of 1,3,5-tris(dimethylpropionylamino)benzene, NMR evidence for $Z' = 1$ was used to restrict possible space groups[286]. Reasonable R factors were obtained in four space groups, with the solutions having similar overall packing, but different local arrangements. The compound was ^{13}C labelled at the carbonyl and the build-up of ^{13}C DQ coherence used to exclude two arrangements which involved a significant spread of intermolecular C,C distances. Subsequently one solution was selected that was favoured by multiple metrics. In a similar vein, the crystal structure of a benzene-1,3,5-trisamide with fluorine-substituted t-butyl groups was solved from PXRD data[339]. Indexing of the diffractogram showed $Z = 4$, while the NMR data indicated $Z' >= 2$, helping to identify compatible space groups. The structure was subsequently solved, but the isoelectronic nature of F and Me means that the conformation of the Me$_2$F groups is not well-determined; Rietveld refinement led to four models with equivalent R factors. As shown in Figure 23, build-up curves of ^{19}F DQ/SQ spectra were fitted to models of local arrangement of nine ^{19}F's, allowing one preferred set of orientations to be identified.

It is difficult to use shift information in a direct way to refine crude structures due to the expense of first principles calculation. In a different approach, a pseudo force field (COSMOS) based on isotropic ^{13}C chemical shifts was included in a molecular dynamics simulation to refine proposed structures for I_α form of cellulose[340]; since cellulose is only semi-crystalline, the quality of the diffraction data is limited. This suggested one of two models of the hydrogen-bonding network as being correct, which was verified using ^{13}C tensor information. Section 4 discusses recent machine-learning based approaches to the problem of efficiently estimating chemical shifts.

3.8 *De novo* structures

A more radical approach in NMR crystallography is to try to determine structures directly from NMR data. This is a distinctly non-trivial problem, since NMR data cannot be realistically "inverted" directly to possible crystal structures, and so it is necessary to hypothesise possible structures and evaluate their agreement with NMR data. The difficulty of this task depends on whether information on the unit cell is available. For example, unit cell parameters, plus limited information about likely space groups from systematic absences in the diffraction pattern, can often be obtained from electron or powder diffraction data. In this case, model structures can be generated using the same tools that are applied in solving structures from powder data[341]. On the other hand, if the diffraction data is good enough to obtain lattice cell information, then it will often be possible to solve the structure from the powder data directly, with varying degrees of assistance from NMR, as discussed in previous sections.

If the unit cell is unknown, Crystal Structure Prediction (CSP) techniques must be used to generate possible structures. CSP is a research area in its own right and the interested reader is referred to recent articles by Price[342, 343]. The number of structures found by CSP depends on the computational resources deployed; it is common, for example, to restrict the number of space groups considered to subsets which account for the largest number of organic structures. While semi-empirical force fields are often used at early stages to estimate lattice energies, it is increasingly common to use DFT to refine likely structures and provide more accurate lattice energies. The current status of different methods can be found in the summary of the most recent (6th) blind test of structure prediction[344]. Interestingly participants in the 2nd blind test[345] were provided with simulated, but unindexed, PXRD patterns. This did not, however, significantly improve the chances of identifying correct structure, presumably reflecting the strong sensitivity of powder patterns to lattice parameters.

3.8.1 Structure determination using dipolar couplings

One approach to determining structures based on NMR information has used measurements of ^{1}H spin-diffusion build-up curves. In work on a crystalline dipeptide[346], spin-diffusion build-up curves were measured for the resolved ^{1}H resonances (only two sites were overlapped). The build-up curves were modelled using a kinetic matrix approach, where the rate of exchange between sites i and j is given by

$$k_{ij} = A \left(\frac{\mu_0 \gamma_H^2 \hbar}{4\pi} \right)^2 \sum_m \frac{1}{(r_{ij}^2)_m^n} \tag{4}$$

where, as in Eq. (3) for the RSS dipolar coupling, the sum runs over the distinct nuclei of type j that are coupled to given spin i. (Note that there is a subtle difference in usage of the term "spin diffusion" between solid and solution-state NMR; here, it includes any transfer of magnetisation between spins i and j, whereas when interpreting, say, NOESY data, the term spin diffusion is restricted to magnetisation transfer via intermediate spins.) The exponent, n, was a fitted parameter in initial work[347], but this value is expected to be close to 6, based on observations with ^{1}H linewidths[42, 348]. The A parameter acts as an overall scaling on the rate of spin diffusion, and decreases with increasing spinning rate. The quality of fit between simulated and experimental data was found to converge with the number of ^{1}H spins included up to a radius of 6 Å. This implies that the build-up curves are sensitive to local packing arrangements, without being swamped by the contributions from

69

very remote and structurally irrelevant spins. In follow-up work on the same system[349], molecular

modelling (MM) techniques were used to generate trial structures, which were refined using a total

pseudo-energy of the energy from the MM force field plus a cost function for the deviation from

experimental spin-diffusion data. The resulting ensemble of similar structures was in good agreement

with the known crystal structure. These structures were subsequently geometry optimised using periodic DFT[350], and essentially converged to the experimental crystal structure, as shown in Figure 24. DFT optimisation of the structures significantly improved the agreement with experimental
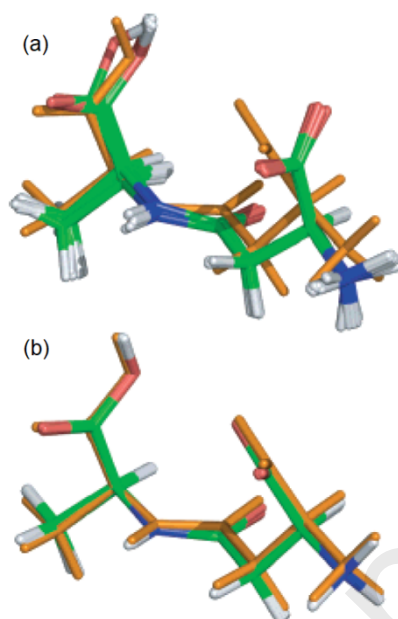

Figure 24 Comparison of the structure of the single molecule in the asymmetric unit of β-L-aspartyl-L-alanine determined by X-ray diffraction (orange structure) and (a) the 16 structures (coloured by element; green C, blue N, red O, white H) obtained from molecular modelling plus ^{1}H spin diffusion data, and (b) the structures obtained after geometry optimisation of these 16 structures. Figure reprinted with permission from Ref. 350, copyright 2007 American Chemical Society.
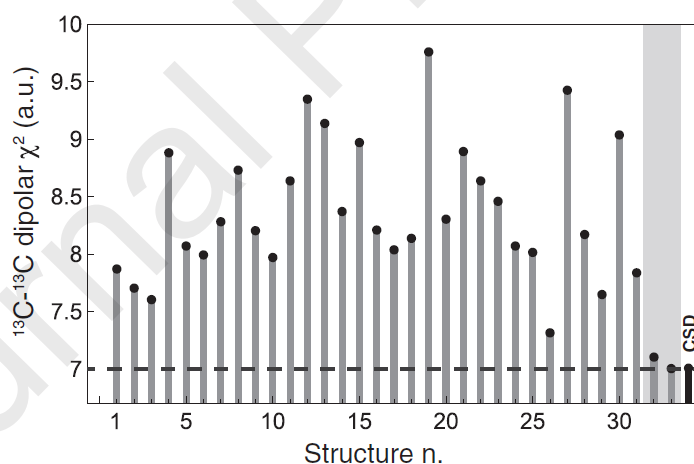

Figure 25 χ^2 parameters for matching ^{13}C double-quantum build-ups between experiment and those calculated for 33 structural models of theophylline obtained by CSP. The structures (32 and 33) showing the best agreement are highlighted in grey, and the dotted line is a guide for the eye identifying the χ^2 minimum. The χ^2 for the CSD structure is also shown for comparison. Figure taken from Ref. 354 © 2019 John Wiley & Sons, Ltd.

chemical shifts (the RMSDs for ^{1}H shifts dropping 2.64 to 0.63 ppm), without significantly affecting agreement with the spin-diffusion data, i.e. refinement against calculated shifts is substantially more precise than using spin-diffusion data. In work on thymol[351], a number of alternative structures were left after DFT refinement. Notably the orientation of a hydroxyl group was not constrained by the spin-diffusion data, but the correct orientation was clearly identified from the RMSD of the ^{1}H chemical shifts, leaving a set of structures with negligible differences (largely in methyl group orientation) and in excellent agreement (0.07 Å RMSD) with the reference diffraction structure.

[13]C, ^{13}C dipolar couplings have also been used to distinguish potential structures. Off-magic-angle spinning was used to measure ^{13}C dipolar couplings in enriched L-alanine and L-histidine[352]. These were generally a good match for RSS couplings determined from the crystal structure. (Note that molecules within a radius of 13 Å needed to be included in the sum to achieve 99% convergence of the RSS coupling.) Rather than use full CSP, artificial unit cells were constructed in different space groups starting with the atomic co-ordinates of the unique molecule in the known unit cell. Although some structures could be clearly ruled out, it was not possible to uniquely identify the correct space group. In related work, ^{13}C,[13]C dipolar couplings were probed using ^{13}C DQ/SQ correlation spectra[353]. Rather than using off-magic-spinning to avoid dipolar truncation, natural abundance samples were used with Dynamic Nuclear Polarisation (DNP) enhancement (see Section 4 for discussion of DNP) to allow the spectra to be obtained in reasonable timescales. The build-up curves could then be fitted to dipolar couplings, and evidence was presented that these could discriminate between different polymorphs. The test system was theophylline, which had proved problematic for structure determination via ^{1}H chemical shifts[192] (see following section). Recent follow-up work has used ^{13}C DQ build-up data to discriminate between a set of 33 candidate structures produced by CSP[354]. Although many build-up curves are dominated by intramolecular distances, there were enough differences across the complete set of build-ups to reduce the choice to two structures with very similar overall packing and unit cells, as shown in Figure 25. These differed in H-bonding arrangements, and so could potentially be distinguished using chemical shifts. As with all dipolar-based methods, calculating the goodness-of-fit to dipolar coupling data takes negligible time compared to calculating shifts, although this advantage largely disappears if DFT is being used to refine initial structures generated by CSP.

[31]P,[13]C REDOR experiments have been used to test candidate structures of four solid forms of *O*-phospho derivatives of serine and threonine[341]. The large gyromagnetic ratio of ^{31}P means that these experiments can probe significantly longer distances (up to 8–10 Å stated) than say between ^{13}C and [1]H. In addition, no isotopic labelling is required, although it was necessary to consider the nearest six P atoms to a given carbon site for the simulated REDOR curves to converge. But this very sensitivity to multiple distances provided good discriminating power. Note that achieving good quantitative agreement between experimental and simulated data required accounting for the significant chemical shift anisotropy (CSA) of ^{31}P, and inhomogeneity of the radio-frequency field. With these precautions, it was clearly possible to discriminate between correct and incorrect candidate structures generated by software, FOX, more typically used to generate structures for fitting PXRD data.

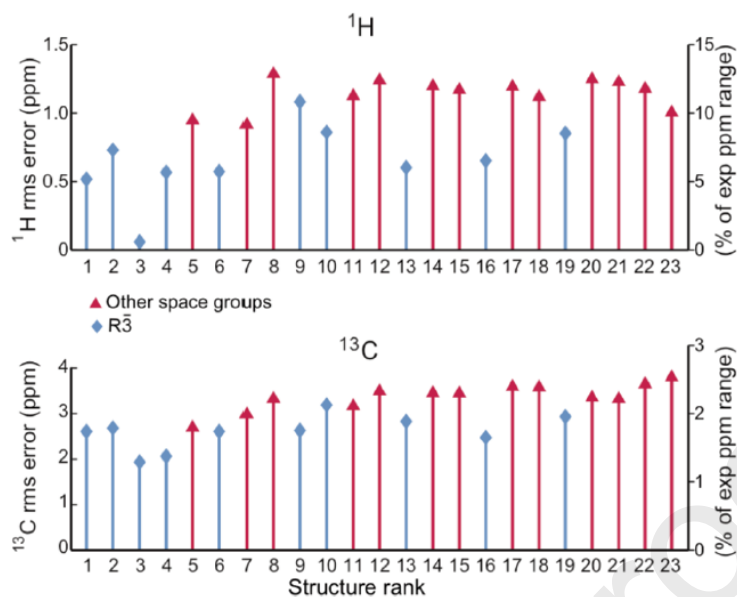*3.8.2 Structure determination using chemical shifts*

Figure 26 Comparison between DFT-calculated and experimental chemical shifts for the 23 lowest-energy structures obtained from CSP of thymol. Figure reprinted with permission from Ref. 133, copyright 2010 American Chemical Society.

Most current *de novo* structure predictions have involved chemical shift data. For example, the structure prediction of thymol was revisited with the aid of ^1H and ^{13}C shifts calculated from the 23 lowest energy (within 10 kJ mol^{-1}) trial structures[133]. Experimental shifts were not assigned, i.e. the GIPAW-predicted order was assumed to match the experimental order. As shown in Figure 26, the correct structure was found to have a much lower ^1H RMSD than the other candidates, while the ^{13}C isotropic shifts failed to clearly distinguish between the candidates. The previously obtained proton spin-diffusion data provided a similar level of discrimination, with the drawback of being technically more demanding and time-consuming to acquire. In later work, a reference set of 15 organic structures was used to establish typical ranges of RMSDs between calculated and experimental shifts, 0.33 ± 0.16 ppm for ^1H, 1.9 ± 0.4 ppm for ^{13}C[192]. These values were then used to determine which NMR data discriminated between trial structures produced by CSP for four drug molecules. In the case of cocaine, the ^1H shifts provided a clear discrimination. For flutamide, the ^1H shifts were also key, although here assignment of the shifts to crystallographic sites was essential for discrimination, since individual aromatic hydrogen sites changed shift depending on intermolecular interactions. Assigned ^1H shifts were also important for flufenamic acid, although in this case four distinct structures fell in the range of potentially valid solutions (note that OH and NH hydrogens were excluded from comparisons due to their temperature dependence). Discrimination between structures was not possible for theophylline, which only has three distinct peaks, although the correct hydrogen bonding pattern could be identified. In general, ^{13}C shifts were insufficient to identify the correct structure. The same methodology was used to predict the structure of a polymorph of a large drug molecule (422 g mol^{-1}) with unknown structure[206]. Good agreement with ^1H shifts was only possible using structures based on a *cis* conformation; CSP predicted the structures with a *trans* conformation to have significantly lower energy, but may have over-estimated the energy difference. A PXRD study independently found the same structure involving the *cis* conformation. Note that assignment is more challenging for *de novo* structure determination since DFT calculations cannot be used to aid assignment prior to the structure being deduced. In this case, even with demanding ^{13}C INADEQUATE experiments, only partial assignment was possible, and all four possible remaining assignments of experimental shifts needed to be considered.

The unknown molecular conformation in the solid state was also an issue in the solution of the structure of decitabine[170]. CSP was used to generate potential structures for three energy-minimised conformers, and shifts calculated for all structures within 10 kJ mol^{-1} of the minimum. One conformer was clearly ruled out by poor agreement with the ^{13}C shifts; as noted previously, ^{13}C shifts are often useful in distinguishing molecular conformations. Selecting structures with a ^{13}C RMSD < 2.0 ppm and ^{1}H RMSD < 0.5 ppm gave two structures which were resolved on the basis of agreement with 2D NMR data (see Figure 4). The result agreed with a structure solution from PXRD. Follow-up work used CSP + NMR to predict the form adopted by decitabine plus sebacic acid crystallising in a polymer matrix[355]. Using the same methodology, the structure of a previously unknown form was predicted, which explained a difference in ^{15}N CP build-up curves between the forms (the previously known form has N...H–N bonds, while the new form does not). The same method was used to predict the form of sebacic acid present, which matched a known structure. Attempts to solve the structure of form I of metergoline form[61] were less successful. CSP failed to find the experimental structure determined from XRD, but the NMR metrics at least clearly indicated that the best-matched CSP structure had markedly poorer statistics (RMSDs of isotropic shifts of 2.98 ppm and 0.85 ppm for ^{13}C and ^{1}H respectively) compared to the XRD structure (RMSDs of 1.38 pm and 0.39 ppm for ^{13}C and ^{1}H respectively).

In a careful study of the role of NMR and PXRD in validating structure solutions, CSP was used to generate potential structures for procyanidin A-2[356]. This is a challenging target, as the crystal structure contains 2 molecules of water per molecule of procyanidin, which itself is large and flexible, with two major torsion angles plus nine rotatable bonds associated with OH groups. Using energies as a function of the major torsion angles from molecular mechanics, seven conformers were used as starting points for CSP, which was restricted to the four space groups in which related molecules were known to crystallise, and to $Z' = 1$ (on the basis that $Z' > 1$ structures are less common when there is more than one molecule in the formula unit). 67 predicted structures were selected for optimisation using DFT, using a threshold of 30 kJ mol^{-1} for each set of structures with a given conformation and space group. The energy rankings provided by dispersion-corrected DFT and the more empirical force field used in the CSP were quite different (e.g. the lowest energy structure by DFT was ranked 52nd by its CSP-predicted energy). Assigned ^{1}H isotropic shifts and ^{13}C shift tensor principal values were used to judge the validity of the solutions. The ^{1}H shifts clearly identified one conformer, while the ^{13}C chemical shift (including individual tensor components) were much more ambiguous in the metrics used (correlation coefficients). Further insight was provided by PXRD; having narrowed the solutions
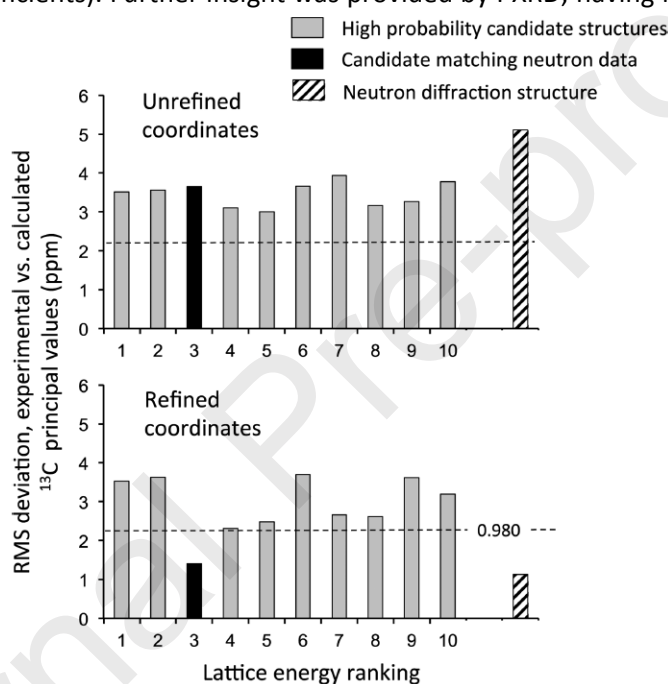

Figure 27 Agreement between experimental and calculated ^{13}C NMR shift tensor principal values for 10 CSP structures of methyl β-D-xylopyranoside. (Top) calculation of shifts within the full crystal structure without optimisation did not allow the correct structure to be identified. (Bottom) the minor bond length and conformational changes on geometry optimisation, however, allowed the correct structure to be selected unambiguously, all other structures being rejected with greater than 98% confidence, as indicated. Note how the NMR agreement for the neutron diffraction structure also improved significantly on optimisation. Figure reprinted with permission from Ref. 358, copyright 2013 American Chemical Society.

to four structures with the same conformation, the agreement of calculated patterns was clearly much better for one of the space groups, allowing the likely space group to be identified without needing to index the powder pattern. Note that it was not possible to distinguish between the different conformations using PXRD alone, i.e. the ^{1}H NMR and PXRD data is strongly complementary. Indeed, insight from both techniques was ultimately necessary to identify the most plausible structure. The final solution was in good overall agreement with the SCXRD structure, but differed in the positioning of some OH groups, which were not considered in the conformational search due to the computational expense of considering all 11 rotatable bonds.

In early work using chemical shift tensor information to improve the quality of CSP predictions[357], considering the agreement between ^{13}C tensor information measured experimentally and calculated

on isolated molecules made it significantly easier to identify the correct structures of four methyl glucosides, although the correct structure was not consistently identified. A follow-up study used GIPAW calculations to optimise and calculate principal values of ^{13}C shift tensors for the 55 structures that had given reasonable fits to tensor values calculated for isolated molecules[358]. As shown in Figure 27, the correct structure was consistently identified once lattice effects were incorporated. Considering just isotropic shifts considerably worsened the discriminating power (three incorrect structures were retained using a 2 standard deviation cut-off criterion), although the correct structure consistently had the lowest RMSD agreement. The optimisation of the geometry under periodic boundary conditions was found to have the largest effect, with the direct effect of neighbouring molecules on chemical shifts estimated to be only ~1 ppm in these systems (where aromatic ring currents are not present). The limited range of chemical environments probably explains the very small ^{13}C shift RMSDs observed in this case.

An example of using CSP + NMR to determine complex structures is a study of a self-assembled material that precipitates from a solution of starting components on exposure to CO_2[289]. The structure cannot be characterised by diffraction methods, particularly since it incorporates a significant fraction of water (15%) and has considerable flexibility, which makes it challenging for CSP. A combination of ^{15}N and ^{13}C experiments (using a partially labelled sample), assisted by DNP enhancement, allowed assignment of the resonances, while cross-peaks in a $^{13}C,^1H$ HETCOR spectrum allowed the value of key torsion angle to be identified. Six trial structures were generated with different stereochemistry, half in agreement with NMR data, and the others deliberately chosen to disagree. These were used as input for CSP structure generation, leading to eight candidate structures which were then relaxed via periodic DFT prior to calculation of NMR parameters. As observed elsewhere, ^{13}C isotropic shifts were not very discriminating, although ^{13}C shift anisotropies clearly ruled out two candidates. One structure was identified that had the lowest overall calculated energy, best fitted the ^1H NMR parameters, and was also compatible with the HETCOR data. Note that comparison of PXRD patterns calculated from the relaxed candidate structures with experiment was uninformative, the incomplete description of the structure (missing the water and the disorder) preventing meaningful comparison.

In addition to examples where desolvated structures have been proposed on the basis of removing solvent molecules from a known solvate structure (see Section 3.4.2), there are cases where structures have been proposed without using CSP techniques. For example, the crystal structure of atorvastatin calcium is unknown, but is challenging for NMR crystallography as $Z' = 2$[217]. The crystallographic splittings are relatively large (up to 8.2 ppm) and are largest for carbons close to the carboxylate, suggesting that the co-ordination of the molecules to the Ca^{2+} ion (via the carboxylate) may be significantly different. A search of the CSD for similar co-ordination environments (Ca^{2+}, carboxylate and water) led to calcium benzoate, and a model was constructed by replacing benzoate with atorvastatin in its conformation observed in an enzyme drug complex. Long-range correlations from $^{13}C,^1H$ HETCOR were used to propose modified orientations for the two hydroxyl groups, prior to optimisation. The predicted crystallographic splittings were a much better match for this model (RMSD of 1.2 ppm over the 33 sites) compared to 2.7 ppm with the original OH positions, and 2.8 ppm when using a different starting structure (based on calcium acetate). Again, correct positioning of OH groups is seen to be critical. Endomorphin-2-OH crystallises with $Z' = 2$ and seven molecules of water in the asymmetric unit (ASU), and dehydrates to form 2 with an estimated three waters[60]. HETCOR shows a similar H-bonding environment around the carbonyl in the two forms, implying retention of water involved in bridging the two unique molecules in the ASU. Full CSP was judged impractical, as were GIPAW calculations on the 35 possible structures obtained by removing four water molecules. Gaussian-type calculations of molecular clusters were used to predict changes in ^{15}N shift tensors, which proved more discriminating than ^{13}C shift tensor values (which were affected by overlap and dynamics). Five structures were selected for GIPAW calculations, and one arrangement was selected as most plausible based on overall agreement of all data.

In an example of a modified-CSP approach, genetic algorithms (GAs) were used to generate crystal structures from amoxicillin trihydrate by minimising the lattice energy (estimated using an atomistic force field with partial atomic charges calculated on amoxicillin) with an additional penalty function based on the deviation of calculated chemical ^{1}H shifts from experiments[191]. Semi-empirical techniques were used to efficiently estimate chemical shifts for an extended cluster (27 unit cells), and a flat-bottomed potential allowed shifts to vary by ±0.25 ppm without penalty. This independent "force" allowed the GA to converge significantly more rapidly, with the chemical shift playing a smaller role as the structures converged; the chemical shift penalty essentially reduces the chance of being trapped in a local minimum. The best 100 structures were optimised using an approximate, but efficient, DFT method ("tight-binding DFT"[359]). The resulting structures showed extensive variation in the water positions, but much less so for the drug molecule, and the structure with significantly lower energy was a good match (RSMD of 0.61 Å over a unit cell) with the known crystal structure. Note, however, that this known crystal structure was exploited in two steps; assignment of ^{13}C and ^{1}H chemical shifts, and fine-tuning of the parameters of the semi-empirical calculation of the ^{1}H shifts.

Although the challenges of crystal structure prediction should not be underestimated, it is clear that the sensitivity of NMR chemical shifts both to the overall structure and individual atomic movements makes it an ideal tool to monitor the agreement between proposed and experimental structures.

3.9 NMR crystallography of disordered materials

NMR is particularly valuable when dealing with materials that are not simple ordered crystals. Diffraction data quickly become ambiguous when the order is insufficiently long-range. For instance, heavy milling of crystalline forms is often said to result in "amorphisation", when all that may have happened is that the particles are too small to give observable X-ray diffraction peaks; NMR will clearly distinguish between a milled crystalline product and a truly amorphous material (e.g. produced by quench cooling of a melt). Ref. [360] and the praziquantel example[317] discussed in Section 3.6.1 are examples of poorly crystalline materials giving well-resolved NMR spectra. NMR also clearly distinguishes between "dynamic disorder", resulting from atomic movements, and "static disorder" due to irregular packing, as these have characteristically different effects on lineshapes. Particularly in the case of dynamics, a wide variety of NMR observables, such as relaxation rates, can be used to characterise the underlying molecular processes; the use of dipolar couplings to observe dynamics was highlighted at the end of Section 2.1. The various techniques classically used to characterise disorder and dynamics in solids have been extensively discussed[25, 361, 362], while relevant review articles include an extensive survey of NMR applied to disordered solids[363], and a review of NMR applied to amorphous solid dispersions[364], i.e. heterogeneous materials involving an API plus excipients. Here we limit discussion to how the NMR crystallographic techniques discussed in the previous sections have been adapted to materials containing disorder.

The presence of disorder often introduces effective additional symmetry. For example, in a set of essentially isomorphous solvates of droperidol, Z' could be either 1 or 2 depending on whether the solvent was disordered (creating a pseudo-inversion centre) or not[327]. In practice, however, strong susceptibility broadenings meant that ^{13}C NMR spectra could not clearly distinguish between ordered vs. disordered solvent arrangements. GIPAW calculations were very helpful in demonstrating that the effects of solvent ordering were small, and confirming that a small (1.0 ppm) splitting observed in ^{15}N spectra was consistent with a $Z' = 2$ ordered structure. First-principles calculations were also used to show that the disordered structures were associated with small differences in energy for inverting the solvent orientation. A similar entropy-driven preference for a disordered structure was also established computationally for the caffeine citric acid cocrystal[128] considered previously in Section 2.4.4. An apparent reduction of Z' from 2 to 1 due to dynamic averaging was also discussed above in the context of structures being solved from crystal structure prediction methods[365]; the averaging introduced by the dynamics significantly reduced the discriminating power of the NMR measurements. In the characterisation of a high temperature phase of barbituric acid, ^{13}C NMR straightforwardly confirms keto vs. enol tautomeric state, while ^{1}H NMR shows the phase is highly dynamic[366]. Note that neutron diffraction was needed to determine the space group since XRD was unable to distinguish between models of the dynamics that exchanged the isoelectronic groups CH_2 and NH.
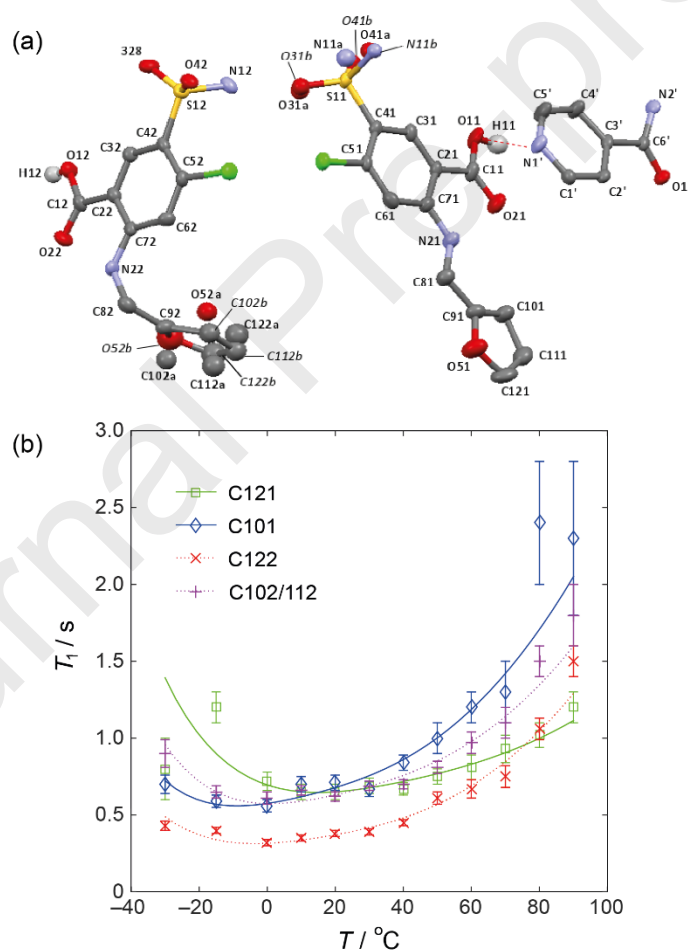
Figure 28 (a) The asymmetric unit of a furosemide-isonicotinamide cocrystal with the minor occupied furan ring and sulphonamide positions drawn as free atoms (correcting a typographical error in original reference), and with most hydrogen atoms removed for clarity. Thermal ellipsoids are shown at the 50% probability level. (b) Temperature dependence of the ^{13}C T_1 relaxation times for the furan ring carbons. Fitting of this data shows the dynamics of the two distinct rings are the same within experimental error, apparently contradicting the structure in (a) in which only one ring is significantly disordered. Figure adapted from data published in Ref. 173, licensed under CC BY 3.0.

In other cases, localised dynamics leads to more subtle changes in the structure observed by diffraction methods. A nice example is a cocrystal of the drug furosemide in which one of the two crystallographically distinct furan rings had been modelled with large-amplitude disorder while the other was modelled without disorder[173]. As shown in Figure 28, ^{13}C relaxation measurements showed that both rings exhibited the same, small-angle libration-type motion, and re-fitting of the XRD data showed that the modelling of the diffraction data was fundamentally ambiguous. In the case of methyl α-L-rhamnofuranoside, the disorder in the structure was readily established to be dynamic by NMR, involving rates on the order of kHz, and slow enough to see multiple peaks per carbon site[367]. 66 molecular conformations were considered and the agreement of ^{13}C NMR shift tensor principal components assessed. It was not, however, feasible to assign individual resonances to a given conformation. Six conformations were judged to be compatible with NMR data, suggesting that the disorder primarily involved re-orientation of a hydroxyl group, a process known in other sugars, but generally too fast to be observed in NMR spectra.

The effects of dynamics are now commonly observed from outliers between calculated and experimental shifts. For example, a 37 ppm discrepancy on an individual ^{13}C shift of an acetic acid solvate of terbutaline sulfate highlighted an unrealistic geometry[368]. A new SCXRD study revealed a mistake in the modelling of the disorder on one acetic acid, and that minor disorder on another hydroxyl group had been missed. ^{13}C shifts calculated after H-only optimisation of the new structure (averaging over the major disorder) showed much better agreement with experiment. Full geometry optimisation further improved agreement, but care is needed when comparing shifts calculated at 0 K to experimental shifts that are clearly influenced by dynamics. Other examples where full optimisation was needed to obtain agreement between calculated and experimental data associated with dynamic fragments include Refs. [92, 187, 369]. In all cases, geometry optimisation resulted in improved agreement and more chemically reasonable bond lengths. Dynamics of groups, such as phenyl rings, also show up as discrepancies between observed and calculated chemical shift anisotropies[59, 370], where this may not observable from isotropic shifts.

Dynamic behaviour is frequently observed in solvate materials, as in the case of sildenafil citrate considered previously[189]. For example, NMR crystallography approaches helped to understand the hydration behaviour of a pharmaceutical material in which the structures of the two key phases provided little insight into the differences in their hydration behaviour[371]. ^{13}C NMR of the HyA phase showed single resonances, consistent with rapid exchange of water molecules between (inequivalent) hydration sites, but the spectra became more complex at low relative humidity. DFT was used to calculate shifts for structures with waters in different sites, and most variation was seen in the calculated shifts where peak splitting was observed experimentally. The DFT calculations and experimental measurements thus helped to provide a consistent understanding of the hydration behaviour. In the case of (+)-catechin, only the structure of the "full" hydrate is available from an NMR crystallographic study discussed previously[180], but there are at (?) least two "lower" hydrates, a crystalline form with 2.5–3 water molecules per formula unit, and a disordered form[197]. Dehydrate structures were produced by removing water molecules from different sites in the 4.5 hydrate (giving 21 structures), and CSP was also used to predict structures of 1-, 2- and 3- hydrates. The lowest energy structures (within 20 kJ mol^{-1} of minimum for each hydrate) from CSP plus the 21 "manual" structures were optimised by GIPAW and calculated shifts compared to experiment, including ^{13}C tensor principal component data. Some carbons showed distinct changes in tensor components that were not apparent in isotropic shifts, i.e. the tensor information increases the chance of observing measurable effects. Two of the "manual" structures were judged to show reasonable agreement with NMR data (although comparison was complicated by the lack of dispersion correction on optimisation, resulting in unit cells that were consistently too large). Given the low number of candidate structures considered (a total of five), it is perhaps not surprising that the correct structure was not identified from CSP.
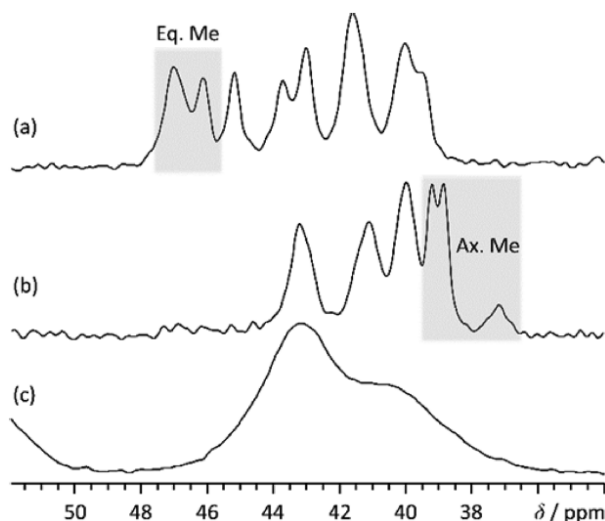
Figure 29 Low frequency region of the ¹³C CP/MAS NMR spectra of forms of the drug tenapanor, with shift ranges associated with methyl group carbons highlighted in grey: (a) anhydrous form, (b) HCl salt and (c) amorphous form of the salt. The different shift ranges of methyl groups in axial vs. equatorial conformations show that the amorphous form has a similar conformational distribution to the salt. Figure reprinted with permission from Ref. 372, copyright 2018 American Chemical Society.

NMR crystallography has also been widely applied to materials exhibiting static disorder. For example, the structure of ranitidine hydrochloride form II shows conformational disorder with *E* vs. *Z*-type conformations[214]. The initial unit cell was doubled in order to accommodate the observed disorder. Calculated lattice energies (including vibrational corrections) of single conformer arrangements were significantly higher than that of form I, but mixed conformations had comparable energy, leading to a revised model with a mix of these similar energy configurations. The PXRD data was unable to distinguish between the initial and revised model, while the experimental ¹³C NMR showed broadenings at low frequency which are compatible with revised model, and the calculated shifts clearly ruled out some packing arrangements (as well as correcting a previous literature assignment). Far-IR spectra provided supportive evidence, but was less clear cut than the ¹³C NMR, while variable temperature inelastic neutron scattering combined with DFT-MD simulations permitted further discrimination between structural models. Conformational disorder was also observed in the structures of a large, and conformationally flexible drug, tenapanor[372]. DNP-enhanced INADEQUATE was used to assign most (37/50) of the ¹³C resonances, and the structure determined from PXRD was validated by ¹³C and ¹H shifts. As shown in Figure 29, different ring conformations were observed for the hydrochloride salt and free base, with DFT-predicted shifts showing distinct ranges for equatorial vs. axial methyl groups depending on conformation, allowing the conformational distribution in an amorphous form of the salt to be determined. This molecular-level information provided a route to reliably forming and stabilising the amorphous form.

Obtaining a structure for the anhydrate phase of orotic acid was challenging due to the presence of disorder, indicated by significant diffuse scattering in the XRD data[373]; depending on the dehydration conditions, broad peaks with differing linewidths were observed in PXRD patterns. ¹³C and ¹⁵N solid-state NMR showed the structure of the anhydrate forms was essentially the same, with only small differences in peak shape (these were clearer in the ¹⁵N spectra). Since the quality of the diffraction data was too poor to allow the structure to be determined directly, CSP was used to predict the anhydrate structure. The proposed structure fitted the PXRD data, and the disorder was rationalised in terms of stacking faults, with the degree of faulting varying with preparation conditions. Diffraction methods have similar problems characterising the solid solutions formed between 5-fluorouracil and thymine[374]. PXRD shows two distinct forms, depending on stoichiometry, and SCXRD of form I showed disordered occupancy of two molecular sites in the asymmetric unit, but with a distinct preference for one site to be occupied by the F of fluorouracil rather than the CH_3 of thymine.

83

This behaviour was also seen in the ^{19}F NMR spectra, although ^{13}C NMR spectra had more structure than would be expected for a simple random disorder, implying that a larger repeating unit would be needed to more completely model the disorder.

The additional parameters provided by measuring ^{13}C shift principal components have been valuable in discriminating between alternative structures affected by disorder. For example, various structures have been proposed for the highly crystalline α form of poly(L-lactide) from wide-angle X-ray and neutron diffraction studies, but the structural quality is limited (e.g. *R* factors about 20%), associated with the limited number of observed reflections (< 100) in these partially crystalline materials. Four models were constructed from initial structures from both X-ray and neutron diffraction. Good agreement with the NMR data was found for only one of the models, a neutron structure where all the atomic coordinates had been relaxed by DFT, confirming the ability of NMR crystallography to distinguish between alternative structural models[375].

In a rare example of a quantitative treatment of static disorder, ^{31}P lineshapes were used to characterise static disorder in a biphosphinoamine[376]. The spectra were assigned using DQ/SQ correlation experiments and synthetic 2D spectra derived from calculated shifts. 2D SQ/SQ spin diffusion spectra showed elongated lines at short mixing times, characteristic of correlations between local chemical shifts[377], but the peaks became more rounded as the mixing time increased. This ruled out the possibility that the broadenings in the 2D spectra are due to susceptibility effects[102], and shows that the disorder is extremely local. The disorder was modelled using chemical shifts calculated for isolated molecules as a function of different vibrational co-ordinates. Some vibrational modes could be discarded as the predicted effects have the wrong sign to match the experiments. The amplitudes of the motions needed to reproduce the experimental shift variations were very small (up to 2°) and compatible with the size of the thermal ellipsoids.

4 Looking forward

Solid-state NMR has often been seen as a technique of last resort, to be attempted if a material is sufficiently disordered or heterogeneous for characterisation by diffraction methods. The developments in methodology discussed above, coupled with growing use of solid-state NMR as a mainstream characterisation technique, have transformed this situation. It remains the case, however, that NMR is most widely applied for those problems where X-ray diffraction struggles. For example, an array of approaches, based on both dipolar couplings and chemical shifts, can be applied to clarify the position of hydrogen atoms (Section 3.2). Similarly, NMR is unrivalled in its ability to probe disorder, whether static or dynamic, at the atomic level – applications that could only be touched on in Section 3.9 for reasons of space.

The major advance in recent decades has come from the ability to calculate chemical shifts in the solid state with reasonable accuracy and with reasonable computational effort. Trying to use chemical shift information using empirical rules has historically been a risky business, given the number of factors that affect the chemical shift in the solid state; this review has highlighted a number of cases where chemical shifts have unusual values, generally due to strong intermolecular effects. Being able to predict chemical shifts for a given crystal structure has allowed us to move beyond using the NMR spectrum solely as a fingerprint of a particular solid form. For example, the strength of intermolecular interactions can be assessed quantitatively via changes in chemical shifts (Section 3.4). Moreover, the abundance of shift information routinely available for organic molecules (^{13}C shifts, ^{1}H shifts, anisotropies as well as isotropic values) provides many more "points of contact" between predicted and experimental results, compared to, for example, dipolar-coupling based techniques. Although dipolar-based approaches have proved their worth in specific cases, for example, in establishing N protonation states, recent progress in structure determination from NMR data has been dominated by chemical shift based approaches (Section 3.8.2).

There are, however, a number of significant challenges and open questions. In contrast to X-ray diffraction, where increasingly brilliant light sources can be used improve data quality, the sensitivity

of conventional NMR is limited by the intrinsically small population difference of the nuclear spin states at thermal equilibrium. Unless isotopically enriched samples are available (which is generally only practical for biomolecular systems), the sophisticated multi-dimensional techniques that are used in biomolecular systems have only been practical in isolated favourable cases. This, in turn, limits the complexity of the systems that can be tackled. Recent developments, however, in dynamic nuclear polarisation (DNP) techniques for transferring the much larger Boltzmann polarisation of unpaired electron spins to nuclear spins, could potentially change this picture dramatically. DNP has significant practical challenges, but recent demonstrations that DNP can be successfully applied to a variety of pharmaceutical materials are very encouraging[378]. Examples of using DNP-enhanced spectra in NMR crystallography can be found in Refs. [289, 353, 372], discussed previously.

Being able to predict chemical shifts for a given structure has been invaluable both for validating crystal structures obtained from diffraction techniques (see Sections 3.3 and 3.6). But incorporating NMR data directly into the structure solution process, e.g. as a constraint during Rietveld refinement of powder data, is complicated by the computational effort required for first-principles calculations. Dipolar couplings can be calculated very quickly for a given model, and have been used with some success in structure solution (Section 3.8.1), but the greater discriminating power of chemical shift information means that efficient techniques to estimate chemical shifts for a trial structure are highly desirable, and some examples have been discussed previously[191, 379]. More recently a Machine Learning (ML) model was developed using GIPAW-calculated shifts on 2000 crystal structures of molecules containing CNHO[380]. Excellent agreement was obtained for the shifts predicted by this model on an independent test set of 500 calculated results; the RMSD on ^{1}H isotropic shifts was 0.49 ppm, compared to about 0.4 ppm expected between GIPAW calculations and experiment. The discriminating power (between correct and next-best solution) was slightly worse for the ML-predicted shifts compared to full DFT-calculated shifts, and the ML model would be less effective in cases where ^{13}C shifts are necessary (the RMSD for ^{13}C isotropic shifts was 4.3 ppm, about twice as large as that expected for DFT-calculated shifts). Ideally, ML models would be trained on experimental shift data, but this would require a large database of robustly assigned chemical shifts covering a wide range of chemical functionality.

NMR crystallography (and structural characterisation in general) is more difficult in situations where initial model structures are not available. Hence NMR studies are increasingly coupled to CSP methods to provide possible structures that can be tested against experimental data (see Section 3.8). CSP is a hard, but actively researched, scientific problem, and so we can hope to see the combination of NMR studies and CSP becoming more widely adopted. Understanding disordered structures is a similarly open research problem, with multiple challenges, e.g. both producing model structures, and calculating NMR parameters for systems without long-range order. NMR has a particularly powerful role here, due to the sensitivity of parameters such as dipolar coupling and chemical shift to local environment. As discussed in Section 3.5, NMR can provide information on molecular conformation, irrespective of the degree of long-range ordering. Fragment-based approaches to DFT (see Section 2.5.2) and ML methods may be particularly useful since these do not require periodic boundary conditions; a good recent example is the application of an ML model trained on shifts calculated from representative crystalline structures to predict shift distributions in amorphous silicates[381].

This review has considered the various ways in which NMR has been applied to crystalline (and some not-so-crystalline) materials, with the aim of demonstrating the insight that can be provided using now-standard solid-state NMR spectrometers and computational chemistry techniques. As both experimental and computational techniques develop, we hope that the wider crystallographic community will come to embrace NMR crystallography as a natural complement to diffraction-based approaches.

5 Acknowledgements

[1] G.E. Pake, Nuclear Resonance Absorption in Hydrated Crystals - Fine Structure of the Proton Line, J. Chem. Phys., 16 (1948) 327-336.

[2] Report of the Executive Committee for 1991, Acta Crystallographica Section A, 48 (1992) 922-946.

[3] D.L. Bryce, F. Taulelle, NMR Crystallography, Acta Cryst. C, 73 (2017) 126-127.

[4] L. Mafra, Preface, Solid State Nucl. Magn. Reson., 65 (2015) 1.

[5] J.A. Ripmeester, R.E. Wasylishen, NMR crystallography, CrystEngComm, 15 (2013) 8598-8598.

[6] NMR Crystallography, R.K. Harris, R.E. Wasylishen, M.J. Duer (Eds.), Wiley, 2009.

[7] M. Dacombe, Report of the Executive Committee for 2014, Acta Cryst. A, 72 (2016) 412-455.

[8] D.L. Bryce, NMR crystallography: structure and properties of materials from solid-state nuclear magnetic resonance observables, IUCrJ, 4 (2017) 350-359.

[9] C. Martineau, J. Senker, F. Taulelle, NMR crystallography, in: Annu. Rep. NMR Spect., Elsevier, 2014, pp. 1-57.

[10] S.E. Ashbrook, D. McKay, Combining solid-state NMR spectroscopy with first-principles calculations–a guide to NMR crystallography, Chem. Commun., 52 (2016) 7186-7204.

[11] S.E. Ashbrook, D.M. Dawson, V.R. Seymour, Recent developments in solid-state NMR spectroscopy of crystalline microporous materials, Phys. Chem. Chem. Phys., 16 (2014) 8223-8242.

[12] M. Dračínský, P. Hodgkinson, Solid-state NMR studies of nucleic acid components, RSC Adv., 5 (2015) 12300-12310.

[13] A. Jeziorna, S. Kazmierski, P. Paluch, E. Skorupska, M.J. Potrzebowski, Recent Progress in the Solid-State NMR Studies of Short Peptides: Techniques, Structure and Dynamics, in: Annu. Rep. NMR Spect., Elsevier, 2014, pp. 67-143.

[14] C. Martineau, NMR crystallography: applications to inorganic materials, Solid State Nucl. Magn. Reson., 63 (2014) 1-12.

[15] P.C. Vioglio, M.R. Chierotti, R. Gobetto, Pharmaceutical aspects of salt and cocrystal forms of APIs and characterization challenges, Advanced Drug Delivery Reviews, 117 (2017) 86-110.

[16] F.G. Vogt, Evolution of solid-state NMR in pharmaceutical analysis, Future Med. Chem., 2 (2010) 915-921.

[17] M.R. Chierotti, R. Gobetto, Solid-state NMR studies of weak interactions in supramolecular systems, Chem. Commun., (2008) 1621-1634.

[18] B.G. Caulkins, R.P. Young, R.A. Kudla, C. Yang, T.J. Bittbauer, B. Bastin, E. Hilario, L. Fan, M.J. Marsella, M.F. Dunn, NMR crystallography of a carbanionic intermediate in tryptophan synthase: chemical structure, tautomerization, and reaction specificity, J. Am. Chem. Soc., 138 (2016) 15214-15226.

[19] J. Bauer, S. Spanton, R. Henry, J. Quick, W. Dziki, W. Porter, J. Morris, Ritonavir: an extraordinary example of conformational polymorphism, Pharm. Res., 18 (2001) 859-866.

[20] I.B. Rietveld, R. Céolin, Rotigotine: Unexpected polymorphism with predictable overall monotropic behavior, J. Pharm. Sci., 104 (2015) 4117-4122.

[21] Polymorphism in pharmaceutical solids, H.G. Brittain (Ed.), Marcel Dekker, Inc., New York, 1999.

[22] Polymorphism: in the Pharmaceutical Industry, R. Hilfiker (Ed.), Wiley-VCH, Weinheim.

[23] Solid state characterization of pharmaceuticals, R.A. Storey, I. Ymen (Eds.), John Wiley & Sons, 2011.

[24] M.J. Duer, Introduction to solid-state NMR spectroscopy, Wiley-Blackwell, 2005.

[25] D.C. Apperley, R.K. Harris, P. Hodgkinson, Solid-State NMR: Basic Principles and Practice, Momentum Press, New York, 2012.

[26] G. Kervern, A. D'Aléo, L. Toupet, O. Maury, L. Emsley, G. Pintacuda, Crystal-Structure Determination of Powdered Paramagnetic Lanthanide Complexes by Proton NMR Spectroscopy, Angew. Chem. Int. Ed., 48 (2009) 3082-3086.

[27] T. Wittmann, A. Mondal, C.B.L. Tschense, J.J. Wittmann, O. Klimm, R. Siegel, B. Corzilius, B. Weber, M. Kaupp, J. Senker, Probing Interactions of N-Donor Molecules with Open Metal Sites within Paramagnetic Cr-MIL-101: A Solid-State NMR Spectroscopic and Density Functional Theory Study, J. Am. Chem. Soc., 140 (2018) 2135-2144.

[28] M.A. Shaibat, L.B. Casabianca, D.Y. Siberio-Pérez, A.J. Matzger, Y. Ishii, Distinguishing polymorphs of the semiconducting pigment copper phthalocyanine by solid-state NMR and Raman spectroscopy, J. Phys. Chem. B, 114 (2010) 4400-4406.

[29] C. Luchinat, G. Parigi, E. Ravera, M. Rinaldelli, Solid-state NMR crystallography through paramagnetic restraints, J. Am. Chem. Soc., 134 (2012) 5006-5009.

[30] A. Bhaumik, C. Luchinat, G. Parigi, E. Ravera, M. Rinaldelli, NMR crystallography on paramagnetic systems: solved and open issues, CrystEngComm, 15 (2013) 8639-8656.

[31] P. Amornsakchai, P. Hodgkinson, R.K. Harris, NMR studies of ^{31}P, ^{1}H spin pairs in solid tin(II) phosphite and tin(II) hydrogen phosphate, Mol. Phys., 102 (2004) 877-882.

[32] L. Seyfarth, J. Senker, An NMR crystallographic approach for the determination of the hydrogen substructure of nitrogen bonded protons, Phys. Chem. Chem. Phys., 11 (2009) 3522-3531.

[33] T. Gullion, J. Schaefer, Rotational-echo Double-Resonance NMR, J. Magn. Reson., 81 (1989) 196-200.

[34] X. Zhao, J.L. Sudmeier, W.W. Bachovchin, M.H. Levitt, Measurement of NH bond lengths by fast magic-angle spinning solid-state NMR spectroscopy: A new method for the quantification of hydrogen bonds, J. Am. Chem. Soc., 123 (2001) 11097-11098.

[35] I. Schnell, K. Saalwächter, ^{15}N-^{1}H Bond Length Determination in Natural Abundance by Inverse Detection in Fast-MAS Solid-State NMR Spectroscopy, J. Am. Chem. Soc., 124 (2002) 10938-10939.

[36] P. Paluch, T. Pawlak, J.-P. Amoureux, M.J. Potrzebowski, Simple and accurate determination of X--H distances under ultra-fast MAS NMR, J. Magn. Reson., 233 (2013) 56-63.

[37] J.W. Emsley, J.C. Lindon, NMR Spectroscopy Using Liquid Crystal Solvents, Pergamon Press, 1975.

[38] D.A. Case, Calculations of NMR dipolar coupling strengths in model peptides, J. Biomol. NMR, 15 (1999) 95-102.

[39] Y. Ishii, T. Terao, S. Hayashi, Theory and simulation of vibrational effects on structural measurements by solid-state nuclear magnetic resonance, J. Chem. Phys., 107 (1997) 2760-2774.

[40] P. Hodgkinson, L. Emsley, The Accuracy of Distance Measurements in Solid-State NMR, J. Magn. Reson., 139 (1999) 46-59.

[41] M.J. Bayro, M. Huber, R. Ramachandran, T.C. Davenport, B.H. Meier, M. Ernst, R.G. Griffin, Dipolar truncation in magic-angle spinning NMR recoupling experiments, J. Chem. Phys., 130 (2009) 114506.

[42] V.E. Zorin, S.P. Brown, P. Hodgkinson, Quantification of homonuclear dipolar coupling from magic-angle spinning ^{1}H NMR, Mol. Phys., 104 (2006) 293-304.

[43] P. Thureau, G. Mollica, F. Ziarelli, S. Viel, Solid-State ^{1}H NMR Studies of Homonuclear Dipolar Couplings, in: Annu. Rep. NMR Spect., Elsevier, 2014, pp. 217-249.

[44] K. Saalwächter, Robust NMR approaches for the determination of homonuclear dipole–dipole coupling constants in studies of solid materials and biomolecules, ChemPhysChem, 14 (2013) 3000-3014.

[45] S.P. Brown, High-resolution ^{1}H 2D Magic-angle Spinning Techniques for Organic Solids, in: P. Hodgkinson (Ed.) Modern Methods in Solid-state NMR: A Practitioner's Guide, The Royal Society of Chemistry, 2018, pp. 39-74.

[46] S.P. Brown, Applications of high-resolution ^{1}H solid-state NMR, Solid State Nucl. Magn. Reson., 41 (2012) 1-27.

[47] T. Gorelik, G. Matveeva, U. Kolb, T. Schleuß, A.F. Kilbinger, J. van de Streek, A. Bohle, G. Brunklaus, H-bonding schemes of di-and tri-*p*-benzamides assessed by a combination of electron diffraction, X-ray powder diffraction and solid-state NMR, CrystEngComm, 12 (2010) 1824-1832.

[48] S.P. Brown, Probing proton-proton proximities in the solid state, Prog. Nucl. Magn. Reson. Spectrosc., (2007) 199-251.

[49] E. Carignani, S. Borsacchi, J.P. Bradley, S.P. Brown, M. Geppi, Strong intermolecular ring current influence on ^{1}H chemical shifts in two crystalline forms of naproxen: a combined solid-state NMR and DFT study, J. Phys. Chem. C, 117 (2013) 17731-17740.

[50] M. Sardo, S.M. Santos, A.A. Babaryk, C. López, I. Alkorta, J. Elguero, R.M. Claramunt, L. Mafra, Diazole-based powdered cocrystal featuring a helical hydrogen-bonded network: Structure determination from PXRD, solid-state NMR and computer modeling, Solid State Nucl. Magn. Reson., 65 (2015) 49-63.

[51] T. Kobayashi, Y. Nishiyama, M. Pruski, Heteronuclear Correlation Solid-state NMR Spectroscopy with Indirect Detection under Fast Magic-angle Spinning, in: P. Hodgkinson (Ed.) Modern Methods in Solid-state NMR: A Practitioner's Guide, The Royal Society of Chemistry, 2018, pp. 1-38.

[52] J.P. Bradley, C. Tripon, C. Filip, S.P. Brown, Determining relative proton–proton proximities from the build-up of two-dimensional correlation peaks in ^{1}H double-quantum MAS NMR: Insight from multi-spin density-matrix simulations, Phys. Chem. Chem. Phys., 11 (2009) 6941-6952.

[53] J.P. Bradley, S.P. Velaga, O.N. Antzutkin, S.P. Brown, Probing intermolecular crystal packing in γ-indomethacin by high-resolution ^{1}H solid-state NMR spectroscopy, Cryst. Growth Des., 11 (2011) 3463-3471.

[54] J.P. Bradley, C.J. Pickard, J.C. Burley, D.R. Martin, L.P. Hughes, S.D. Cosgrove, S.P. Brown, Probing intermolecular hydrogen bonding in sibenadet hydrochloride polymorphs by high-resolution ^{1}H double-quantum solid-state NMR spectroscopy, J. Pharm. Sci., 101 (2012) 1821-1830.

[55] V.E. Zorin, M. Ernst, S.P. Brown, P. Hodgkinson, Insights into homonuclear decoupling from efficient numerical simulation: Techniques and examples, J. Magn. Reson., 192 (2008) 183-196.

[56] M.R. Hansen, R. Graf, H.W. Spiess, Interplay of structure and dynamics in functional macromolecular and supramolecular systems as revealed by magnetic resonance spectroscopy, Chem. Rev., 116 (2015) 1272-1308.

[57] S.P. Brown, Advanced solid-state NMR methods for characterising structure and self-assembly in supramolecular chemistry, polymers and hydrogels, Current Opinion in Colloid & Interface Science, (2018).

[58] M.R. Chierotti, R. Gobetto, NMR crystallography: the use of dipolar interactions in polymorph and co-crystal investigation, CrystEngComm, 15 (2013) 8599-8612.

[59] T. Pawlak, M.J. Potrzebowski, Fine refinement of solid-state molecular structures of Leu-and Met-Enkephalins by NMR crystallography, J. Phys. Chem. B, 118 (2014) 3298-3309.

[60] M.K. Dudek, T. Pawlak, P. Paluch, A. Jeziorna, M.J. Potrzebowski, A multi-technique experimental and computational approach to study the dehydration processes in the crystals of endomorphin opioid peptide derivative, Cryst. Growth Des., 16 (2016) 5312-5322.

[61] J. Czernek, M. Urbanova, J. Brus, NMR Crystallography of the Polymorphs of Metergoline, Crystals, 8 (2018) 378.

[62] U.J. Griesser, R.K. Jetti, M.F. Haddow, T. Brehmer, D.C. Apperley, A. King, R.K. Harris, Conformational polymorphism in oxybuprocaine hydrochloride, Cryst. Growth Des., 8 (2008) 44-56.

[63] S.V. Dvinskikh, Characterization of Liquid-crystalline Materials by Separated Local Field Methods, in: P. Hodgkinson (Ed.) Modern Methods in Solid-state NMR: A Practitioner's Guide, The Royal Society of Chemistry, 2018, pp. 391-423.

[64] P. Schanda, M. Ernst, Studying dynamics by magic-angle spinning solid-state NMR spectroscopy: principles and applications to biomolecules, Prog. Nucl. Magn. Reson. Spectrosc., 96 (2016) 1-46.

[65] T.N. Pham, J.M. Griffin, S. Masiero, S. Lena, G. Gottarelli, P. Hodgkinson, C. Filip, S.P. Brown, Quantifying hydrogen-bonding strength: the measurement of $^{2h}J_{NN}$ couplings in self-assembled guanosines by solid-state ^{15}N spin-echo MAS NMR, Phys. Chem. Chem. Phys., 9 (2007) 3416-3423.

[66] P. Schanda, M. Huber, R. Verel, M. Ernst, B.H. Meier, Direct Detection of $^{3h}J_{NC'}$ Hydrogen-Bond Scalar Couplings in Proteins by Solid-State NMR Spectroscopy, Angew. Chem., 121 (2009) 9486-9489.

[67] R.R. Vold, Deuterium NMR studies of dynamics in solids and liquid crystals, in: R. Tycko (Ed.) Nuclear Magnetic Resonance Probes of Molecular Dynamics, Kluwer Academic Publishers, 1994, pp. 27-112.

[68] C.M. Widdifield, G. Cavallo, G.A. Facey, T. Pilati, J. Lin, P. Metrangolo, G. Resnati, D.L. Bryce, Multinuclear Solid-State Magnetic Resonance as a Sensitive Probe of Structural Changes upon the Occurrence of Halogen Bonding in Co-crystals, Chem.-Eur. J., 19 (2013) 11949-11962.

[69] A.M. Namespetra, D.A. Hirsh, M.P. Hildebrand, A.R. Sandre, H. Hamaed, J.M. Rawson, R.W. Schurko, ^{35}Cl solid-state NMR spectroscopy of HCl pharmaceuticals and their polymorphs in bulk and dosage forms, CrystEngComm, 18 (2016) 6213-6232.

[70] N. Zencirci, U.J. Griesser, T. Gelbrich, V. Kahlenberg, R.K. Jetti, D.C. Apperley, R.K. Harris, New solvates of an old drug compound (phenobarbital): structure and stability, J. Phys. Chem. B, 118 (2014) 3267-3280.

[71] F. Taulelle, NMR crystallography: crystallochemical formula and space group selection, Solid State Sci., 6 (2004) 1053-1057.

[72] I.J. King, F. Fayon, D. Massiot, R.K. Harris, J.S.O. Evans, A space group assignment of ZrP$_2$O$_7$ obtained by ^{31}P solid state NMR, Chem. Commun., (2001) 1766-1767.

[73] S.E. Lister, A. Soleilhavoup, R.L. Withers, P. Hodgkinson, J.S.O. Evans, Structures and Phase Transitions in (MoO$_2$)$_2$P$_2$O$_7$, Inorg. Chem., 49 (2010) 1188-1194.

[74] M.R. Chierotti, L. Ferrero, N. Garino, R. Gobetto, L. Pellegrino, D. Braga, F. Grepioni, L. Maini, The Richest Collection of Tautomeric Polymorphs: The Case of 2-Thiobarbituric Acid, Chem.-Eur. J., 16 (2010) 4347-4358.

[75] E. Brunner, U. Sternberg, Solid-state NMR investigations on the nature of hydrogen bonds, Prog. Nucl. Magn. Reson. Spectrosc., 32 (1998) 21-57.

[76] G.M. Reddy, A. Marsh, J.T. Davis, S. Masiero, S.P. Brown, Interplay of Noncovalent Interactions in Ribbon-like Guanosine Self-Assembly: An NMR Crystallography Study, Cryst. Growth Des., 15 (2015) 5945-5954.

[77] G.M. Reddy, D.S. Cook, D. Iuga, R.I. Walton, A. Marsh, S.P. Brown, An NMR crystallography study of the hemihydrate of 2',3'-O-isopropylidineguanosine, Solid State Nucl. Magn. Reson., 65 (2015) 41-48.

[78] H. Kimura, K. Nakamura, A. Eguchi, H. Sugisawa, K. Deguchi, K. Ebisawa, E.-i. Suzuki, A. Shoji, Structural study of α-amino-acid crystals by ^{1}H CRAMPS NMR spectroscopy, J. Mol. Struct., 447 (1998) 247-255.

[79] T. Oikawa, M. Okumura, T. Kimura, Y. Nishiyama, Solid-state NMR meets electron diffraction: determination of crystalline polymorphs of small organic microcrystalline samples, Acta Cryst. C, 73 (2017) 219-228.

[80] J.T. Damron, K.M. Kersten, M.K. Pandey, K.H. Mroue, J.R. Yarava, Y. Nishiyama, A.J. Matzger, A. Ramamoorthy, Electrostatic Constraints Assessed by ^{1}H MAS NMR Illuminate Differences in Crystalline Polymorphs, J. Phys. Chem. Lett., 8 (2017) 4253-4257.

[81] C.J. Pickard, F. Mauri, All-electron magnetic response with pseudopotentials: NMR chemical shifts, Phys. Rev. B, 63 (2001) 245101.

[82] S.J. Clark, M.D. Segall, C.J. Pickard, P.J. Hasnip, M.I. Probert, K. Refson, M.C. Payne, First principles methods using CASTEP, Zeitschrift für Kristallographie-Crystalline Materials, 220 (2005) 567-570.

[83] P.C.M.M. Magusin, I.D. Seymour, O. Pecher, C.P. Grey, NMR Studies of Electrochemical Storage Materials, in: P. Hodgkinson (Ed.) Modern Methods in Solid-state NMR: A Practitioner's Guide, The Royal Society of Chemistry, 2018, pp. 322-355.

[84] G.J. Beran, Modeling polymorphic molecular crystals with electronic structure theory, Chem. Rev., 116 (2016) 5567-5613.

[85] C. Bonhomme, C. Gervais, F. Babonneau, C. Coelho, F. Pourpoint, T. Azais, S.E. Ashbrook, J.M. Griffin, J.R. Yates, F. Mauri, First-principles calculation of NMR parameters using the gauge including projector augmented wave method: a chemist's point of view, Chem. Rev., 112 (2012) 5733-5779.

[86] M. Bühl, T. van Mourik, NMR spectroscopy: quantum-chemical calculations, Wiley Interdisciplinary Reviews: Computational Molecular Science, 1 (2011) 634-647.

[87] A.A. Korlyukov, M.Y. Antipin, Structural studies of crystals of organic and organoelement compounds using modern quantum chemical calculations within the framework of the density functional theory, Russian Chemical Reviews, 81 (2012) 105-129.

[88] P.J. Hasnip, K. Refson, M.I. Probert, J.R. Yates, S.J. Clark, C.J. Pickard, Density functional theory in the solid state, Phil. Trans. R. Soc. A, 372 (2014) 20130270.

[89] J. Hoja, A.M. Reilly, A. Tkatchenko, First-principles modeling of molecular crystals: structures and stabilities, temperature and pressure, Wiley Interdisciplinary Reviews: Computational Molecular Science, 7 (2017) e1294.

[90] J.C. Facelli, Chemical shift tensors: Theory and application to molecular structural problems, Prog. Nucl. Magn. Reson. Spectrosc., 58 (2011) 176.

[91] V. Gowda, B. Sarma, S. Öberg, V.V. Telkki, A.C. Larsson, P. Lantto, O.N. Antzutkin, Structure Elucidation of an Yttrium Diethyldithiocarbamato-Phenanthroline Complex by X-ray Crystallography, Solid-State NMR, and ab-initio Quantum Chemical Calculations, Eur. J. Inorg. Chem., 2016 (2016) 3278-3291.

[92] V. Gowda, R.S. Laitinen, V.-V. Telkki, A.-C. Larsson, O.N. Antzutkin, P. Lantto, DFT calculations in the assignment of solid-state NMR and crystal structure elucidation of a lanthanum (III) complex with dithiocarbamate and phenanthroline, Dalton Transactions, 45 (2016) 19473-19484.

[93] T. Helgaker, S. Coriani, P. Jørgensen, K. Kristensen, J. Olsen, K. Ruud, Recent advances in wave function-based methods of molecular-property calculations, Chem. Rev., 112 (2012) 543-631.

[94] J.P. Perdew, K. Burke, M. Ernzerhof, Generalized gradient approximation made simple, Phys. Rev. Lett., 77 (1996) 3865.

[95] H.J. Monkhorst, J.D. Pack, Special points for Brillouin-zone integrations, Phys. Rev. B, 13 (1976) 5188.

[96] A. Baldereschi, Mean-value point in the Brillouin zone, Phys. Rev. B, 7 (1973) 5212.

[97] A.J. Morris, C.J. Pickard, R.J. Needs, Hydrogen/silicon complexes in silicon from computational searches, Phys. Rev. B, 78 (2008) 184102.

[98] M. Deschamps, S. Cadars, E. Gilbert, P. Azaïs, E. Raymundo-Pinero, F. Béguin, D. Massiot, A solid-state NMR study of C_{70}: A model molecule for amorphous carbons, Solid State Nucl. Magn. Reson., 42 (2012) 81-86.

[99] D. Presti, A. Pedone, M.C. Menziani, Unraveling the polymorphism of [(p-cymene)Ru(κN-INA)Cl$_2$] through dispersion-corrected DFT and NMR GIPAW calculations, Inorg. Chem., 53 (2014) 7926-7935.

[100] R.K. Harris, P. Hodgkinson, C.J. Pickard, V. Zorin, J.R. Yates, Chemical Shift Computations on a Crystallographic Basis: Some Reflections and Comments, Magn. Reson. Chem., 45 (2007) S174-186.

[101] A. Sadoc, M. Body, C. Legein, M. Biswal, F. Fayon, X. Rocquefelte, F. Boucher, NMR parameters in alkali, alkaline earth and rare earth fluorides from first principle calculations, Phys. Chem. Chem. Phys., 13 (2011) 18539-18550.

[102] A.J. Robbins, W.T.K. Ng, D. Jochym, T.W. Keal, S.J. Clark, D.J. Tozer, P. Hodgkinson, Combining insights from solid-state NMR and first principles calculation: applications to the ^{19}F NMR of octafluoronaphthalene, Phys. Chem. Chem. Phys., 9 (2007) 2389-2396.

[103] D. Vanderbilt, Soft self-consistent pseudopotentials in a generalized eigenvalue formalism, Phys. Rev. B, 41 (1990) 7892.

[104] J.R. Yates, C.J. Pickard, F. Mauri, Calculation of NMR chemical shifts for extended systems using ultrasoft pseudopotentials, Phys. Rev. B, 76 (2007) 024401.

[105] K. Lejaeghere, G. Bihlmayer, T. Bjorkman, P. Blaha, S. Blugel, V. Blum, D. Caliste, I.E. Castelli, S.J. Clark, A. Dal Corso, S. de Gironcoli, T. Deutsch, J.K. Dewhurst, I. Di Marco, C. Draxl, M. Dulak, O. Eriksson, J.A. Flores-Livas, K.F. Garrity, L. Genovese, P. Giannozzi, M. Giantomassi, S. Goedecker, X. Gonze, O. Granas, E.K. Gross, A. Gulans, F. Gygi, D.R. Hamann, P.J. Hasnip, N.A. Holzwarth, D. Iusan, D.B. Jochym, F. Jollet, D. Jones, G. Kresse, K. Koepernik, E. Kucukbenli, Y.O. Kvashnin, I.L. Locht, S. Lubeck, M. Marsman, N. Marzari, U. Nitzsche, L. Nordstrom, T. Ozaki, L. Paulatto, C.J. Pickard, W. Poelmans, M.I. Probert, K. Refson, M. Richter, G.M. Rignanese, S. Saha, M. Scheffler, M. Schlipf, K. Schwarz, S. Sharma, F. Tavazza, P. Thunstrom, A. Tkatchenko, M. Torrent, D. Vanderbilt, M.J. van Setten, V. Van Speybroeck, J.M. Wills, J.R. Yates, G.X. Zhang, S. Cottenier, Reproducibility in density functional theory calculations of solids, Science, 351 (2016) aad3000.
[106] J. Czernek, On the solid-state NMR spectra of naproxen, Chem. Phys. Lett., 619 (2015) 230-235.
[107] S.A. Joyce, J.R. Yates, C.J. Pickard, F. Mauri, A first principles theory of nuclear magnetic resonance J-coupling in solid-state systems, J. Chem. Phys., 127 (2007) 204107.
[108] S.A. Joyce, J.R. Yates, C.J. Pickard, S.P. Brown, Density functional theory calculations of hydrogen-bond-mediated NMR J coupling in the solid state, J. Am. Chem. Soc., 130 (2008) 12663-12670.
[109] J.R. Yates, Prediction of NMR J-coupling in solids with the planewave pseudopotential approach, Magn. Reson. Chem., 48 (2010) S23-S31.
[110] J. Rezac, Y. Huang, P. Hobza, G.J. Beran, Benchmark calculations of three-body intermolecular interactions and the performance of low-cost electronic structure methods, J. Chem. Theory Comput., 11 (2015) 3065-3079.
[111] J. Klimeš, A. Michaelides, Perspective: Advances and challenges in treating van der Waals dispersion forces in density functional theory, J. Chem. Phys., 137 (2012) 120901.
[112] S.T. Holmes, R.J. Iuliucci, K.T. Mueller, C. Dybowski, Semi-empirical refinements of crystal structures using ^{17}O quadrupolar-coupling tensors, J. Chem. Phys., 146 (2017) 064201.
[113] S.T. Holmes, R.W. Schurko, Refining Crystal Structures with Quadrupolar NMR and Dispersion-Corrected Density Functional Theory, J. Phys. Chem. C, 122 (2018) 1809-1820.
[114] A. Tkatchenko, M. Scheffler, Accurate molecular van der Waals interactions from ground-state electron density and free-atom reference data, Phys. Rev. Lett., 102 (2009) 073005.
[115] A.M. Reilly, A. Tkatchenko, van der Waals dispersion interactions in molecular materials: beyond pairwise additivity, Chem. Sci., 6 (2015) 3289-3301.
[116] J. Binns, M.R. Healy, S. Parsons, C.A. Morrison, Assessing the performance of density functional theory in optimizing molecular crystal structure parameters, Acta Cryst. B, 70 (2014) 259-267.
[117] D.V. Dudenko, J.R. Yates, K.D. Harris, S.P. Brown, An NMR crystallography DFT-D approach to analyse the role of intermolecular hydrogen bonding and π–π interactions in driving cocrystallisation of indomethacin and nicotinamide, CrystEngComm, 15 (2013) 8797-8807.
[118] V.L. Deringer, V. Hoepfner, R. Dronskowski, Accurate hydrogen positions in organic crystals: Assessing a quantum-chemical aide, Cryst. Growth Des., 12 (2012) 1014-1021.
[119] J.R. Yates, C.J. Pickard, M.C. Payne, R. Dupree, M. Profeta, F. Mauri, Theoretical investigation of oxygen-17 NMR shielding and electric field gradients in glutamic acid polymorphs, J. Phys. Chem. A, 108 (2004) 6032-6037.
[120] M. Dračínský, P. Jansa, K. Ahonen, M. Buděšínský, Tautomerism and the Protonation/Deprotonation of Isocytosine in Liquid-and Solid-States Studied by NMR Spectroscopy and Theoretical Calculations, Eur. J. Org. Chem., 2011 (2011) 1544-1551.
[121] J. van de Streek, M.A. Neumann, Validation of experimental molecular crystal structures with dispersion-corrected density functional theory calculations, Acta Cryst. B, 66 (2010) 544-558.
[122] J. van de Streek, M.A. Neumann, Validation of molecular crystal structures from powder diffraction data with dispersion-corrected density functional theory (DFT-D), Acta Cryst. B, 70 (2014) 1020-1032.

[123] R.K. Harris, P. Hodgkinson, V. Zorin, J.-N. Dumez, B. Elena-Herrmann, L. Emsley, E. Salager, R. Stein, Computation and NMR crystallography of terbutaline sulfate, Magn. Reson. Chem., 48 (2010) S103-S112.

[124] J.K. Harper, R. Iuliucci, M. Gruber, K. Kalakewich, Refining crystal structures with experimental ^{13}C NMR shift tensors and lattice-including electronic structure methods, CrystEngComm, 15 (2013) 8693-8704.

[125] K. Kalakewich, R. Iuliucci, K.T. Mueller, H. Eloranta, J.K. Harper, Monitoring the refinement of crystal structures with ^{15}N solid-state NMR shift tensor data, J. Chem. Phys., 143 (2015) 194702.

[126] J.C. Johnston, R.J. Iuliucci, J.C. Facelli, G. Fitzgerald, K.T. Mueller, Intermolecular shielding contributions studied by modeling the ^{13}C chemical-shift tensors of organic single crystals with plane waves, J. Chem. Phys., 131 (2009) 144503.

[127] D. Alderman, M. Sherwood, D. Grant, Comparing, modeling, and assigning chemical-shift tensors in the Cartesian, irreducible spherical, and icosahedral representations, J. Magn. Reson., Ser. A, 101 (1993) 188-197.

[128] H.E. Kerr, H.E. Mason, H.A. Sparkes, P. Hodgkinson, Testing the limits of NMR crystallography: the case of caffeine-citric acid hydrate, CrystEngComm, 18 (2016) 6700-6707.

[129] M.W. Lodewyk, M.R. Siebert, D.J. Tantillo, Computational prediction of ^{1}H and ^{13}C chemical shifts: A useful tool for natural product, mechanistic, and synthetic organic chemistry, Chem. Rev., 112 (2011) 1839-1862.

[130] M. Arhangelskis, M.D. Eddleston, D.G. Reid, G.M. Day, D.K. Bučar, A.J. Morris, W. Jones, Rationalization of the color properties of fluorescein in the solid state: a combined computational and experimental study, Chem.-Eur. J., 22 (2016) 10065-10073.

[131] J.D. Hartman, R.A. Kudla, G.M. Day, L.J. Mueller, G.J. Beran, Benchmark fragment-based ^{1}H, ^{13}C, ^{15}N and ^{17}O chemical shift predictions in molecular crystals, Phys. Chem. Chem. Phys., 18 (2016) 21686-21709.

[132] J.D. Hartman, G.M. Day, G.J.O. Beran, Enhanced NMR Discrimination of Pharmaceutically Relevant Molecular Crystal Forms through Fragment-Based Ab Initio Chemical Shift Predictions, Cryst. Growth Des., 16 (2016) 6479-6493.

[133] E. Salager, G.M. Day, R.S. Stein, C.J. Pickard, B. Elena, L. Emsley, Powder Crystallography by Combined Crystal Structure Prediction and High-Resolution ^{1}H Solid-State NMR Spectroscopy, J. Am. Chem. Soc., 132 (2010) 2564-2566.

[134] C.M. Widdifield, H. Robson, P. Hodgkinson, Furosemide's one little hydrogen atom: NMR crystallography structure verification of powdered molecular organics, Chem. Commun., 52 (2016) 6685-6688.

[135] S.D. Gumbert, M. Körbitzer, E. Alig, M.U. Schmidt, M.R. Chierotti, R. Gobetto, X. Li, J. Van De Streek, Crystal structure and tautomerism of Pigment Yellow 138 determined by X-ray powder diffraction and solid-state NMR, Dyes and Pigments, 131 (2016) 364-372.

[136] I. Fonseca, M. Baias, S.E. Hayes, C.J. Pickard, M. Bertmer, Effects of Aromatic Substitution on the Photodimerization Kinetics of β-trans Cinnamic Acid Derivatives Studied with ^{13}C Solid-State NMR, J. Phys. Chem. C, 116 (2012) 12212-12218.

[137] M. Profeta, F. Mauri, C.J. Pickard, Accurate first principles prediction of ^{17}O NMR parameters in SiO$_2$: Assignment of the zeolite ferrierite spectrum, J. Am. Chem. Soc., 125 (2003) 541-548.

[138] J. Czernek, J. Brus, The covariance of the differences between experimental and theoretical chemical shifts as an aid for assigning two-dimensional heteronuclear correlation solid-state NMR spectra, Chem. Phys. Lett., 608 (2014) 334-339.

[139] J. Czernek, J. Brus, Theoretical predictions of the two-dimensional solid-state NMR spectra: A case study of the ^{13}C–^{1}H correlations in metergoline, Chem. Phys. Lett., 586 (2013) 56-60.

[140] S. Sturniolo, T.F.G. Green, R.M. Hanson, M. Zilka, K. Refson, P. Hodgkinson, S.P. Brown, J.R. Yates, Visualization and processing of computed solid-state NMR parameters: MagresView and MagresPython, Solid State Nucl. Magn. Reson., 78 (2016) 64-70.

[141] R.P. Young, C.R. Lewis, C. Yang, L. Wang, J.K. Harper, L.J. Mueller, TensorView: A software tool for displaying NMR tensors, Magn. Reson. Chem., 57 (2019) 211-223.

[142] P. Giannozzi, S. Baroni, N. Bonini, M. Calandra, R. Car, C. Cavazzoni, D. Ceresoli, G.L. Chiarotti, M. Cococcioni, I. Dabo, A. Dal Corso, S. de Gironcoli, S. Fabris, G. Fratesi, R. Gebauer, U. Gerstmann, C. Gougoussis, A. Kokalj, M. Lazzeri, L. Martin-Samos, N. Marzari, F. Mauri, R. Mazzarello, S. Paolini, A. Pasquarello, L. Paulatto, C. Sbraccia, S. Scandolo, G. Sclauzero, A.P. Seitsonen, A. Smogunov, P. Umari, R.M. Wentzcovitch, QUANTUM ESPRESSO: a modular and open-source software project for quantum simulations of materials, J. Phys.: Condens. Matter, 21 (2009) 395502.

[143] R. Radeglia, On the pictorial representation of the magnetic screening tensor: Ellipsoid or ovaloid?, Solid State Nucl. Magn. Reson., 4 (1995) 317-321.

[144] J. Hester, A validating CIF parser: PyCIFRW, J. Appl. Crystallogr., 39 (2006) 621-625.

[145] C.R. Groom, I.J. Bruno, M.P. Lightfoot, S.C. Ward, The Cambridge Structural Database, Acta Cryst. B, 72 (2016) 171-179.

[146] A. Hjorth Larsen, J. Jørgen Mortensen, J. Blomqvist, I.E. Castelli, R. Christensen, M. Dułak, J. Friis, M.N. Groves, B. Hammer, C. Hargus, E.D. Hermes, P.C. Jennings, P. Bjerre Jensen, J. Kermode, J.R. Kitchin, E. Leonhard Kolsbjerg, J. Kubal, K. Kaasbjerg, S. Lysgaard, J. Bergmann Maronsson, T. Maxson, T. Olsen, L. Pastewka, A. Peterson, C. Rostgaard, J. Schiøtz, O. Schütt, M. Strange, K.S. Thygesen, T. Vegge, L. Vilhelmsen, M. Walter, Z. Zeng, K.W. Jacobsen, The atomic simulation environment—a Python library for working with atoms, J. Phys.: Condens. Matter, 29 (2017) 273002.

[147] G.J. Beran, J.D. Hartman, Y.N. Heit, Predicting molecular crystal properties from first principles: Finite-temperature thermochemistry to NMR crystallography, Acc. Chem. Res., 49 (2016) 2501-2508.

[148] M. Dračínský, P. Hodgkinson, A molecular dynamics study of the effects of fast molecular motions on solid-state NMR parameters, CrystEngComm, 15 (2013) 8705-8712.

[149] J.N. Dumez, C.J. Pickard, Calculation of NMR chemical shifts in organic solids: Accounting for motional effects, J. Chem. Phys., 130 (2009) 104701.

[150] L.A. O'Dell, C.I. Ratcliffe, X. Kong, G. Wu, Multinuclear solid-state nuclear magnetic resonance and density functional theory characterization of interaction tensors in taurine, J. Phys. Chem. A, 116 (2012) 1008-1014.

[151] M. Robinson, P.D. Haynes, Dynamical effects in ab initio NMR calculations: Classical force fields fitted to quantum forces, J. Chem. Phys., 133 (2010) 084109.

[152] X. Li, L. Tapmeyer, M. Bolte, J. van de Streek, Crystallographic and Dynamic Aspects of Solid-State NMR Calibration Compounds: Towards ab Initio NMR Crystallography, ChemPhysChem, 17 (2016) 2496-2502.

[153] M.A. Neumann, Tailor-made force fields for crystal-structure prediction, J. Phys. Chem. B, 112 (2008) 9810-9829.

[154] X. Li, M.A. Neumann, J. van de Streek, The application of tailor-made force fields and molecular dynamics for NMR crystallography: a case study of free base cocaine, IUCrJ, 4 (2017) 175-184.

[155] M. Dračínský, P. Bouř, P. Hodgkinson, Temperature Dependence of NMR Parameters Calculated from Path Integral Molecular Dynamics Simulations, J. Chem. Theory Comput., 12 (2016) 968-973.

[156] B. Monserrat, Vibrational averages along thermal lines, Phys. Rev. B, 93 (2016) 014302.

[157] S. Sene, D. Berthomieu, B. Donnadieu, S. Richeter, J. Vezzani, D. Granier, S. Bégu, H. Mutin, C. Gervais, D. Laurencin, A combined experimental-computational study of benzoxaborole crystal structures, CrystEngComm, 16 (2014) 4999-5011.

[158] E. Carignani, S. Borsacchi, A. Marini, B. Mennucci, M. Geppi, ^{13}C chemical shielding tensors: A combined solid-state NMR and DFT study of the role of small-amplitude motions, J. Phys. Chem. C, 115 (2011) 25023-25029.

[159] E. Carignani, S. Borsacchi, M. Concistrè, O.G. Johannessen, M. Geppi, Direct observation of the effects of small-amplitude motions on ^{13}C nuclear shielding tensors by means of low-temperature 2D MAS NMR spectroscopy, Chem. Phys. Lett., 706 (2018) 107-112.

[160] I.D. Gortari, G. Portella, X. Salvatella, V.S. Bajaj, P.C. van der Wel, J.R. Yates, M.D. Segall, C.J. Pickard, M.C. Payne, M. Vendruscolo, Time averaging of NMR chemical shifts in the MLF peptide in the solid state, J. Am. Chem. Soc., 132 (2010) 5993-6000.

[161] J.D. Dunitz, E.F. Maverick, K.N. Trueblood, Atomic motions in molecular crystals from diffraction measurements, Ange. Chem. Int. Ed., 27 (1988) 880-895.

[162] S.T. Holmes, R.J. Iuliucci, K.T. Mueller, C. Dybowski, Density functional investigation of intermolecular effects on ^{13}C NMR chemical-shielding tensors modeled with molecular clusters, J. Chem. Phys., 141 (2014) 164121.

[163] I. Poltavsky, A. Tkatchenko, Modeling quantum nuclei with perturbed path integral molecular dynamics, Chem. Sci., 7 (2016) 1368-1372.

[164] C. John, T. Spura, S. Habershon, T.D. Kühne, Quantum ring-polymer contraction method: Including nuclear quantum effects at no additional computational cost in comparison to ab initio molecular dynamics, Phys. Rev. E, 93 (2016) 043305.

[165] O. Marsalek, T.E. Markland, Ab initio molecular dynamics with nuclear quantum effects at classical cost: Ring polymer contraction for density functional theory, J. Chem. Phys., 144 (2016) 054112.

[166] M. Dračínský, P. Hodgkinson, Effects of Quantum Nuclear Delocalisation on NMR Parameters from Path Integral Molecular Dynamics, Chem.-Eur. J., 20 (2014) 2201-2207.

[167] B. Monserrat, R.J. Needs, C.J. Pickard, Temperature effects in first-principles solid state calculations of the chemical shielding tensor made simple, J. Chem. Phys., 141 (2014) 134113.

[168] A.L. Webber, B. Elena, J.M. Griffin, J.R. Yates, T.N. Pham, F. Mauri, C.J. Pickard, A.M. Gil, R. Stein, A. Lesage, L. Emsley, S.P. Brown, Complete ^{1}H resonance assignment of β-maltose from ^{1}H–^{1}H DQ-SQ CRAMPS and ^{1}H (DQ-DUMBO)–^{13}C SQ refocused INEPT 2D solid-state NMR spectra and first principles GIPAW calculations, Phys. Chem. Chem. Phys., 12 (2010) 6970-6983.

[169] M. Hušák, A. Jegorov, J. Rohlíček, A. Fitch, J. Czernek, L. Kobera, J. Brus, Determining the crystal structures of peptide analogs of boronic acid in the absence of single crystals: Intricate motifs of ixazomib citrate revealed by XRPD guided by ss-NMR, Cryst. Growth Des., 18 (2018) 3616-3625.

[170] J. Brus, J. Czernek, L. Kobera, M. Urbanova, S. Abbrent, M. Husak, Predicting the crystal structure of decitabine by powder NMR crystallography: Influence of long-range molecular packing symmetry on NMR parameters, Cryst. Growth Des., 16 (2016) 7102-7111.

[171] A.D. Boese, Density functional theory and hydrogen bonds: are we there yet?, ChemPhysChem, 16 (2015) 978-985.

[172] S. Sadhukhan, D. Muñoz, C. Adamo, G.E. Scuseria, Predicting proton transfer barriers with density functional methods, Chem. Phys. Lett., 306 (1999) 83-87.

[173] H.E. Kerr, L.K. Softley, K. Suresh, A. Nangia, P. Hodgkinson, I.R. Evans, A furosemide-isonicotinamide cocrystal: an investigation of properties and extensive structural disorder, CrystEngComm, 17 (2015) 6707-6715.

[174] N. Mercadal, S.P. Day, A. Jarmyn, M.B. Pitak, S.J. Coles, C. Wilson, G.J. Rees, J.V. Hanna, J.D. Wallis, *O*-vs. *N*-protonation of 1-dimethylaminonaphthalene-8-ketones: formation of a peri N–C bond or a hydrogen bond to the pi-electron density of a carbonyl group, CrystEngComm, 16 (2014) 8363-8374.

[175] J.R. Yates, S.E. Dobbins, C.J. Pickard, F. Mauri, P.Y. Ghi, R.K. Harris, A combined first principles computational and solid-state NMR study of a molecular crystal: flurbiprofen, Phys. Chem. Chem. Phys., 7 (2005) 1402-1407.

[176] C.M. Gowda, F. Vasconcelos, E. Schwartz, E.R. van Eck, M. Marsman, J.J. Cornelissen, A.E. Rowan, G.A. de Wijs, A.P. Kentgens, Hydrogen bonding and chemical shift assignments in carbazole functionalized isocyanides from solid-state NMR and first-principles calculations, Phys. Chem. Chem. Phys., 13 (2011) 13082-13095.

[177] P. Stephens, F. Devlin, C. Chabalowski, M.J. Frisch, Ab initio calculation of vibrational absorption and circular dichroism spectra using density functional force fields, J. Phys. Chem., 98 (1994) 11623-11627.

[178] C. Adamo, V. Barone, Toward reliable density functional methods without adjustable parameters: The PBE0 model, J. Chem. Phys., 110 (1999) 6158-6170.

[179] J.D. Hartman, S. Monaco, B. Schatschneider, G.J.O. Beran, Fragment-based ^{13}C nuclear magnetic resonance chemical shift predictions in molecular crystals: An alternative to planewave methods, J. Chem. Phys., 143 (2015) 102809.

[180] J.K. Harper, J.A. Doebbler, E. Jacques, D.M. Grant, R.B. Von Dreele, A Combined Solid-State NMR and Synchrotron X-ray Diffraction Powder Study on the Structure of the Antioxidant (+)-Catechin 4.5-hydrate, J. Am. Chem. Soc., 132 (2010) 2928-2937.

[181] R. Laskowski, P. Blaha, F. Tran, Assessment of DFT functionals with NMR chemical shifts, Phys. Rev. B, 87 (2013) 195130.

[182] S.T. Holmes, R.J. Iuliucci, K.T. Mueller, C. Dybowski, Critical analysis of cluster models and exchange-correlation functionals for calculating magnetic shielding in molecular solids, J. Chem. Theory Comput., 11 (2015) 5229-5241.

[183] S.E. Soss, P.F. Flynn, R.J. Iuliucci, R.P. Young, L.J. Mueller, J. Hartman, G.J. Beran, J.K. Harper, Measuring and Modeling Highly Accurate [15]N Chemical Shift Tensors in a Peptide, ChemPhysChem, 18 (2017) 2225-2232.

[184] F. Alkan, S.T. Holmes, C. Dybowski, Role of Exact Exchange and Relativistic Approximations in Calculating [19]F Magnetic Shielding in Solids Using a Cluster Ansatz, J. Chem. Theory Comput., 13 (2017) 4741-4752.

[185] R.K. Harris, S.A. Joyce, C.J. Pickard, S. Cadars, L. Emsley, Assigning carbon-13 NMR spectra to crystal structures by the INADEQUATE pulse sequence and first principles computation: a case study of two forms of testosterone, Phys. Chem. Chem. Phys., 8 (2006) 137-143.

[186] I. Alkorta, R.M. Claramunt, J. Elguero, M.B. Ferraro, J.C. Facelli, P.F. Provasi, F. Reviriego, The origin of the splitting of ^{13}C and ^{15}N NMR signals of 3(5)-phenyl-5(3)-methylpyrazolium chloride and bromide in the solid state: Quantum Espresso calculations, J. Mol. Struct., 1075 (2014) 551-558.

[187] M. Dracinsky, M. Buděšínský, B. Warzajtis, U. Rychlewska, Solution and solid-state effects on NMR chemical shifts in sesquiterpene lactones: NMR, X-ray, and theoretical methods, J. Phys. Chem. A, 116 (2011) 680-688.

[188] D.H. Brouwer, K.P. Langendoen, Q. Ferrant, Measurement and calculation of ^{13}C chemical shift tensors in α-glucose and α-glucose monohydrate, Can. J. Chem., 89 (2011) 737-744.

[189] A. Abraham, D.C. Apperley, S.J. Byard, A.J. Ilott, A.J. Robbins, V. Zorin, R.K. Harris, P. Hodgkinson, Characterising the role of water in sildenafil citrate by NMR crystallography, CrystEngComm, 18 (2016) 1054-1063.

[190] Ł. Szeleszczuk, D.M. Pisklak, M. Zielińska-Pisklak, Does the choice of the crystal structure influence the results of the periodic DFT calculations? A case of glycine alpha polymorph GIPAW NMR parameters computations, J. Comput. Chem., 39 (2018) 853-861.

[191] S.M. Santos, J. Rocha, L. Mafra, NMR crystallography: toward chemical shift-driven crystal structure determination of the β-lactam antibiotic amoxicillin trihydrate, Cryst. Growth Des., 13 (2013) 2390-2395.

[192] M. Baias, C.M. Widdifield, J.-N. Dumez, H.P. Thompson, T.G. Cooper, E. Salager, S. Bassil, R.S. Stein, A. Lesage, G.M. Day, Powder crystallography of pharmaceutical materials by combined crystal structure prediction and solid-state ^{1}H NMR spectroscopy, Phys. Chem. Chem. Phys., 15 (2013) 8069-8080.

[193] T. Kobayashi, K. Mao, P. Paluch, A. Nowak-Król, J. Sniechowska, Y. Nishiyama, D.T. Gryko, M.J. Potrzebowski, M. Pruski, Study of Intermolecular Interactions in the Corrole Matrix by Solid-State NMR under 100 kHz MAS and Theoretical Calculations, Angew. Chem. Int. Ed., 52 (2013) 14108-14111.

[194] N. Mifsud, B. Elena, C.J. Pickard, A. Lesage, L. Emsley, Assigning powders to crystal structures by high-resolution [1]H–[1]H double quantum and [1]H–^{13}C J-INEPT solid-state NMR spectroscopy and first principles computation. A case study of penicillin G, Phys. Chem. Chem. Phys., 8 (2006) 3418-3422.

[195] A.L. Webber, L. Emsley, R.M. Claramunt, S.P. Brown, NMR crystallography of campho[2,3-c]pyrazole (Z'= 6): Combining high-resolution ^{1}H-^{13}C solid-state MAS NMR spectroscopy and GIPAW chemical-shift calculations, J. Phys. Chem. A, 114 (2010) 10435-10442.

[196] A.L. Webber, S. Masiero, S. Pieraccini, J.C. Burley, A.S. Tatton, D. Iuga, T.N. Pham, G.P. Spada, S.P. Brown, Identifying guanosine self assembly at natural isotopic abundance by high-resolution ^{1}H and ^{13}C solid-state NMR spectroscopy, J. Am. Chem. Soc., 133 (2011) 19777-19795.

[197] M.K. Dudek, A. Jeziorna, M.J. Potrzebowski, Computational and experimental study of reversible hydration/dehydration processes in molecular crystals of natural products–a case of catechin, CrystEngComm, 18 (2016) 5267-5277.

[198] T. Pawlak, P. Paluch, K. Trzeciak-Karlikowska, A. Jeziorna, M.J. Potrzebowski, Study of the thermal processes in molecular crystals of peptides by means of NMR crystallography, CrystEngComm, 15 (2013) 8680-8692.

[199] G.M. Reddy, M. Malon, A. Marsh, Y. Nishiyama, S.P. Brown, Fast Magic-Angle Spinning Three-Dimensional NMR Experiment for Simultaneously Probing H–H and N–H Proximities in Solids, Anal. Chem., 88 (2016) 11412-11419.

[200] F.G. Vogt, G.R. Williams, M. Strohmeier, M.N. Johnson, R.C. Copley, Solid-state NMR analysis of a complex crystalline phase of ronacaleret hydrochloride, J. Phys. Chem. B, 118 (2014) 10266-10284.

[201] F.G. Vogt, G.R. Williams, R.C. Copley, Solid-State NMR Analysis of a Boron-Containing Pharmaceutical Hydrochloride Salt, J. Pharm. Sci., 102 (2013) 3705-3716.

[202] J.K. Harper, M. Strohmeier, D.M. Grant, Pursuing structure in microcrystalline solids with independent molecules in the unit cell using ^{1}H–^{13}C correlation data, J. Magn. Reson., 189 (2007) 20-31.

[203] E.M. Heider, J.K. Harper, D.M. Grant, Structural characterization of an anhydrous polymorph of paclitaxel by solid-state NMR, Phys. Chem. Chem. Phys., 9 (2007) 6083-6097.

[204] L. Mafra, S.M. Santos, R. Siegel, I.M. Alves, F.A.A. Paz, D. Dudenko, H.W. Spiess, Packing interactions in hydrated and anhydrous forms of the antibiotic ciprofloxacin: a solid-state NMR, X-ray diffraction and computer simulation study, J. Am. Chem. Soc., 134 (2012) 71-74.

[205] R.K. Harris, S. Cadars, L. Emsley, J.R. Yates, C.J. Pickard, R.K.R. Jetti, U.J. Griesser, NMR crystallography of oxybuprocaine hydrochloride, modification II°, Phys. Chem. Chem. Phys., 9 (2007) 360-368.

[206] M. Baias, J.-N. Dumez, P.H. Svensson, S. Schantz, G.M. Day, L. Emsley, De novo determination of the crystal structure of a large drug molecule by crystal structure prediction-based powder NMR crystallography, J. Am. Chem. Soc., 135 (2013) 17501-17507.

[207] J. Brus, A. Jegorov, Through-bonds and through-space solid-state NMR correlations at natural isotopic abundance: Signal assignment and structural study of simvastatin, J. Phys. Chem. A, 108 (2004) 3955-3964.

[208] Y. Nishiyama, Fast magic-angle sample spinning solid-state NMR at 60–100 kHz for natural abundance samples, Solid State Nucl. Magn. Reson., 78 (2016) 24-36.

[209] T. Asakura, K. Yazawa, K. Horiguchi, F. Suzuki, Y. Nishiyama, K. Nishimura, H. Kaji, Difference in the structures of alanine tri- and tetra-peptides with antiparallel β-sheet assessed by X-ray diffraction, solid-state NMR and chemical shift calculations by GIPAW, Biopolymers, 101 (2014) 13-20.

[210] N.J. Vigilante, M.A. Mehta, A ^{13}C solid-state NMR investigation of four cocrystals of caffeine and theophylline, Acta Cryst. C, 73 (2017) 234-243.

[211] S. Ando, J. Kikuchi, Y. Fujimura, Y. Ida, K. Higashi, K. Moribe, K. Yamamoto, Physicochemical characterization and structural evaluation of a specific 2:1 cocrystal of naproxen–nicotinamide, J. Pharm. Sci., 101 (2012) 3214-3221.

[212] M. Aguiar, S. Menezes, A. Gemal, R. San Gil, Solid-state ^{13}C nuclear magnetic resonance spectra of 6-aminopenicillanic acid, Solid State Nucl. Magn. Reson., 4 (1995) 179-185.

[213] N.J. Clayden, C.M. Dobson, L.-Y. Lian, J.M. Twyman, A solid-state ^{13}C nuclear magnetic resonance study of the conformational states of penicillins, J. Chem. Soc. Perkin Trans. 2, (1986) 1933-1940.

[214] K. Drużbicki, A. Pajzderska, D. Chudoba, J. Jenczyk, M. Jarek, J. Mielcarek, J. Wąsicki, Elucidating the Structure of Ranitidine Hydrochloride Form II: Insights from Solid-State Spectroscopy and ab initio Simulations, Cryst. Growth Des., 18 (2018) 4671-4681.

[215] X. Filip, I.-G. Grosu, M. Miclăuş, C. Filip, NMR crystallography methods to probe complex hydrogen bonding networks: application to structure elucidation of anhydrous quercetin, CrystEngComm, 15 (2013) 4131-4142.

[216] D.M. Pisklak, M.A. Zielińska-Pisklak, Ł. Szeleszczuk, I. Wawer, ^{13}C solid-state NMR analysis of the most common pharmaceutical excipients used in solid drug formulations, Part I: Chemical shifts assignment, J. Pharm. Biomed. Anal., 122 (2016) 81-89.

[217] W.D. Wang, X. Gao, M. Strohmeier, W. Wang, S. Bai, C. Dybowski, Solid-state NMR studies of form I of atorvastatin calcium, J. Phys. Chem. B, 116 (2012) 3641-3649.

[218] L. Shao, J.R. Yates, J.J. Titman, Carbon-13 chemical shift tensors of disaccharides: measurement, computation and assignment, J. Phys. Chem. A, 111 (2007) 13126-13132.

[219] J.R. Smith, W. Xu, D. Raftery, Analysis of conformational polymorphism in pharmaceutical solids using solid-state NMR and electronic structure calculations, J. Phys. Chem. B, 110 (2006) 7766-7776.

[220] R.I. Cooper, A.L. Thompson, D.J. Watkin, CRYSTALS enhancements: dealing with hydrogen atoms in refinement, J. Appl. Crystallogr., 43 (2010) 1100-1107.

[221] M. Woińska, S. Grabowsky, P.M. Dominiak, K. Woźniak, D. Jayatilaka, Hydrogen atoms can be located accurately and precisely by X-ray crystallography, Science advances, 2 (2016) e1600192.

[222] L. Rajput, M. Banik, J.R. Yarava, S. Joseph, M.K. Pandey, Y. Nishiyama, G.R. Desiraju, Exploring the salt–cocrystal continuum with solid-state NMR using natural-abundance samples: implications for crystal engineering, IUCrJ, 4 (2017) 466-475.

[223] D. Wiechert, D. Mootz, Molecular beside ionic: Crystal structures of a 1/1 and a 1/4 adduct of pyridine and formic acid, Angew. Chem. Int. Ed., 38 (1999) 1974-1976.

[224] F. Spinelli, E. Dichiarante, M. Curzi, S.L. Giaffreda, M.R. Chierotti, R. Gobetto, F. Rossi, L. Chelazzi, D. Braga, F. Grepioni, Molecular salts of the antidepressant venlafaxine: an effective route to solubility properties modifications, Cryst. Growth Des., 17 (2017) 4270-4279.

[225] F.A. Martin, M.M. Pop, G. Borodi, X. Filip, I. Kacso, Ketoconazole salt and co-crystals with enhanced aqueous solubility, Cryst. Growth Des., 13 (2013) 4295-4304.

[226] G.J. Rees, S.P. Day, A. Lari, A.P. Howes, D. Iuga, M.B. Pitak, S.J. Coles, T.L. Threlfall, M.E. Light, M.E. Smith, A multinuclear solid state NMR, density functional theory and X-ray diffraction study of hydrogen bonding in Group I hydrogen dibenzoates, CrystEngComm, 15 (2013) 8823-8839.

[227] Z. Gu, A. McDermott, Chemical shielding anisotropy of protonated and deprotonated carboxylates in amino acids, J. Am. Chem. Soc., 115 (1993) 4282-4285.

[228] J. Powell, K. Kalakewich, F.J. Uribe-Romo, J.K. Harper, Solid-state NMR and DFT predictions of differences in COOH hydrogen bonding in odd and even numbered n-alkyl fatty acids, Phys. Chem. Chem. Phys., 18 (2016) 12541-12549.

[229] L. Wang, F.J. Uribe-Romo, L.J. Mueller, J.K. Harper, Predicting anisotropic thermal displacements for hydrogens from solid-state NMR: a study on hydrogen bonding in polymorphs of palmitic acid, Phys. Chem. Chem. Phys., 20 (2018) 8475-8487.

[230] A. Hofstetter, L. Emsley, Positional variance in NMR crystallography, J. Am. Chem. Soc., 139 (2017) 2573-2576.

[231] M. Jaworska, P.B. Hrynczyszyn, M. Wełniak, A. Wojtczak, K. Nowicka, G. Krasinski, H. Kassassir, W. Ciesielski, M.J. Potrzebowski, Solid state NMR spectroscopy as a precise tool for assigning the tautomeric form and proton position in the intramolecular bridges of o-hydroxy Schiff bases, J. Phys. Chem. A, 114 (2010) 12522-12530.

[232] E. Kolehmainen, B. Ośmiałowski, ^{15}N NMR Studies of tautomerism, Int. Rev. Phys. Chem., 31 (2012) 567-629.

[233] S. Yaghmaei, S. Khodagholian, J.M. Kaiser, F.S. Tham, L.J. Mueller, T.H. Morton, Chelation of a proton by an aliphatic tertiary diamine, J. Am. Chem. Soc., 130 (2008) 7836-7838.

[234] M.U. Schmidt, J. Brüning, J. Glinnemann, M.W. Hützler, P. Mörschel, S.N. Ivashevskaya, J. van de Streek, D. Braga, L. Maini, M.R. Chierotti, The thermodynamically stable form of solid barbituric acid: the enol tautomer, Angew. Chem. Int. Ed., 50 (2011) 7924-7926.

[235] C. Gervais, F. Babonneau, J. Maquet, C. Bonhomme, D. Massiot, E. Framery, M. Vaultier, ^{15}N cross-polarization using the inversion–recovery cross-polarization technique and ^{11}B magic angle spinning NMR studies of reference compounds containing B—N bonds, Magn. Reson. Chem., 36 (1998) 407-414.

[236] M. Skotnicki, D.C. Apperley, J.A. Aguilar, B. Milanowski, M. Pyda, P. Hodgkinson, Characterization of two distinct amorphous forms of valsartan by solid-state NMR, Mol. Pharm., 13 (2015) 211-222.

[237] A. Lesage, S. Steuernagel, L. Emsley, Carbon-13 Spectral Editing in Solid-State NMR Using Heteronuclear Scalar Couplings, J. Am. Chem. Soc., 120 (1998) 7095-7100.

[238] A.S. Tatton, T.N. Pham, F.G. Vogt, D. Iuga, A.J. Edwards, S.P. Brown, Probing intermolecular interactions and nitrogen protonation in pharmaceuticals by novel ^{15}N-edited and 2D [14]N-^{1}H solid-state NMR, CrystEngComm, 14 (2012) 2654-2659.

[239] I.C.B. Martins, M. Sardo, S.M. Santos, A. Fernandes, A. Antunes, V. André, L. Mafra, M.T. Duarte, Packing Interactions and Physicochemical Properties of Novel Multicomponent Crystal Forms of the Anti-Inflammatory Azelaic Acid Studied by X-ray and Solid-State NMR, Cryst. Growth Des., 16 (2015) 154-166.

[240] F. Rossi, P. Cerreia Vioglio, S. Bordignon, V. Giorgio, C. Nervi, E. Priola, R. Gobetto, K. Yazawa, M.R. Chierotti, Unraveling the Hydrogen Bond Network in a Theophylline–Pyridoxine Salt Cocrystal by a Combined X-ray Diffraction, Solid-State NMR, and Computational Approach, Cryst. Growth Des., 18 (2018) 2225-2233.

[241] Z.J. Li, Y. Abramov, J. Bordner, J. Leonard, A. Medek, A.V. Trask, Solid-state acid-base interactions in complexes of heterocyclic bases with dicarboxylic acids: crystallography, hydrogen bond analysis, and ^{15}N NMR spectroscopy, J. Am. Chem. Soc., 128 (2006) 8199-8210.

[242] D. Braga, L. Chelazzi, F. Grepioni, E. Dichiarante, M.R. Chierotti, R. Gobetto, Molecular salts of anesthetic lidocaine with dicarboxylic acids: solid-state properties and a combined structural and spectroscopic study, Cryst. Growth Des., 13 (2013) 2564-2572.

[243] D. Luedeker, G. Brunklaus, NMR crystallography of ezetimibe co-crystals, Solid State Nucl. Magn. Reson., 65 (2015) 29-40.

[244] J.S. Stevens, S.J. Byard, C.A. Muryn, S.L. Schroeder, Identification of protonation state by XPS, solid-state NMR, and DFT: characterization of the nature of a new theophylline complex by experimental and computational methods, J. Phys. Chem. B, 114 (2010) 13961-13969.

[245] J.S. Stevens, S.J. Byard, S.L. Schroeder, Salt or co-crystal? Determination of protonation state by X-ray photoelectron spectroscopy (XPS), J. Pharm. Sci., 99 (2010) 4453-4457.

[246] J.S. Stevens, S.J. Byard, C.C. Seaton, G. Sadiq, R.J. Davey, S.L. Schroeder, Proton transfer and hydrogen bonding in the organic solid state: a combined XRD/XPS/ssNMR study of 17 organic acid–base complexes, Phys. Chem. Chem. Phys., 16 (2014) 1150-1160.

[247] R. Koike, K. Higashi, N. Liu, W. Limwikrant, K. Yamamoto, K. Moribe, Structural determination of a novel polymorph of sulfathiazole–oxalic acid complex in powder form by solid-state NMR spectroscopy on the basis of crystallographic structure of another polymorph, Cryst. Growth Des., 14 (2014) 4510-4518.

[248] Y.l. Hong, T. Asakura, Y. Nishiyama, 3D ^{14}N/[1]H Double Quantum/[1]H Single Quantum Correlation Solid-State NMR for Probing the Parallel and Anti-Parallel Beta-Sheet Arrangement of Oligo-Peptides at Natural Abundance, ChemPhysChem, 19 (2018) 1841-1845.

[249] K. Bouchmella, S.G. Dutremez, B. Alonso, F. Mauri, C. Gervais, ^{1}H, ^{13}C, and ^{15}N solid-state NMR studies of imidazole-and morpholine-based model compounds possessing halogen and hydrogen bonding capabilities, Cryst. Growth Des., 8 (2008) 3941-3950.

[250] R.K. Harris, P. Jackson, L.H. Merwin, B.J. Say, G. Hägele, Perspectives in high-resolution solid-state nuclear magnetic resonance, with emphasis on combined rotation and multiple-pulse spectroscopy, J. Chem. Soc., Faraday Trans. 1, 84 (1988) 3649-3672.

[251] K. Yamauchi, S. Kuroki, I. Ando, The amide proton NMR chemical shift and hydrogen-bonded structure of glycine-containing peptides and polypeptides in the solid state as studied by multi-pulse-associated high-speed MAS ^{1}H NMR, J. Mol. Struct., 602 (2002) 9-16.

[252] R. Gobetto, C. Nervi, M.R. Chierotti, D. Braga, L. Maini, F. Grepioni, R.K. Harris, P. Hodgkinson, Hydrogen Bonding and Dynamic Behaviour in Crystals and Polymorphs of Dicarboxylic-Diamine Adducts: A Comparison between NMR Parameters and X-ray Diffraction Studies, Chem.-Eur. J., 11 (2005) 7461-7471.

[253] R. Gobetto, C. Nervi, E. Valfrè, M.R. Chierotti, D. Braga, L. Maini, F. Grepioni, R.K. Harris, P.Y. Ghi, ^{1}H MAS, ^{15}N CPMAS, and DFT investigation of hydrogen-bonded supramolecular adducts between the diamine 1,4-diazabicyclo-[2.2.2] octane and dicarboxylic acids of variable chain length, Chem. Mater., 17 (2005) 1457-1466.

[254] K. Yazawa, F. Suzuki, Y. Nishiyama, T. Ohata, A. Aoki, K. Nishimura, H. Kaji, T. Shimizu, T. Asakura, Determination of accurate ^{1}H positions of an alanine tripeptide with anti-parallel and parallel β-sheet structures by high resolution ^{1}H solid state NMR and GIPAW chemical shift calculation, Chem. Commun., 48 (2012) 11199-11201.

[255] T. Emmler, S. Gieschler, H. Limbach, G. Buntkowsky, A simple method for the characterization of OHO-hydrogen bonds by ^{1}H-solid state NMR spectroscopy, J. Mol. Struct., 700 (2004) 29-38.

[256] J.W. Blanchard, T.L. Groy, J.L. Yarger, G.P. Holland, Investigating Hydrogen-Bonded Phosphonic Acids with Proton Ultrafast MAS NMR and DFT Calculations, J. Phys. Chem. C, 116 (2012) 18824-18830.

[257] R.K. Harris, P.Y. Ghi, R.B. Hammond, C.-Y. Ma, K.J. Roberts, Refinement of Hydrogen Atomic Positions in a Hydrogen Bond using a Combination of Solid-State NMR and Computation, Chem. Commun., (2003) 2834-2835.

[258] H.E. Kerr, L.K. Softley, K. Suresh, P. Hodgkinson, I.R. Evans, Structure and physicochemical characterization of a naproxen-picolinamide cocrystal, Acta Cryst. C, 73 (2017) 168-175.

[259] M. Kibalchenko, D. Lee, L. Shao, M.C. Payne, J.J. Titman, J.R. Yates, Distinguishing hydrogen bonding networks in α-D-galactose using NMR experiments and first principles calculations, Chem. Phys. Lett., 498 (2010) 270-276.

[260] J. Nyman, G.M. Day, Static and lattice vibrational energy differences between polymorphs, CrystEngComm, 17 (2015) 5154-5165.

[261] H.K. Miah, R. Cresswell, D. Iuga, J.J. Titman, ^{1}H CSA parameters by ultrafast MAS NMR: measurement and applications to structure refinement, Solid State Nucl. Magn. Reson., 87 (2017) 67-72.

[262] R. Webber, G.H. Penner, A combined deuterium NMR and quantum chemical investigation of inequivalent hydrogen bonds in organic solids, Solid State Nucl. Magn. Reson., 47 (2012) 10-18.

[263] G.H. Penner, R. Webber, L.A. O'Dell, A multinuclear NMR and quantum chemical study of solid trimethylammonium chloride, Can. J. Chem., 89 (2011) 1036-1046.

[264] G. Wu, Oxygen-17 NMR Studies of Organic and Biological Molecules, in: R.E. Wasylishen, S.E. Ashbrook, S. Wimperis (Eds.) NMR of quadrupolar nuclei in solid materials, John Wiley & Sons, 2012, pp. 273-290.

[265] A. Wong, F. Poli, Solid-state ^{17}O NMR studies of biomolecules, in: Annu. Rep. NMR Spect., Elsevier, 2014, pp. 145-220.

[266] G. Wu, Solid-state ^{17}O NMR studies of organic and biological molecules: recent advances and future directions, Solid State Nucl. Magn. Reson., 73 (2016) 1-14.

[267] J. Zhu, J.Y. Lau, G. Wu, A solid-state ^{17}O NMR study of L-tyrosine in different ionization states: Implications for probing tyrosine side chains in proteins, J. Phys. Chem. B, 114 (2010) 11681-11688.

[268] X. Kong, M. Shan, V. Terskikh, I. Hung, Z. Gan, G. Wu, Solid-state ^{17}O NMR of pharmaceutical compounds: Salicylic acid and aspirin, J. Phys. Chem. B, 117 (2013) 9643-9654.

[269] F.G. Vogt, H. Yin, R.G. Forcino, L. Wu, ^{17}O solid-state NMR as a sensitive probe of hydrogen bonding in crystalline and amorphous solid forms of diflunisal, Mol. Pharm., 10 (2013) 3433-3446.

[270] C. Gardiennet-Doucet, X. Assfeld, B. Henry, P. Tekely, Revealing successive steps of deprotonation of l-phosphoserine through ^{13}C and ^{31}P chemical shielding tensor fingerprints, J. Phys. Chem. A, 110 (2006) 9137-9144.

[271] P. Paluch, T. Pawlak, M. Oszajca, W. Lasocha, M.J. Potrzebowski, Fine refinement of solid state structure of racemic form of phospho-tyrosine employing NMR crystallography approach, Solid State Nucl. Magn. Reson., 65 (2015) 2-11.

[272] J. Czernek, T. Pawlak, M.J. Potrzebowski, J. Brus, The comparison of approaches to the solid-state NMR-based structural refinement of vitamin B1 hydrochloride and of its monohydrate, Chem. Phys. Lett., 555 (2013) 135-140.

[273] E. Pindelska, L. Szeleszczuk, D.M. Pisklak, A. Mazurek, W. Kolodziejski, Solid-state NMR as an effective method of polymorphic analysis: Solid dosage forms of clopidogrel hydrogensulfate, J. Pharm. Sci., 104 (2015) 106-113.

[274] F. Rossi, P.C. Vioglio, M.R. Chierotti, R. Gobetto, Solid-state NMR in the Study of Intermolecular Interactions, in: D. Chopra (Ed.) Understanding Intermolecular Interactions in the Solid State: Approaches and Techniques, The Royal Society of Chemistry, 2019, pp. 243-284.

[275] A.S. Tatton, T.N. Pham, F.G. Vogt, D. Iuga, A.J. Edwards, S.P. Brown, Probing hydrogen bonding in cocrystals and amorphous dispersions using [14]N–^{1}H HMQC solid-state NMR, Mol. Pharm., 10 (2013) 999-1007.

[276] F.G. Vogt, J.S. Clawson, M. Strohmeier, A.J. Edwards, T.N. Pham, S.A. Watson, Solid-state NMR analysis of organic cocrystals and complexes, Cryst. Growth Des., 9 (2009) 921-937.

[277] J.R. Patel, R.A. Carlton, T.E. Needham, C.O. Chichester, F.G. Vogt, Preparation, structural analysis, and properties of tenoxicam cocrystals, Int. J. Pharm., 436 (2012) 685-706.

[278] K. Gaglioti, M.R. Chierotti, F. Grifasi, R. Gobetto, U. Griesser, D. Hasa, D. Voinovich, Improvement of the water solubility of tolfenamic acid by new multiple-component crystals produced by mechanochemical methods, CrystEngComm, 16 (2014) 8252-8262.

[279] T. Venâncio, L.M. Oliveira, J. Ellena, N. Boechat, S.P. Brown, Probing intermolecular interactions in a diethylcarbamazine citrate salt by fast MAS ^{1}H solid-state NMR spectroscopy and GIPAW calculations, Solid State Nucl. Magn. Reson., 87 (2017) 73-79.

[280] K. Maruyoshi, D. Iuga, O.N. Antzutkin, A. Alhalaweh, S.P. Velaga, S.P. Brown, Identifying the intermolecular hydrogen-bonding supramolecular synthons in an indomethacin–nicotinamide cocrystal by solid-state NMR, Chem. Commun., 48 (2012) 10844-10846.

[281] F.G. Vogt, L.M. Katrincic, S.T. Long, R.L. Mueller, R.A. Carlton, Y.T. Sun, M.N. Johnson, R.C. Copley, M.E. Light, Enantiotropically-related polymorphs of {4-(4-chloro-3-fluorophenyl)-2-[4-(methyloxy)phenyl]-1,3-thiazol-5-yl} acetic acid: Crystal structures and multinuclear solid-state NMR, J. Pharm. Sci., 97 (2008) 4756-4782.

[282] H. Fenniri, G.A. Tikhomirov, D.H. Brouwer, S. Bouatra, M. El Bakkari, Z. Yan, J.-Y. Cho, T. Yamazaki, High Field Solid-State NMR Spectroscopy Investigation of ^{15}N-Labeled Rosette Nanotubes: Hydrogen Bond Network and Channel-Bound Water, J. Am. Chem. Soc., 138 (2016) 6115-6118.

[283] D. Sebastiani, Current densities and nucleus-independent chemical shift maps from reciprocal-space density functional perturbation theory calculations, ChemPhysChem, 7 (2006) 164-175.

[284] J. Schmidt, A. Hoffmann, H.W. Spiess, D. Sebastiani, Bulk chemical shifts in hydrogen-bonded systems from first-principles calculations and solid-state-NMR, J. Phys. Chem. B, 110 (2006) 23204-23210.

[285] M. Zilka, S. Sturniolo, S.P. Brown, J.R. Yates, Visualising crystal packing interactions in solid-state NMR: Concepts and applications, J. Chem. Phys., 147 (2017) 144203.

[286] M. Schmidt, J.J. Wittmann, R. Kress, D. Schneider, S. Steuernagel, H.-W. Schmidt, J. Senker, Crystal structure of a highly efficient clarifying agent for isotactic polypropylene, Cryst. Growth Des., 12 (2012) 2543-2551.

[287] A.-C. Pöppler, E.K. Corlett, H. Pearce, M.P. Seymour, M. Reid, M.G. Montgomery, S.P. Brown, Single-crystal X-ray diffraction and NMR crystallography of a 1: 1 cocrystal of dithianon and pyrimethanil, Acta Cryst. C, 73 (2017) 149-156.

[288] A.-C. Pöppler, D. Walker, S.P. Brown, A combined NMR crystallographic and PXRD investigation of the structure-directing role of water molecules in orotic acid and its lithium and magnesium salts, CrystEngComm, 19 (2017) 224-236.

[289] J. Leclaire, G. Poisson, F. Ziarelli, G. Pepe, F. Fotiadu, F.M. Paruzzo, A.J. Rossini, J.-N. Dumez, B. Elena-Herrmann, L. Emsley, Structure elucidation of a complex CO_2-based organic framework material by NMR crystallography, Chem. Sci., 7 (2016) 4379-4390.

[290] J.R. Yates, T.N. Pham, C.J. Pickard, F. Mauri, A.M. Amado, A.M. Gil, S.P. Brown, An Investigation of Weak CH...O Hydrogen Bonds in Maltose Anomers by a Combination of Calculation and Experimental Solid-State NMR Spectroscopy, J. Am. Chem. Soc., 127 (2005) 10216-10220.

[291] A.C. Uldry, J.M. Griffin, J.R. Yates, M. Pérez-Torralba, M.D. Santa María, A.L. Webber, M.L.L. Beaumont, A. Samoson, R.M. Claramunt, C.J. Pickard, S.P. Brown, Quantifying Weak Hydrogen Bonding in Uracil and 4-Cyano-4'-ethynylbiphenyl: A Combined Computational and Experimental Investigation of NMR Chemical Shifts in the Solid State, J. Am. Chem. Soc., 130 (2008) 945-954.

[292] D.H. Brouwer, S. Alavi, J.A. Ripmeester, NMR crystallography of *p-tert*-butylcalix[4]arene host-guest complexes using ^{1}H complexation-induced chemical shifts, Phys. Chem. Chem. Phys., 10 (2008) 3857-3860.

[293] A. Comotti, S. Bracco, P. Sozzani, S.M. Hawxwell, C. Hu, M.D. Ward, Guest molecules confined in amphipathic crystals as revealed by X-ray diffraction and MAS NMR, Cryst. Growth Des., 9 (2009) 2999-3002.

[294] P.C. Vioglio, M. Chierotti, R. Gobetto, Solid-state nuclear magnetic resonance as a tool for investigating the halogen bond, CrystEngComm, 18 (2016) 9173-9184.

[295] P.M.J. Szell, D.L. Bryce, Solid-State NMR Studies of Halogen Bonding, in: G.A. Webb (Ed.) Modern Magnetic Resonance, Springer International Publishing, Cham, 2016, pp. 1-18.

[296] G. Cavallo, P. Metrangolo, R. Milani, T. Pilati, A. Priimagi, G. Resnati, G. Terraneo, The halogen bond, Chem. Rev., 116 (2016) 2478-2601.

[297] M. Weingarth, N. Raouafi, B. Jouvelet, L. Duma, G. Bodenhausen, K. Boujlel, B. Schöllhorn, P. Tekely, Revealing molecular self-assembly and geometry of non-covalent halogen bonding by solid-state NMR spectroscopy, Chem. Commun., (2008) 5981-5983.

[298] P.M. Szell, S.A. Gabriel, R.D. Gill, S.Y. Wan, B. Gabidullin, D.L. Bryce, ^{13}C and ^{19}F solid-state NMR and X-ray crystallographic study of halogen-bonded frameworks featuring nitrogen-containing heterocycles, Acta Cryst. C, 73 (2017) 157-167.

[299] P.M. Szell, G. Cavallo, G. Terraneo, P. Metrangolo, B. Gabidullin, D.L. Bryce, Comparing the Halogen Bond to the Hydrogen Bond by Solid-State NMR: Anion Coordinated Dimers from 2- & 3-Iodoethynylpyridine Salts, Chem.-Eur. J., (2018).

[300] L.B. Krivdin, Computational protocols for calculating ^{13}C NMR chemical shifts, Prog. Nucl. Magn. Reson. Spectrosc., 112-113 (2019) 103-156.

[301] D.A. Middleton, C.S. Le Duff, X. Peng, D.G. Reid, D. Saunders, Molecular Conformations of the Polymorphic Forms of Cimetidine from ^{13}C Solid-State NMR Distance and Angle Measurements, J. Am. Chem. Soc., 122 (2000) 1161-1170.

[302] A. Arakcheeva, P. Pattison, A. Bauer-Brandl, H. Birkedal, G. Chapuis, Cimetidine, $C_{10}H_{16}N_6S$, form C: crystal structure and modelling of polytypes using the superspace approach, J. Appl. Crystallogr., 46 (2013) 99-107.

[303] D.A. Middleton, X. Peng, D. Saunders, K. Shankland, W.I.F. David, A.J. Markvardsen, Conformational analysis by solid-state NMR and its application to restrained structure determination from powder diffraction data, Chem. Commun., (2002).

[304] J. Madine, D.A. Middleton, An NMR strategy for obtaining multiple conformational constraints for ^{15}N–^{13}C spin-pair labelled organic solids, Phys. Chem. Chem. Phys., 8 (2006) 5223-5228.

[305] I. Sack, S. Macholl, J. Fuhrhop, G. Buntkowsky, Conformational studies of polymorphic *N*-octyl-D-gluconamide with ^{15}N (labeled) ^{13}C (natural abundance) REDOR spectroscopy, Phys. Chem. Chem. Phys., 2 (2000) 1781-1788.

[306] S. Macholl, F. Börner, G. Buntkowsky, Revealing the Configuration and Crystal Packing of Organic Compounds by Solid-State NMR Spectroscopy: Methoxycarbonylurea, a Case Study, Chem.-Eur. J., 10 (2004) 4808-4816.

[307] G.M. Pope, I. Hung, Z. Gan, H. Mobarak, G. Widmalm, J.K. Harper, Exploiting ^{13}C/^{14}N solid-state NMR distance measurements to assign dihedral angles and locate neighboring molecules, Chem. Commun., 54 (2018) 6376-6379.

[308] D.A. Middleton, Solid-state NMR detection of ^{14}N-^{13}C dipolar couplings between amino acid side groups provides constraints on amyloid fibril architecture, Magn. Reson. Chem., 49 (2011) 65-69.

[309] M. Strohmeier, D.M. Grant, Experimental and Theoretical Investigation of the ^{13}C and ^{15}N Chemical Shift Tensors in Melanostatin Exploring the Chemical Shift Tensor as a Structural Probe, J. Am. Chem. Soc., 126 (2004) 966-977.

[310] J. Żabiński, D. Maciejewska, P. Kaźmierczak, Structural analysis of bis-amidines and bis-nitriles in solid-state by combining NMR spectroscopy and molecular modeling, J. Mol. Struct., 923 (2009) 132-140.

[311] Structure determination from powder diffraction data, W.I. David, K. Shankland, C. Baerlocher, L. McCusker (Eds.), Oxford University Press, 2002.

[312] I. Jastrzebska, T. Pawlak, R. Arcos-Ramos, E. Florez-Lopez, N. Farfán, D. Czajkowska-Szczykowska, J. Maj, R. Santillan, J.W. Morzycki, M.J. Potrzebowski, Synthesis, structure, and local molecular dynamics for crystalline rotors based on hecogenin/botogenin steroidal frameworks, Cryst. Growth Des., 16 (2016) 5698-5709.

[313] C.M. Widdifield, J.D. Farrell, J.C. Cole, J.A.K. Howard, P. Hodgkinson, Resolving alternative organic crystal structures using density functional theory and NMR chemical shifts, Chem. Sci., (2020).

[314] M. Hušák, A. Jegorov, J. Brus, W. van Beek, P. Pattison, M. Christensen, V. Favre-Nicolin, J. Maixner, Metergoline II: structure solution from powder diffraction data with preferred orientation and from microcrystal, Struct. Chem., 19 (2008) 517-525.

[315] J.A. Fernandes, M. Sardo, L. Mafra, D. Choquesillo-Lazarte, N. Masciocchi, X-ray and NMR crystallography studies of novel theophylline cocrystals prepared by liquid assisted grinding, Cryst. Growth Des., 15 (2015) 3674-3683.

[316] P. Li, Y. Chu, L. Wang, R.M. Wenslow, K. Yu, H. Zhang, Z. Deng, Structure determination of the theophylline–nicotinamide cocrystal: a combined powder XRD, 1D solid-state NMR, and theoretical calculation study, CrystEngComm, 16 (2014) 3141-3147.

[317] D. Zanolla, B. Perissutti, N. Passerini, M.R. Chierotti, D. Hasa, D. Voinovich, L. Gigli, N. Demitri, S. Geremia, J. Keiser, A new soluble and bioactive polymorph of praziquantel, European Journal of Pharmaceutics and Biopharmaceutics, 127 (2018) 19-28.

[318] A.E. Watts, K. Maruyoshi, C.E. Hughes, S.P. Brown, K.D. Harris, Combining the advantages of powder X-ray diffraction and NMR crystallography in structure determination of the pharmaceutical material cimetidine hydrochloride, Cryst. Growth Des., 16 (2016) 1798-1804.

[319] E.D. Smith, R.B. Hammond, M.J. Jones, K.J. Roberts, J.B. Mitchell, S.L. Price, R.K. Harris, D.C. Apperley, J.C. Cherryman, R. Docherty, The determination of the crystal structure of anhydrous theophylline by X-ray powder diffraction with a systematic search algorithm, lattice energy

calculations, and ^{13}C and ^{15}N solid-state NMR: a question of polymorphism in a given unit cell, J. Phys. Chem. B, 105 (2001) 5818-5826.

[320] Ł. Szeleszczuk, T. Gubica, A. Zimniak, D.M. Pisklak, K. Dąbrowska, M.K. Cyrański, M. Kańska, The potential for the indirect crystal structure verification of methyl glycosides based on acetates' parent structures: GIPAW and solid-state NMR approaches, Chem. Phys. Lett., 686 (2017) 7-11.

[321] X. Filip, G. Borodi, C. Filip, Testing the limits of sensitivity in a solid-state structural investigation by combined X-ray powder diffraction, solid-state NMR, and molecular modelling, Phys. Chem. Chem. Phys., 13 (2011) 17978-17986.

[322] A.S. Tatton, H. Blade, S.P. Brown, P. Hodgkinson, L.P. Hughes, S.O. Nilsson Lill, J.R. Yates, Improving Confidence in Crystal Structure Solutions Using NMR Crystallography: The Case of β-Piroxicam, Cryst. Growth Des., 18 (2018) 3339-3351.

[323] E. Mugnaioli, T. Gorelik, U. Kolb, "Ab initio" structure solution from electron diffraction data obtained by a combination of automated diffraction tomography and precession technique, Ultramicroscopy, 109 (2009) 758-765.

[324] T.E. Weirich, First-principles calculations as a tool for structure validation in electron crystallography, Acta Crystallogr. Sect. A: Found. Crystallogr., 60 (2004) 75-81.

[325] L. Maini, D. Braga, F. Grepioni, G. Lampronti, K. Gaglioti, R. Gobetto, M.R. Chierotti, From isomorphous to "anisomorphous" ionic co-crystals of barbituric acid upon dehydration and return, CrystEngComm, 18 (2016) 4651-4657.

[326] M. Schmidt, C.S. Zehe, R. Siegel, J.U. Heigl, C. Steinlein, H.-W. Schmidt, J. Senker, NMR-crystallographic study of two-dimensionally self-assembled cyclohexane-based low-molecular-mass organic compounds, CrystEngComm, 15 (2013) 8784-8796.

[327] A. Bērziņš, P. Hodgkinson, Solid-state NMR and computational investigation of solvent molecule arrangement and dynamics in isostructural solvates of droperidol, Solid State Nucl. Magn. Reson., 65 (2015) 12-20.

[328] G.K. Lim, K. Fujii, K.D.M. Harris, D.C. Apperley, Structure determination from powder X-ray diffraction data of a new polymorph of a high-density organic hydrate material, with an assessment of hydrogen-bond disorder by Rietveld refinement, Cryst. Growth Des., 11 (2011) 5192-5199.

[329] S.L. Bekö, D. Urmann, A. Lakatos, C. Glaubitz, M.U. Schmidt, Nimustine hydrochloride: the first crystal structure determination of a 2-chloroethyl-*N*-nitrosourea hydrochloride derivative by X-ray powder diffraction and solid-state NMR, Acta Crystallogr. Sect. C: Cryst. Struct. Commun., 68 (2012) o144-o148.

[330] L. Seyfarth, J. Sehnert, N. El-Gamel, W. Milius, E. Kroke, J. Breu, J. Senker, Structure elucidation of cyameluric acid by combining solid-state NMR spectroscopy, molecular modeling and direct-space methods, J. Mol. Struct., 889 (2008) 217-228.

[331] X. Li, A.D. Bond, K.E. Johansson, J. Van de Streek, Distinguishing tautomerism in the crystal structure of (*Z*)-*N*-(5-ethyl-2,3-dihydro-1,3,4-thiadiazol-2-ylidene)-4-methylbenzenesulfonamide using DFT-D calculations and ^{13}C solid-state NMR, Acta Cryst. C, 70 (2014) 784-789.

[332] A. Hangan, G. Borodi, X. Filip, C. Tripon, C. Morari, L. Oprean, C. Filip, Structure of *N*-(5-ethyl-[1,3,4]-thiadiazole-2-yl)toluenesulfonamide by combined X-ray powder diffraction, ^{13}C solid-state NMR and molecular modelling, Acta Cryst. B, 66 (2010) 615-621.

[333] J.K. Harper, D.M. Grant, Y. Zhang, P.L. Lee, R. Von Dreele, Characterizing challenging microcrystalline solids with solid-state NMR shift tensor and synchrotron X-ray powder diffraction data: structural analysis of ambuic acid, J. Am. Chem. Soc., 128 (2006) 1547-1552.

[334] X. Filip, C. Filip, Can the conformation of flexible hydroxyl groups be constrained by simple NMR crystallography approaches? The case of the quercetin solid forms, Solid State Nucl. Magn. Reson., 65 (2015) 21-28.

[335] X. Filip, M. Miclaus, F. Martin, C. Filip, I.G. Grosu, Optimized multi-step NMR-crystallography approach for structural characterization of a stable quercetin solvate, J. Pharm. Biomed. Anal., 138 (2017) 22-28.

[336] M. Miclaus, I.-G. Grosu, X. Filip, C. Tripon, C. Filip, Optimizing structure determination from powders of crystalline organic solids with high molecular flexibility: the case of lisinopril dihydrate, CrystEngComm, 16 (2014) 299-303.

[337] C.E. Hughes, G.M. Reddy, S. Masiero, S.P. Brown, P.A. Williams, K.D. Harris, Determination of a complex crystal structure in the absence of single crystals: analysis of powder X-ray diffraction data, guided by solid-state NMR and periodic DFT calculations, reveals a new 2′-deoxyguanosine structural motif, Chem. Sci., 8 (2017) 3971-3979.

[338] C. Yang, L. Zhu, R.A. Kudla, J.D. Hartman, R.O. Al-Kaysi, S. Monaco, B. Schatschneider, A. Magalhães, G.J. Beran, C.J. Bardeen, Crystal structure of the meta-stable intermediate in the photomechanical, crystal-to-crystal reaction of 9-*tert*-butyl anthracene ester, CrystEngComm, 18 (2016) 7319-7329.

[339] C. Zehe, M. Schmidt, R. Siegel, K. Kreger, V. Daebel, S. Ganzleben, H.-W. Schmidt, J. Senker, Influence of fluorine side-group substitution on the crystal structure formation of benzene-1,3,5-trisamides, CrystEngComm, 16 (2014) 9273-9283.

[340] R. Witter, U. Sternberg, S. Hesse, T. Kondo, F.-T. Koch, A.S. Ulrich, ^{13}C chemical shift constrained crystal structure refinement of cellulose I$_\alpha$ and its verification by NMR anisotropy experiments, Macromolecules, 39 (2006) 6125-6132.

[341] A.I. Greenwood, M.C. Clay, C.M. Rienstra, ^{31}P-dephased, ^{13}C-detected REDOR for NMR crystallography at natural isotopic abundance, J. Magn. Reson., 278 (2017) 8-17.

[342] S.L. Price, Predicting crystal structures of organic compounds, Chem. Soc. Rev., 43 (2014) 2098-2111.

[343] S.L. Price, Is zeroth order crystal structure prediction (CSP_0) coming to maturity? What should we aim for in an ideal crystal structure prediction code?, Faraday Discuss., 211 (2018) 9-30.

[344] A.M. Reilly, R.I. Cooper, C.S. Adjiman, S. Bhattacharya, A.D. Boese, J.G. Brandenburg, P.J. Bygrave, R. Bylsma, J.E. Campbell, R. Car, Report on the sixth blind test of organic crystal structure prediction methods, Acta Cryst. B, 72 (2016) 439-459.

[345] W.D.S. Motherwell, H.L. Ammon, J.D. Dunitz, A. Dzyabchenko, P. Erk, A. Gavezzotti, D.W.M. Hofmann, F.J.J. Leusen, J.P.M. Lommerse, W.T.M. Mooij, S.L. Price, H. Scheraga, B. Schweizer, M.U. Schmidt, B.P. van Eijck, P. Verwer, D.E. Williams, Crystal structure prediction of small organic molecules: a second blind test, Acta Cryst. B, 58 (2002) 647-661.

[346] L. Emsley, Spin diffusion in crystalline solids, in: NMR Crystallography, John Wiley & Sons Ltd., 2009.

[347] B. Elena, L. Emsley, Powder crystallography by proton solid-state NMR, J. Am. Chem. Soc., 127 (2005) 9140-9146.

[348] V.E. Zorin, S.P. Brown, P. Hodgkinson, Origins of linewidth in ^{1}H magic-angle spinning NMR, J. Chem. Phys., 125 (2006) 144508:144501-144513.

[349] B. Elena, G. Pintacuda, N. Mifsud, L. Emsley, Molecular structure determination in powders by NMR crystallography from proton spin diffusion, J. Am. Chem. Soc., 128 (2006) 9555-9560.

[350] C.J. Pickard, E. Salager, G. Pintacuda, B. Elena, L. Emsley, Resolving structures from powders by NMR crystallography using combined proton spin diffusion and plane wave DFT calculations, J. Am. Chem. Soc., 129 (2007) 8932-8933.

[351] E. Salager, R.S. Stein, C.J. Pickard, B. Elena, L. Emsley, Powder NMR crystallography of thymol, Phys. Chem. Chem. Phys., 11 (2009) 2610-2621.

[352] G. Mollica, M. Dekhil, F. Ziarelli, P. Thureau, S. Viel, Probing crystal packing of uniformly ^{13}C-enriched powder samples using homonuclear dipolar coupling measurements, Solid State Nucl. Magn. Reson., 65 (2015) 114-121.

[353] G. Mollica, M. Dekhil, F. Ziarelli, P. Thureau, S. Viel, Quantitative Structural Constraints for Organic Powders at Natural Isotopic Abundance Using Dynamic Nuclear Polarization Solid-State NMR Spectroscopy, Angew. Chem. Int. Ed., 54 (2015) 6028-6031.

[354] P. Thureau, S. Sturniolo, M. Zilka, F. Ziarelli, S. Viel, J. Yates, G. Mollica, Reducing the computational cost of NMR crystallography of organic powders at natural isotopic abundance with the help of ^{13}C-^{13}C dipolar couplings, Magn. Reson. Chem., 57 (2019) 256-264.

[355] J. Brus, J. Czernek, M. Hruby, P. Svec, L. Kobera, S. Abbrent, M. Urbanova, Efficient strategy for determining the atomic-resolution structure of micro-and nanocrystalline solids within polymeric microbeads: Domain-edited NMR crystallography, Macromolecules, 51 (2018) 5364-5374.

[356] M.K. Dudek, G. Bujacz, M.J. Potrzebowski, Experimental tests for quality validation of computationally predicted crystal structures–a case of a conformationally flexible procyanidin A-2 dihydrate, CrystEngComm, 19 (2017) 2903-2913.

[357] J.K. Harper, D.M. Grant, Enhancing crystal-structure prediction with NMR tensor data, Cryst. Growth Des., 6 (2006) 2315-2321.

[358] K. Kalakewich, R. Iuliucci, J.K. Harper, Establishing Accurate High-Resolution Crystal Structures in the Absence of Diffraction Data and Single Crystals—An NMR Approach, Cryst. Growth Des., 13 (2013) 5391-5396.

[359] G. Seifert, Tight-Binding Density Functional Theory: An Approximate Kohn–Sham DFT Scheme, J. Phys. Chem. A, 111 (2007) 5609-5613.

[360] M. Khan, V. Enkelmann, G. Brunklaus, Heterosynthon mediated tailored synthesis of pharmaceutical complexes: a solid-state NMR approach, CrystEngComm, 13 (2011) 3213-3223.

[361] NMR Crystallography, R. Harris, R. Wasylishen, M. Duer (Eds.), Wiley, Chichester, 2009.

[362] Modern Methods in Solid-state NMR, P. Hodgkinson (Ed.), The Royal Society of Chemistry, 2018.

[363] R.F. Moran, D.M. Dawson, S.E. Ashbrook, Exploiting NMR spectroscopy for the study of disorder in solids, Int. Rev. Phys. Chem., 36 (2017) 39-115.

[364] A. Paudel, M. Geppi, G. Van den Mooter, Structural and dynamic properties of amorphous solid dispersions: the role of solid-state nuclear magnetic resonance spectroscopy and relaxometry, J. Pharm. Sci., 103 (2014) 2635-2662.

[365] C.M. Widdifield, S.O.N. Lill, A. Broo, M. Lindkvist, A. Pettersen, A.S. Ankarberg, P. Aldred, S. Schantz, L. Emsley, Does Z' equal 1 or 2? Enhanced powder NMR crystallography verification of a disordered room temperature crystal structure of a p38 inhibitor for chronic obstructive pulmonary disease, Phys. Chem. Chem. Phys., 19 (2017) 16650-16661.

[366] D.M. Többens, J. Glinneman, M.R. Chierotti, J. van de Streek, D. Sheptyakov, On the high-temperature phase of barbituric acid, CrystEngComm, 14 (2012) 3046-3055.

[367] J.K. Harper, D. Tishler, D. Richardson, J. Lokvam, R. Pendrill, G. Widmalm, Solid-State NMR Characterization of the Molecular Conformation in Disordered Methyl α-L-Rhamnofuranoside, J. Phys. Chem. A, 117 (2013) 5534-5541.

[368] D.C. Apperley, A.S. Batsanov, S.J. Clark, R.K. Harris, P. Hodgkinson, D.B. Jochym, Computation of magnetic shielding to simultaneously validate a crystal structure and assign a solid-state NMR spectrum, J. Mol. Struct., 1015 (2012) 192-201.

[369] D.C. Apperley, A.F. Markwell, R.K. Harris, P. Hodgkinson, NMR characterisation of structure in solvates and polymorphs of formoterol fumarate, Magn. Reson. Chem., 50 (2012) 680-690.

[370] J. Czernek, T. Pawlak, M.J. Potrzebowski, Benchmarks for the ^{13}C NMR chemical shielding tensors in peptides in the solid state, Chem. Phys. Lett., 527 (2012) 31-35.

[371] D.E. Braun, L.H. Koztecki, J.A. McMahon, S.L. Price, S.M. Reutzel-Edens, Navigating the waters of unconventional crystalline hydrates, Mol. Pharm., 12 (2015) 3069-3088.

[372] S.O. Nilsson Lill, C.M. Widdifield, A. Pettersen, A. Svensk Ankarberg, M. Lindkvist, P. Aldred, S. Gracin, N. Shankland, K. Shankland, S. Schantz, Elucidating an Amorphous Form Stabilization Mechanism for Tenapanor Hydrochloride: Crystal Structure Analysis Using X-ray Diffraction, NMR Crystallography, and Molecular Modeling, Mol. Pharm., 15 (2018) 1476-1487.

[373] D.E. Braun, K.P. Nartowski, Y.Z. Khimyak, K.R. Morris, S.R. Byrn, U.J. Griesser, Structural Properties, Order–Disorder Phenomena, and Phase Stability of Orotic Acid Crystal Forms, Mol. Pharm., 13 (2016) 1012-1029.

[374] F.G. Vogt, J.A. Vena, M. Chavda, J.S. Clawson, M. Strohmeier, M.E. Barnett, Structural analysis of 5-fluorouracil and thymine solid solutions, J. Mol. Struct., 932 (2009) 16-30.

[375] T. Pawlak, M. Jaworska, M.J. Potrzebowski, NMR Crystallography of α-Poly(L-lactide), Phys. Chem. Chem. Phys., 15 (2013) 3137-3145.

[376] S. Cadars, A. Lesage, C.J. Pickard, P. Sautet, L. Emsley, Characterizing slight structural disorder in solids by combined solid-state NMR and first principles calculations, J. Phys. Chem. A, 113 (2009) 902-911.

[377] D. Sakellariou, S.P. Brown, A. Lesage, S. Hediger, M. Bardet, C.A. Meriles, A. Pines, L. Emsley, High-resolution NMR correlation spectra of disordered solids, J. Am. Chem. Soc., 125 (2003) 4376-4380.

[378] A.J. Rossini, A. Zagdoun, F. Hegner, M. Schwarzwälder, D. Gajan, C. Copéret, A. Lesage, L. Emsley, Dynamic Nuclear Polarization NMR Spectroscopy of Microcrystalline Solids, J. Am. Chem. Soc., 134 (2012) 16899-16908.

[379] U. Sternberg, R. Witter, A.S. Ulrich, Crystal Structure Refinement Using Chemical Shifts, Modern Magnetic Resonance, (2006) 71-78.

[380] F.M. Paruzzo, A. Hofstetter, F. Musil, S. De, M. Ceriotti, L. Emsley, Chemical shifts in molecular solids by machine learning, Nat. Commun., 9 (2018) 4501.

[381] J. Cuny, Y. Xie, C.J. Pickard, A.A. Hassanali, Ab Initio Quality NMR Parameters in Solid-State Materials Using a High-Dimensional Neural-Network Representation, J. Chem. Theory Comput., 12 (2016) 765-773.

6 Glossary

API   Active Pharmaceutical Ingredient

APT   Attached Proton Test

CIF   Crystallographic Information File

CP   Cross-Polarisation

CSA   Chemical Shift Anisotropy

CSD   Cambridge Structural Database

CSP   Crystal Structure Prediction

dc-DFT   dispersion-corrected DFT

DFT   Density Functional Theory

DNP   Dynamic Nuclear Polarisation

DQ   Double Quantum

ED   Electron Diffraction

GGA   Generalised Gradient Approximation

GIPAW   Gauge Including Projector Augmented Waves

GTO   Gaussian Type Orbitals

HETCOR   HETeronuclear CORrelation

INADEQUATE   Incredible Natural Abundance DoublE QUAntum Transfer Experiment

INEPT   Insensitive Nuclei Enhanced by Polarisation Transfer

LDA   Localised Density Approximation

MAE   Mean Average Error

MAS   Magic-Angle Spinning

MC   Monte Carlo

MD   Molecular Dynamics

ML   Machine Learning

NICS   Nucleus Independent Chemical Shift
PBE   Perdew, Burke and Ernzerhof (exchange correlation energy functional)
PI(MD) Path Integral (Molecular Dynamics)
PXRD   Powder X-Ray Diffraction
REDOR   Rotational Echo Double Resonance
RF   Radio Frequency
RMS(D) Root Mean Square (Deviation)
RSS   Root Sum Square
SCXRD   Single Crystal X-Ray Diffraction
SEDC   Semi-Empirical Dispersion Correction
TS   Tkatchenko-Scheffler (SEDC scheme)
SQ   Single Quantum
XRD   X-Ray Diffraction

Graphical abstract
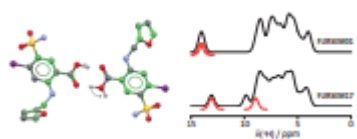
Highlights

The state-of-the-art for NMR crystallographic methods for organic solids is presented

NMR is seen to be effective in identifying protonation states and hydrogen positions

NMR is now widely used as a complement to powder and electron diffraction studies

Approaches for obtaining crystal structures purely from NMR data are reviewed

Future challenges and directions in NMR crystallography are discussed